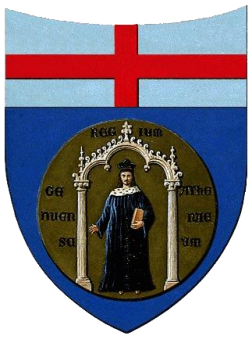

UNIVERSITY OF GENOVA

Ph.D. in NEUROSCIENCES

CLINICAL AND EXPERIMENTAL NEUROSCIENCES

MISGLYCOSYLATION IN CHARCOT-MARIE-TOOTH NEUROPATHIES ASSOCIATED TO *MPZ* MUTATIONS

Tutor

Dr. Marina Grandis

Ph.D. candidate

Francesca Veneri

Coordinator of Ph.D. program

Prof. Angelo Schenone

XXXII CYCLE

2019/2020

"Science, my lad, is made up of mistakes, but they are mistakes which it is useful to make, because they lead little by little to the truth."

Jules Verne, A Journey to the Center of the Earth

ABSTRACT

Charcot-Marie-Tooth disease is the most common neuromuscular disorder, with a prevalence of 1:2500. Despite the phenotypical similarities among patients, it is characterized by a remarkable genetic heterogeneity. Among the different genes that are responsible for CMT, mutations in *Myelin Protein Zero* (*MPZ*) gene cause CMT1B and represent the 5% of all CMT cases. *MPZ* gene encodes for the P0 protein, the principal myelin protein of the peripheral nervous system; at the moment, more than 200 mutations in these gene are known and almost all mutations are pathogenic. The phenotype of *MPZ* related neuropathies is also variable, implying multiple pathogenic mechanisms. We focused our interest on misglycosylation, which is increasingly recognized as a cause of different diseases, but has never been investigated in inherited neuropathies, even if peripheral myelin is largely composed of glycoproteins.

We identified two groups of mutations in *MPZ* gene: one group is composed by variants introducing a new glycosylation site in the P0 sequence, the other one includes mutations that eliminate the constitutive glycosylation site of the P0 protein. Through transient transfection in different cellular lines (HeLa cells and Schwannoma rat cells), and through different techniques of cell and molecular biology, we founded that mutant protein with a double oligosaccharide are partially retained intracellularly, with consequences on their adhesion capacity; instead, mutant proteins that loose the constitutive glycosylation site were less affected in localization or adhesion capacity. To further investigate how peripheral myelination is affected by misglycosylation, in particular, we generated a mouse model carrying the mutation $D^{61}\rightarrow N$ to evaluate *in vivo* the effects of hyperglycosylation. This mouse model, that represent the first knock-in model of CMT1B generated using the CRISPR/Cas9 technology, faithfully recapitulates the human pathology and confirms hyperglycosylation as a novel pathomechanism for CMT1B. We characterized the mice with behavioral test and with electrophysiological analysis, finding a severe impairment in nerve functionality; this was further confirmed by morphological analysis that revealed a de/dysmyelinating phenotype with the presence in sciatic nerves of myelin

abnormalities similar to tomacula structures. Starting from evidences founded in literature, we evaluated the possibility to test a molecule, belonging to a class of compounds called iminosugars, that are potentially able to inhibits some enzymes involved in glycosylation cascade, and that are already used for the treatment of other pathologies. We obtained encouraging results from the treatment of cells transfected with the $D^{61}\rightarrow N$ mutation, in terms of protein localization and adhesion capacity; also the treatment of mutant DRGs that were characterized by myelin abnormalities, ameliorated the morphology. However, more in depth experiments showed that this molecule didn't act modifying the glycosidic structure but decreasing the amount of myelin proteins.

The ineffectiveness of the treatment showed that, before proceeding, it is necessary to know the glycosidic composition of the new oligosaccharide but also of the constitutive one, to find a molecule able to modify glycans in a targeted way.

TABLE OF CONTENTS

INTRODUCTION

1. MYELIN

The nervous system can be divided in two parts: the Central Nervous System (CNS) and the Peripheral Nervous System (PNS). The CNS is formed by brain and spinal cord, whereas the PNS is constituted by fibers that convey informations from both external environment and internal organs to the CNS or from the CNS to muscles, organs and glands.

The nervous system is mainly constituted by two types of specialized cells: neurons and glial cells, even if cells of the immune system, blood cells and fibroblasts are also present. Glial cells are located near neuron cell bodies and axons and they have the important role to guide axonal growth and to form myelin. The principal role of the myelin is to insulate axons to allow a rapid impulse propagation, necessary for motor, sensory and cognitive function of the nervous system; the myelin ensheathment of axons provides the structural basis for saltatory action potential propagation [1-5]. Neuronal signals are transmitted in the form of electrochemical waves, called action potentials that travel along the axons and reach specific target cells via electrical or chemical synapses.

Myelin is a multilamellar structure present both in the CNS and in the PNS. In the CNS, myelin is formed by oligodendrocytes [6] whereas in the PNS it is formed by Schwann Cells (SCs) [7]. Glial cells, that have different developmental origin (neural crest for SCs and subventricular zone for oligodendrocytes), enwrap the axons forming myelin as a protrusion of their own plasma membrane; however, SCs and oligodendrocytes differ for the number of myelinated axonal segment per myelinating cell: oligodendrocytes contact multiple axons simultaneously in order to form myelin (60:1), whereas SCs enwrap one axon at time (1:1) and provide myelin to a single internode, i.e. the space included between two nodes of Ranvier [8] (Figure 1).

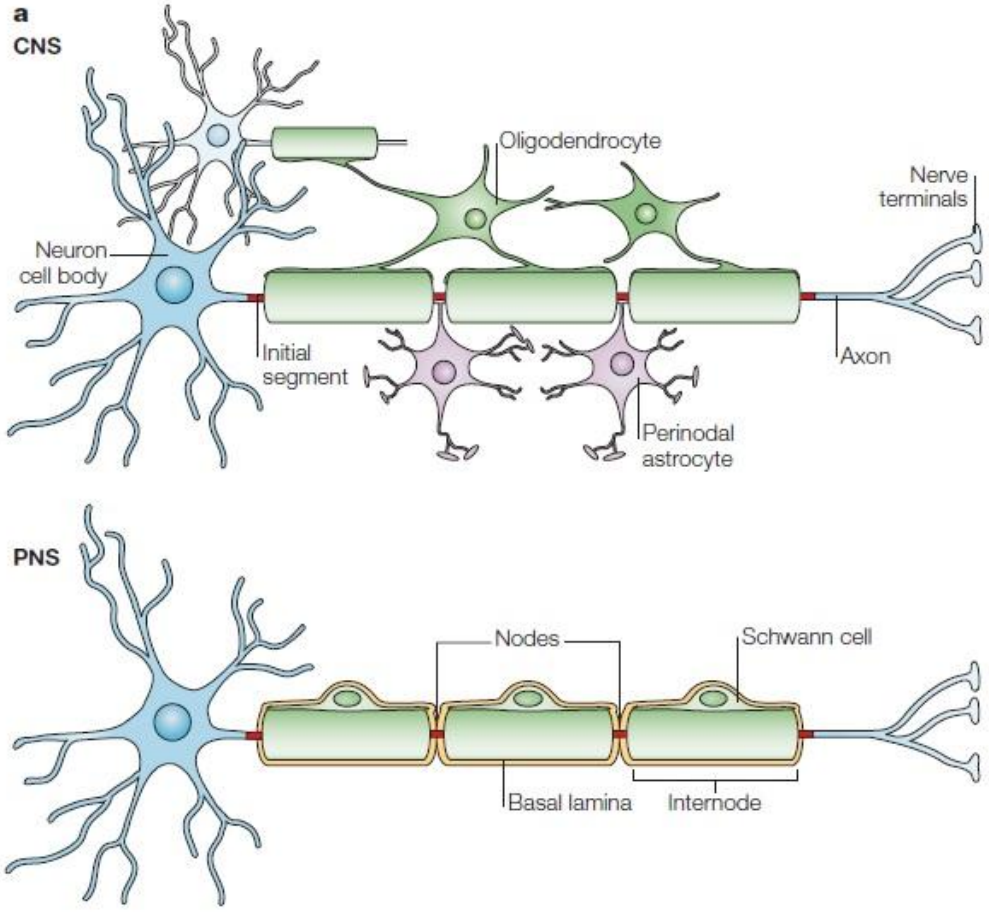

Figure 1: Schematic representation of the structure of myelinated axons. Myelinating glial cells, oligodendrocytes in the CNS and Schwann cells in the PNS, form the myelin sheath by enwrapping their membrane several times around the axon. Myelinated tracts (internodes) are interspersed with gaps, the nodes of Ranvier. Oligodendrocytes can myelinate different axons and several internodes per axon, whereas Schwann cells myelinate a single internode in a single axon (Part of Poliak, S. and E. Peles 2003).

At the electron microscope, in transversal sections, the myelin appears as a spiral extension of a glial plasma membrane (Figure 2A, B) and present a dark zone, called electron-dense "major dense line" (MDL) and a clearer area called "intraperiod line" (IPL) (Figure 2C). Longitudinally, the myelin sheath surrounding each internode can be divided into compact and non-compact myelin. The non-compacted myelin is composed by mesaxons, paranodal loops and Schmidt-Lanterman incisures. The paranodal loops, in particular, are responsible

for myelin anchorage to the axon and the correct structure of the nodes. The Schmidt-Lanterman incisures seem to be the connections between inner and outer compacted myelin (Figure 2D). Finally, Cajal bands are cytoplasmic compartments on the abaxonal surface of SCs, required for the longitudinal extension of the myelinated internode [9-11].

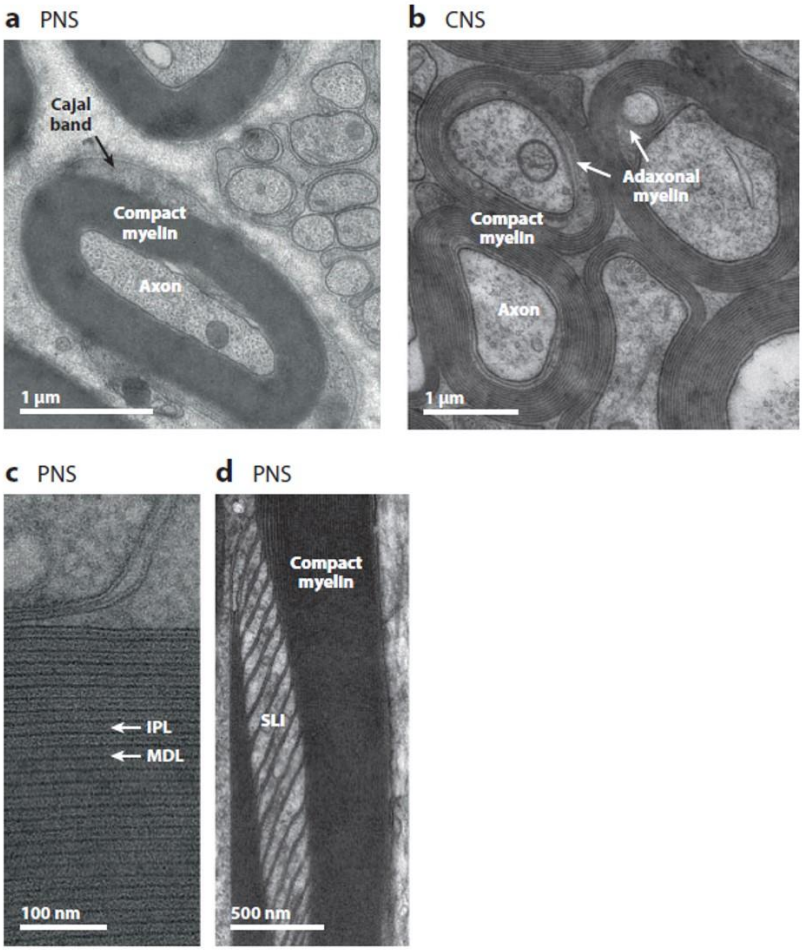

Figure 2: Myelinated axons in PNS and CNS.

A) Electron microscopy of a peripheral sciatic nerve with a myelinating Schwann Cell forming consecutive wrapping around the axon.

B) Electron microscopy of an optic nerve in which oligodendrocyte myelinate multiple axonal segments.

C) Magnification of myelin in which are distinguishable the intraperiod lines (IPL) and the major dense line (MDL).

D) Schmidt-Lanterman incisures provide cytosolic channels through compact peripheral myelin. (Adapted from Nave, K.A. and H.B. Werner 2014).

Furthermore, the Node of Ranvier (Figure 3) is a non-insulated axonal segment that is characterized by a high density (>1200/μm^2) of Na^+ channels that are essential for the generation of the action potential [12]. Nodes of Ranvier have a central role in the conduction of the electric impulse along the axon also because myelin is a very lipid rich compartment, which blocks the passage of water and of soluble ions as Na^+ and K^+. The nerve impulse is a self-regenerating electrical current that travels along the axon due to ion movements. The action potential is first generated in the nerve cell body, then the current moves quickly towards the internode. Along the internode, there is electrotonic spread of depolarization of the axonal membrane [13, 14]. At the next node of Ranvier this depolarization leads to the opening of the sodium channels clustered in the Node of Ranvier, allowing the entrance of positive ions that regenerate the action potential. At the juxtaparanodal level, instead, the exit of the K^+ ions re-polarizes the membrane. The wave generated from the entrance of positive sodium ions in the axon, can again passively diffuse along the internode to the following node of Ranvier, where the action potential is newly re-generated. In this way the "saltatory" conduction of the impulse is generated, as the action potential seems to leap from one node to the next one [15]. In the unmyelinated axons generation of the action potential follows the same process, even if the propagation of the signal is 25-fold slower. The main difference is that in the unmyelinated fibers, sodium channels are not clustered but they are diffused along the axon.

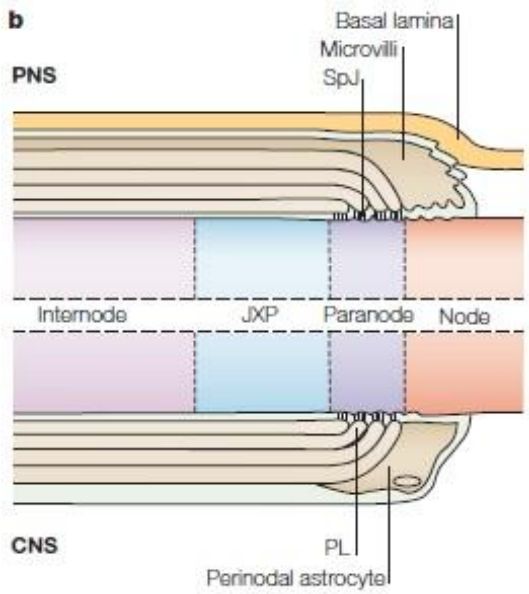

Figure 3: Schematic longitudinal cut of a myelinated fiber around the node of Ranvier. The node is contacted by Schwann cell microvilli in the PNS or by processes from perinodal astrocytes in the CNS. Myelinated fibers in the PNS are surrounded by a basal lamina. The paranodal loops form septate-like junctions (SpJ) with the axon. The juxtaparanodal region, surrounded by compact myelin, is adjacent to the paranode. The internode extends from the juxtaparanodes and is also wrapped by compact myelin (Part of Poliak, S. and E. Peles 2003).

2. MYELIN IN THE PERIPHERAL NERVOUS SYSTEM

2.1 PNS MYELINATION

In vertebrates, SCs originate from a population of multipotent cells derived from the neural crest, a transient group of cells that delaminates from the neural tube during embryonic development [16]. Cells of the neural crest also give rise to other cell types, such as neurons of the sensory, sympathetic and parasympathetic ganglia, chromaffin cells and melanocytes. How the glial lineage originates from the neural crest is still unclear, even if appeared that many crest cells have entered glial lineage at the onset of cell migration. *In vivo* and *in vitro* studies showed the instructive signals that regulate crest diversification: one of these signal seems to be Neuregulin-1 that block the entry to the neuronal lineage [17, 18].

The final goal of SCs development is the formation of myelinating and non-myelinating cells ensheathing large and small diameter axons, respectively. However, this events are preceded by the generation of other two cells types: Schwann cell precursors, which are the glial cells that migrate from neural crest during embryonic (E) day 14-15 in rat (mouse E12-13), and immature Schwann cells, which derive from the proliferation of SC precursor during E15 to E17 in rat (mouse E13-15) until the time of birth. At this point, immature SCs mature and their fate depends on the diameter of the axon they contact: in fact, all mature SCs are potentially able to form myelin by establishing a one to one relationship with axon. However, when mature SCs contact axons with a diameter greater than 1 µm, they form myelin (myelinating Schwann cells), instead, when they contact small calibre axons, they surround them forming Remak boundles (non myelinating Schwann cells) [19] [20] (Figure 4).

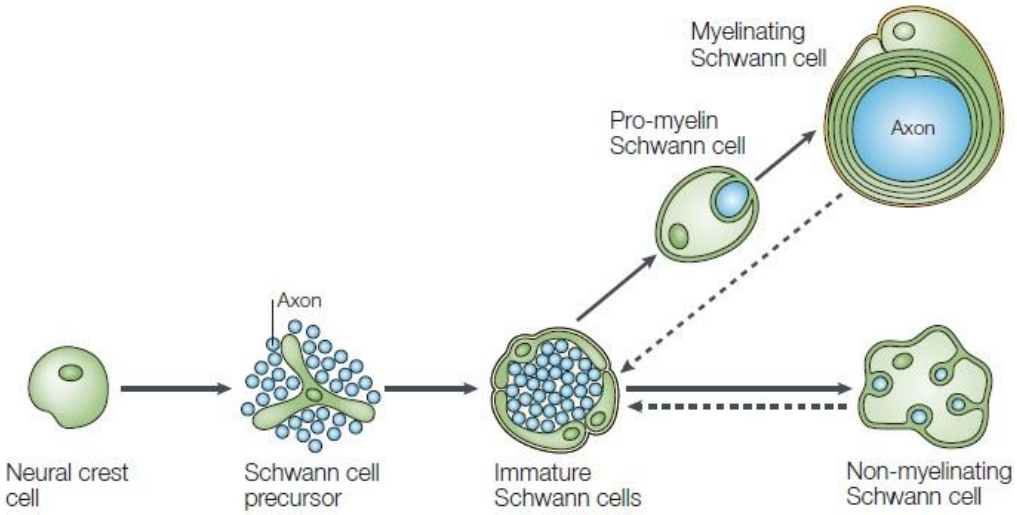

Figure 4: Schwann cell lineage. Schematic representation of the main cell types and developmental transitions occurring during Schwann cell development (Jessen, KR. and Mirsky, R. 2005).

The final nerve morphogenesis is reached also with the contribution of immature SCs that, in a process called radial sorting, separate axon according to diameter; indeed, they signal to perineurial cells and other nerve components to promote their differentiation. Radial sorting is an important process that serves to separate large caliber axons intended to be myelinated, from small caliber axons, which will be part of Remak bundles, and involves different steps: first, axons are grouped in bundles by a "family" of 3-8 immature SCs that deposit a common basal lamina around them; then there is the recognition of large caliber axons, the radial segregation of large axons to the periphery, the defasciculation and establishment of 1:1 relationship between an axon and a promyelinating Schwann cells. The promyelinated SC will differentiate into a myelinating SC, while the SCs in contact with small caliber axons will surround them and differentiate into a non-myelinating SC to form Remak bundles (Figure 5) [21, 22].

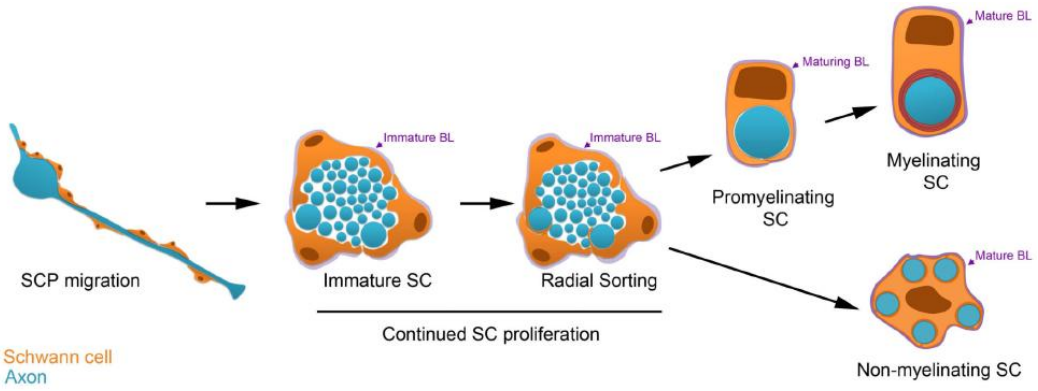

Figure 5: Development of myelinating and non-myelinating Schwann cells. Representation of radial sorting process that separates large diameter axons from small diameter axons (Monk, KR. et al. 2015).

The interaction between axons and glial cells is fundamental for nervous system development. Axonal signals control SC migration, survival and proliferation to guarantee the correct SC-axon match; indeed, axons regulate SC differentiation into myelinating and non-myelinating population [19]. On the other hand, SCs provide trophic support for the development of neurons and control axonal properties [23]. Signals deriving from SCs guide the assembly of multi-protein complexes, such as cell adhesion molecules, ion channels and scaffolding proteins; myelinating SCs regulate the axon cytoskeleton, organelle content and rates of axonal transport [24]. Finally, interaction between axons and SCs has an important role after axonal damage. For example, during Wallerian degeneration axons degenerate distally and, in parallel, distal SCs de-differentiate to an immature stage. At this point, glial cells proliferate and fill the endoneural basal lamina tube (bands of Bungner) required for axonal regeneration. After re-contacting axons, SCs stop proliferating [25, 26].

The regulation of radial sorting and SCs differentiation require extracellular component and signalling pathways that control polarity, cytoskeletal remodelling and proliferation [21, 22, 27, 28]. The main pathway that regulates SC development in the PNS is the NRG1/ErbB2-3 signalling [29-31]. In particular, the axonal NRG1 type III, among all NRG1 isoforms expressed in the PNS, determines the fate of SC differentiation in both myelinating and non-myelinating SCs and regulates myelin thickness [32, 33]. Other important players that regulate

SC myelination are the Notch1 signalling [34], BDNF and NT-3 neurotrophins [35], the Necl family of proteins [36] and GPCR receptors such as GPR126 [37] and GPR44 [38]. Important signalling pathways downstream these molecules are the PI-3 Kinase/AKT/mTOR pathway [39, 40], the ERK/MAPK pathway [41, 42], the cAMP signalling [43] and the Calcineurin/NFAT signalling [44]. Both positive and negative regulators of myelination have been identified [24, 45]. Among positive transcriptional regulators, the transcription factor Sox10 is responsible for precursor SC differentiation, SCs maturation and myelin maintenance during adulthood, together with Krox20/Egr2 [46, 47]. Along with Sox10, the POU domain transcription factors Oct-6 and Brn2 [48] control the expression of Krox20, the master regulator of SC myelination *in vitro* and *in vivo* [49]. Krox20 directly represses negative regulators of PNS myelination, in particular Sox2 and Id2, and activates myelin genes expression in SCs [26, 49].

2.2 MYELIN COMPOSITION

Myelin has a peculiar biochemical composition: ~70-80% of myelin dry-weight is composed by lipids, that guarantee the insulating properties of myelin sheaths; instead, the remaining ~20-30% of myelin dry-weight is constitute by proteins, whose role is to maintain myelin compaction, stability and functionality.

2.2.1 Lipids in PNS myelin

The principal lipid classes, such as neutral lipids, phosphoglycerides and sphingolipids, are present in myelin membranes, even if there are no myelin-specific lipids. Myelin lipids and glycoproteins are synthesized in the Endoplasmic Reticulum (ER) and altered ER homeostasis impairs lipid biogenesis suggesting a tight coordination between the two biosynthetic events [50].

Cholesterol represent 20-30% of the total lipids in PNS myelin. In mouse sciatic nerves, this lipid accumulates throughout the period of neo-myelinogenesis and during the period of myelin maturation; the accumulation of the cholesterol can be explained taking into account the proposed role in stabilization and compaction of the multilamellar myelin membrane [51, 52]. The importance of this lipid is

demonstrated by the fact that mice in which there is a reduction in cholesterol synthesis develop hypomyelination [53].

The other kind of most represented lipids are phospholipids, which account for 40% of the total lipid content. Finally, glycosphingolipids, a subclass of glycolipids, are the most myelin-specific type of lipids and include Galactosylceramide (GalC), which represents 20% of the total dry mass of myelin.

2.2.2 Proteins in PNS myelin

Differently from the lipids, in PNS myelin there is a very specific set of proteins (Table 1 and Figure 6). At least 60% of the proteins are glycoproteins, 20-30% of total proteins have basic properties, while the remaining 10-20% is a dyshomogeneous group of proteins with very low levels of expression such as CNP, PLP and Connexin 32 [2, 15, 54].

Characteristics of peripheral nervous system myelin proteins

	Abundance in myelin (% of total myelin proteins)	Molecular mass (mature protein) (kDa)	Transmembrane domain(s)	Protein localization (compact or non-compact myelin)	Gene localization (human)
Glycoproteins					
P0	50–70%	28	1	Compact	1
PMP22	2–5%	22	4	Compact	17
MAG	1%	100	1	Non-compact	19
Periaxin	5%	170	None	Non-compact	7 (mouse)
E-cadherin	< 0.5	130	1	Non-compact	16
Basic proteins					
MBP	5-15%	14–21.5	None	Compact	18
P2	1–10%	14.8	None	Compact	8
Other proteins					
CNP	< 0.5%	46/48	None	Compact	17
PLP/DM20	< 0.5%	30/25	4	Controversial	X
Cx32	< 0.5%	32	4	Non-compact	X

Table 1: Protein composition of peripheral nerve myelin (Garbay, B. et al. 2000).

The main proteins are:

Myelin Basic Protein (MBP): MBP is expressed in both PNS and CNS. In mouse the gene coding for MBP is composed by seven exons on chromosome 18. The transcriptional regulation of MBP is characterized by an alternative splicing that produces different MBP protein isoforms with diverse molecular weights and developmental regulation [55, 56]. In the PNS four MBP isoforms of 21.5, 18.5, 17 and 14 kDa have been described [57]. MBP accounts for 5-15% of all PNS

myelin proteins and localizes in the major dense line of compact myelin. MBP has an important role in the compaction and maintenance of myelin itself via interactions with the lipids of the membrane; however, MBP is not necessary for the formation of myelin lamella in the PNS [58]. Maybe for these reason, transgenic mice lacking MBP showed minimal signs of PNS myelin alterations [59], while the absence of the protein in the CNS severely impairs myelin compaction [60].

Peripheral Myelin Protein 22kDa (PMP22): PMP22 is a 22 kDa glycoprotein that represent 2-5% of total PNS myelin proteins [61]. The gene encoding for PMP22 is on chromosome 17 in humans and chromosome 11 in mice, and contains six exons. The predicted amino acid sequence of PMP22 defines four transmembrane domains, two extracellular loops (ECL1 and ECL2), a N-terminus into the membrane bilayer and a cytoplasmic C-terminus [62]. The protein is synthesized into the ER and, after synthesis, it undergoes post-translational modifications and folding reactions, such as the N-glycosylation on asparagine 41, an amino acid of the first extracellular loop, before entering the Golgi compartment and being trafficked to the myelin sheath. The turnover of the protein is very rapid, its half-life is about 1 hour and up to 50% of the newly synthesized protein is degraded by the proteasome, while only a small portion can reach the cell surface [63, 64]. PMP22 is localized in the compacted myelin with a dual role of myelin formation and maintenance [65, 66]. The two extracellular loops are thought to be responsible for the adhesiveness of PMP22, while extracellular domains (ECD) were suggested to mediate both homophilic interaction between PMP22 molecules and heterophilic interaction with P0 [67, 68]. However, the protein is ubiquitously expressed also in non-neural tissue, suggesting alternative roles for PMP22 [69].

Expression of PMP22 is strictly regulated. Indeed, misregulation of the protein levels causes neuropathy in both humans and mice [70, 71]. In particular, deletion of the gene causes a HNPP (Hereditary Neuropathy with Pressure Palsy) [61], whereas duplication of the gene causes CMT1A (Charcot-Marie-Tooth 1A) neuropathy [72].

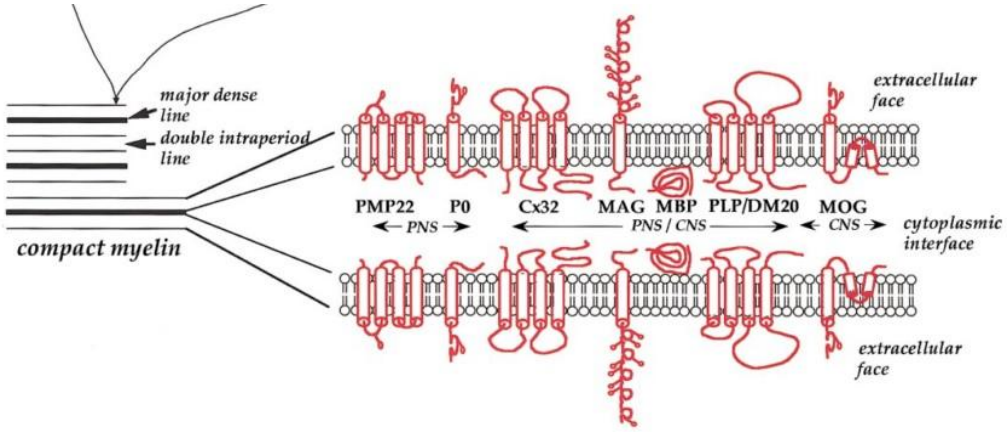

Figure 6: Schematic representation of the most abundant proteins localized in compact myelin of peripheral nerves (Part of Baumann, N. and Pham-Dinh, D. 2001).

3. MYELIN PROTEIN ZERO

Myelin Protein Zero (P0) is the most abundant protein in the PNS. It represents around 20-50% of all the proteins synthesized by SCs [73] and its principal role is to mediate myelin compaction [58].

3.1 THE *MPZ* GENE

P0 protein is encoded by the *MPZ* gene; the gene is located on chromosome 1, in humans and in mice, and is divided into six exons distributed along 7kb of DNA [74-76]. *MPZ* is expressed by SCs mainly during myelination although its expression is detectable also in neural crest cells, in precursor SCs, in immature SCs and in non-myelinating SCs [77]. P0 protein is expressed from the start of myelination, around birth, specifically in myelinating SCs, and the expression reaches the peak between P21 and P28; finally, the level of expression decreases, but remaining still significant during adulthood [78, 79].

The expression of P0 at high levels, and the maintenance of the expression, depend on the contact of SCs with axons [80]. Different factors can regulate *MPZ* expression both *in vitro* and *in vivo*: axons can regulate P0 expression through intracellular stimuli such as cAMP [81], via interaction between cytoskeleton and SC basal lamina [82], via hormone stimulation [83] or via NRG-1 type III [33]; negative regulators have been also detected, such as the treatment with glial growth factor (GGF), tumor growth factor β (FGF β) and fibroblast growth factor

2 (FGF 2) [84, 85]. Finally, Oct6, SOX10 and Krox20 are transcription factors that regulate P0 transcription: Oct6 is expressed highly before myelination [86], Krox20 is expressed mainly in promyelinating and myelinating SCs [87], while SOX10 can activate Krox20 expression and the consecutive *MPZ* expression during myelination [88, 89].

3.2 P0 PROTEIN STRUCTURE AND SYNTHESIS

P0 is a transmembrane glycoprotein that belongs to the Immunoglobulin (Ig)-like superfamily [90]. The protein has a molecular weight of ~29 kDa and the P0 sequence consists of 248 amino acids (aa) that can be divided in three domains: an N-terminal extracellular domain (ECD; aa 30-153), a single transmembrane domain (TMD; aa 154-179) and a C-terminal intracellular cytoplasmic domain (ICD; aa 180-248) (Figure 7) [90-92].

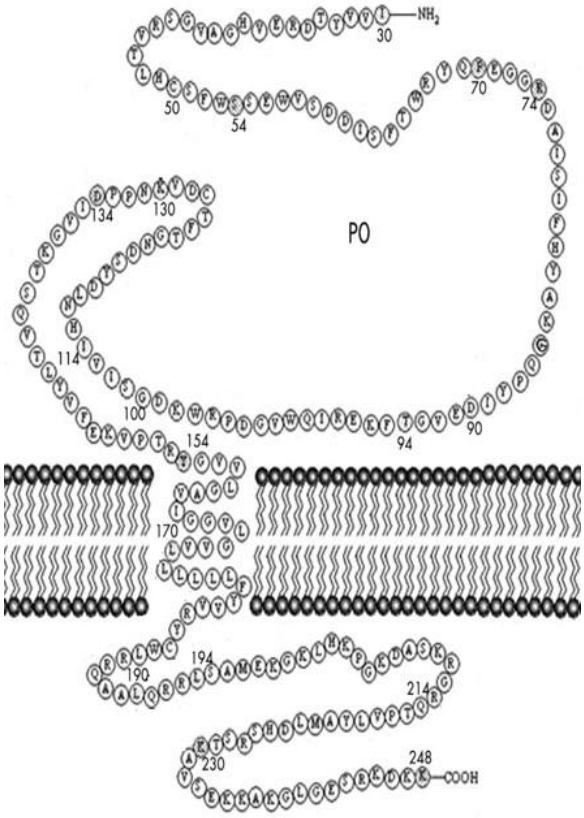

Figure 7: Schematic representation of P0 protein (Adapted from Makowska, A. 2007).

P0 is synthesized by the ribosomes associated to ER membranes, is processed through ER and in the Golgi compartment, is sorted into specific vesicles and transported to myelin sheaths via a microtubule dependent pathway. P0 synthesis and maturation are very rapid, in about 30 min the protein is synthesized and incorporated into the myelin sheaths [93]. The first 29 aa of the extracellular domain encode for the hydrophobic signal peptide that drives the synthesis of P0 through the ER, where the signal peptide is cleaved by ER proteases [90]. The remaining part of the extracellular domain is constituted by ten β-strands organized in two β-sheets; the two β-sheets are linked to each other by the formation of a disulphide bond between Cystein 50 and Cystein 127 [94, 95]. In the extracellular domain is also present the glycosylation sequence Asn122-X-Thr124; analysis of rabbit sciatic nerves revealed that the carbohydrate is N-linked to asparagine 122 and is composed of a single, nine-sugars chain, including one sialyl, one galactosyl, one fucosyl, three mannosyl and three N-acetylglucosamine moieties [96-98]. The ECD contains a sequence that is the more conserved, SDNGT (aa 120-124) that has a role in mediating homophilic P0 interaction; however, crystal structure analysis of P0 indicates that this region is also implicated in the formation of P0 homotetramers *in trans* [94], keeping together adjacent wraps of myelin (Figure 8).

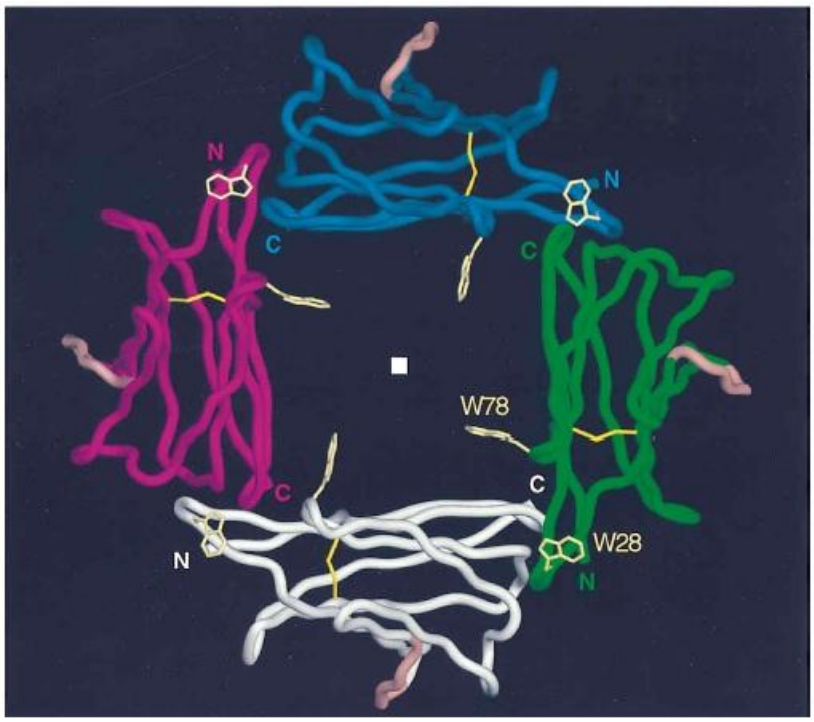

Figure 8: Crystallographic model of putative tetramers formed via interaction of the extracellular domain of P0 (Part of Shapiro, L. 1996).

The transmembrane domain, highly hydrophobic, contains a glycine sequence important for protein dimerization, while the C-terminal cytoplasmic domain is the most basic region of the protein and undergoes acylation at C153 and phosphorylation on several residues [99, 100]. Finally, the cytoplasmic domain contains a sequence YAML (aa 220-223), that targets P0 for microtubular transport to the myelin sheath [99].

3.3 P0 FUNCTION

The principal function of P0 is to mediate compaction of adjacent wraps of myelin, forming the intracellular "major dense line" and extracellular intraperiod line. *In vitro* and *in vivo* studies showed that P0 is essential for normal wrapping, compaction and maintenance of peripheral myelin. Expression of the protein in an ectopic system, like CHO cells, caused adhesion between different cells and the formation of aggregates, supporting the hypothesis that the extracellular domain, which presents homology with members of the immunoglobulin superfamily, plays a role in homophilic interactions [90, 101]. Many data about the role of P0 have been obtained from P0 knock out and P0/+ mice [58, 102, 103]. Peripheral nerves from P0 KO mice are characterized by hypomyelination and myelin uncompaction, with a reduced SC number and increased number of axons without myelin. Nerves of P0 KO mice also presented active demyelination and the formation of "onion bulbs", formed by concentric layers of a SC cytoplasm surrounding the axon but no in contact with it [58]. P0/+ nerves presented a milder phenotype compared to P0 KO, characterized by normal development, but slow demyelination with aging [104].

P0 not only has a structural role in myelin, but is also important for the regulation of myelination: the absence of P0 causes the misregulation of other myelin genes, such as PMP22, whose expression is reduced, and MAG, whose expression is increased [102, 105]. Beside altering myelin gene expression, the absence of P0 caused also the mislocalization of junctions [106], suggesting that P0 can regulate

SCs polarization, junction distribution and gene expression during myelination; indeed, P0 can participate in inside-outside signalling to mediate adhesion.

4. CHARCOT-MARIE-TOOTH DISEASE

Charcot-Marie-Tooth (CMT) disease and related neuropathies represent a heterogeneous group of hereditary disorders, with more than 90 genes associated, many of which have been discovered in the last few years thanks to the next generation sequencing (NGS) technology.

4.1 CLINICAL FEATURES AND CLASSIFICATION OF CMTs

Named after the three physicians who first characterized this disorder in the late 19th century, CMT disease is the most common inherited neurological condition with a prevalence of around 1:2500 [107, 108].

The disease presents common clinical phenotype (Table 2): onset usually occurs in the first two decades of life with a subsequent slow progression over decades. However, late onset mild forms or highly severe early onset CMTs have been reported, the latter known as Dejerine-Scottas syndrome (DSS) or Congenital Hypomyelination (CH), based on different pathological hallmarks. Motor and sensory symptoms gradually affect the leg, producing the typical distal atrophy and sensory loss of the lower limbs, later spreading to the hands. Patients develop skeletal abnormalities, *pes cavus*, distal sensory loss, reduced/absent deep tendon reflexes, distal muscle weakness and atrophy, impaired proprioception, balance difficulty and, in some cases, neuropathic pain [108-110]. Using neurophysiological parameters, CMTs can be divided into two main different groups: a demyelinating form, CMT1, characterized by reduced nerve conduction velocities (<38 m/s) and myelin abnormalities; an axonal form, CMT2, with normal or mildly slowed nerve conduction velocities (>38 m/s) and evidence of axonal degeneration and regeneration (Table 2) [111, 112].

	Inheritance	Phenotype	Mutated genes
CMT1	AD	Usually typical clinical phenotype Uniform and diffuse motor and sensory NCV slowing (<38 m/s in upper-limb motor nerves) Nerve biopsy: onion bulbs or other myelin abnormalities; secondary axonal degenerationabnormalities; secondary axonal degeneration	*PMP22* duplication, *PMP22* point mutations, *MPZ*, *EGR2*, *SIMPLE/LITAF*, *NEFL*
CMT2	AD or AR	Usually typical phenotype Normal or slightly reduced NCV (>38 m/s in upper-limb motor nerves) and decreased amplitudes Nerve biopsy: chronic axonal neuropathy usually without any specific diagnostic featuresneuropathy usually without any specific diagnostic features	*MFN2*, *MPZ*, *NEFL*, *HSPB1* (*HSP27*), *HASB8* (*HSP22*), *RAB7*, *GARS*, *GDAP1* (AD/AR), *LMNA* (AD/AR), *MED25* (AR)
CMTX	X-linked	CMTX1: men more affected than women; motor NCV commonly intermediate in men (30–45 m/s) and in the lower range of CMT2 in women; NCV slowing can be non-uniform and asymmetrical. Nerve biopsy: axonal loss and some demyelination, few onion bulbs; occasional CNS involvement Other CMTX types: only males affected	*GJB1/Cx32*, *PRPS1*
Intermediate CMT	AD	Mild to moderate severity. NCVs intermediate between CMT1 and CMT2 (25–45 m/s). Pathological features of both CMT1 and CMT2	*MPZ*, *DNM2*, *YARS*, (*NEFL*)
CMT3 (HMSN III; DSN-CHN)	AD or AR	Early onset; more severe than CMT1 Very slow NCVs Nerve biopsy: dysmyelination, onion bulbs CHN: congenital onset, extreme severity, hypomyelination	*PMP22*, *MPZ*, *EGR2*, *PRX*
CMT4	AR	Earlier onset and more severe course than CMT1 Vocal cord paresis, sensorineural deafness, and facial and diaphragmatic weakness can occur Slowed NCV (<38 m/s)	*GDAP1*, *MTMR2*, *SBF2/MTMR13*, *KIAA1985/SH3TC2*, *NDRG1*, *EGR2*, *PRX*, *FGD4*, *FIG4*
dHMN	AD or AR X-linked	Pure motor involvement on clinical, electrophysiological, and morphological basis Preserved or mildly slowed NCVs; >38 m/s in upper-limb motor nerves; normal sensory action potential Sural nerve biopsy normal or near-normal	*HSBP1*, *HSBP8*, *GARS*, *BSCL2*, *DCTN1*, (*IGHMBP2*)
CMT5 with pyramidal features (HMSN V)	AD	Pyramidal involvement ranges from increased deep-tendon reflexes with Babinski sign to spastic paraplegia Electrophysiology: usually axonal loss; reduced sensory action potential amplitudes	*MFN2*, *BSCL2*, *GJB1*
CMT6 with optic atrophy (HMSN VI)	AD	Early onset Severe visual loss with optic atrophy NCVs preserved or mildly slowed	*MFN2*

AD=autosomal dominant. AR=autosomal recessive. BSCL2=Berardinelli-Seip congenital lipodystrophy type 2. CHN=congenital hypomyelinating neuropathy. CMT=Charcot–Marie–Tooth disease. CMTX=X-linked CMT. DCTN1=dynactin. dHMN=distal hereditary motor neuronopathy. DNM2=dynamin 2. EGR2=early-growth-response 2. DSN=Déjèrine-Sottas neuropathy. FGD4=FGD1-related F-actin binding protein. FIG4=FIG4 homologue of Saccharomyces cerevisiae. GARS=glycil-tRNA synthetase. GDAP1=ganglioside-induced differentiation-associated protein 1. GJB1/Cx32=gap junction B1/connexin 32. HMSN=hereditary motor and sensory neuropathy. HSPB1/HSP27=heat shock 27-kDa protein 1. HSPB8/HSP22=heat shock 22-kDa protein 8. IGHMBP2=immunoglobulin mu binding protein 2. KIAA1985/SH3TC2=SH3 domain and tetratricopeptide repeat domain 2. LMNA=lamin A/C nuclear envelope protein. MED25=mediator of RNA polymerase II transcription, subunit 25. MFN2=mitofusin 2. MPZ=myelin protein zero. MTMR2=myotubularin-related protein 2. NCV=nerve-conduction velocity. NDRG1=N-myc downstream-regulated gene 1. NEFL=neurofilament light chain. PMP22=peripheral myelin protein 22. PRPS1=phosphoribosylpyrophosphate synthetase 1. PRX=periaxin. RAB7=small GTPase late endosomal protein RAB7. SBF2/MTMR13=set-binding factor 2/myotubularin-related protein 13. SIMPLE/LITAF=small integral membrane protein of lysosome/late endosome; lipopolysaccharide-induced tumour necrosis factor-alpha factor. YARS=tyrosyl-tRNA synthetase.

Table 2: CMT subtypes with their associated phenotype (Adapted from Pareyson, D. 2009).

Is possible to divide the CMTs also based on the mode of inheritance: autosomal dominant demyelinating CMT is indicated as CMT type 1 (CMT1), autosomal dominant axonal CMT is CMT type 2 (CMT2), X-linked CMT is CMTX, and autosomal recessive CMT is CMT type 4 (CMT4). Since the continuous discovery of genes associated with CMT, the new subtypes have been defined by the addition of a letter after the number of a specific type of CMT [113]. CMT is

caused by mutations in genes that encode for different proteins, that are involved in different functions, such as myelin compaction and maintenance or cytoskeleton formation, axonal transport or mitochondrial metabolism [114, 115]. Many studies found that about 90% of patient with CMT had a mutation in one of these gene: *PMP22*, *GJB1*, *MPZ*, *MFN2* or *GDAP1* (Table 3) [116].

The most common CMT type, accounting for ~50% of all CMTs, is CMT1A caused by duplication of 1.4 Mb on chromosome 17p11.2, a region that includes the *PMP22* gene; less commonly, CMT1 is caused by point mutations in *PMP22* or in *MPZ* gene (5% of CMT cases) [117, 118]. CMTX1 is the second most common CMT type (~15-20% of all patients) and is caused by mutation in the *gap-junction B1* (*GJB1*) gene, which encode for Connexin-32 [119]; instead, CMT2 has an heterogeneous genotype without a prevalent gene involved: the most often mutated gene is *Mitofusin 2* (*MFN2*), followed by mutations in *MPZ* and in *Neurofilament Light Chain* (*NEFL*) [120].

	Phenotype	Location and function of gene product
PMP22	CMT1A, DSN, (CHN, HNPP)	Compact myelin protein; myelination, cell growth, differentiation
MPZ/P0	CMT1B, CMT2I/J, DI-CMTD, DSN, CHN	Compact myelin protein; adhesion role
SIMPLE/LITAF	CMT1C	Schwann-cell cytoplasm; stimulator of monocytes and macrophages; causes secretion of tumor necrosis factor-α and other inflammatory mediators; might play a part in protein-degradation pathways
EGR2	CMT1D, CMT4E, DSN, CHN	Schwann cells; transcription factor; activates transcription of several myelin-associated genes; plays a part in peripheral nervous system myelin development and maintenance
NEFL	CMT1F, CMT2E	Cytoskeleton; neurofilament organisation; axonal transport
GJB1/Cx32	CMTX1	Schwann cells, oligodendrocytes; gap-junction-forming protein in non-compact myelin
PRPS1	CMTX5	Ubiquitously expressed in human tissues, including cochlea; mediates biochemical step in purine metabolism and nucleotide biosynthesis; mutation causes reduced enzyme activity
DNM2	DI-CMTB	Family of large GTPases; part of cellular fusion–fission of cellular membrane apparatus
YARS	DI-CMTC	Ubiquitous expression, including brain and spinal cord; concentrated in granular structures in growth cones, branch points and distal neuritis; aminoacil tRNA synthetase, catalyses aminoacylation of tRNAtyr with tyrosine
NFM2	CMT2A, CMT5, CMT6	Mitochondrial outer membrane and endoplasmic reticulum; fusion of mitochondria and endoplasmic reticulum–mitochondria interactions
RAB7	CMT2B	Late endosomes; family of RAS-related GTP-binding proteins; regulator of vesicular transport and membrane trafficking; might have a role in linking vesicles and target membranes to the cytoskeleton
GARS	CMT2D, dHMN V	Ubiquitous expression; aminoacyl tRNA synthetases; protein synthesis
HSPB1 (HSP27)	CMT2F, dHMN	Member of the small heat shock protein family; regulation and maintenance of cytoskeleton; interacts with intermediate filament proteins
HSPB8 (HSP22)	CMT2L, dHMN II	High expression in motor and sensory neurons of spinal cord; member of the small heat shock protein family; interacts with heat shock binding protein 1 ; mutated protein promotes formation of intracellular aggregates
GDAP1	CMT2H/K, AR-CMT2, CMT4A	Expressed in neurons (brain and spinal cord) and Schwann cells; localised in mitochondria; function might be associated with the maintenance of the mitochondrial network
LMNA	CMT2B1	Intermediate filament; structural protein of the nuclear lamina network; gene transcription
MED25	CMT2B2	Subunit of the human activator-recruited cofactor, a family of large transcriptional coactivator complexes related to the yeast mediator; exact physiological function in transcriptional regulation remains obscure
MTMR2	CMT4B1	High levels in neurons, myelinating and non-myelinating Schwann cells; belongs to the myotubularin family; dephosphorylates phosphatidylinositol 3-phosphate and phosphatidylinositol 3,5-bisphosphate
SBF2/MTMR13	CMT4B2	Belongs to the myotubularin family; phosphatase, involved in phosphoinositides metabolism; possibly associated with control of myelination
KIAA1985 (SH3TC2)	CMT4C	Neural tissues, including peripheral nerve; possible role in assembly of protein complexes
NDRG1	CMT4D	Ubiquitous expression, high levels in Schwann cells; possible functions are growth arrest and cell differentiation, and signalling protein shuttling between cytoplasm and nucleus
PRX	CMT4F, DSN	Membrane protein of Schwann cells; interaction between plasma membrane, proteins, and cytoskeleton; maintenance of peripheral nerve myelin
FGD4	CMT4H	Cytoplasm; binds along sides of actin fibres; family of Rho GDP/GTP nucleotide exchange factors; alters Schwann cell shape: induces formation of filopodia and lamellipodia; possible disease mechanism: impaired Rho GTPase signalling
FIG4	CMT4J	Vacuolar membrane localisation; phosphatase, involved in phosphoinositides content and vesicular trafficking
BSCL2	dHMN V, Silver syndrome, CMT2	Seipin, membrane protein of the endoplasmic reticulum, widely expressed in the CNS; involved in RNA transport and glycosylation
DCTN1	dHMN VIIB	Mediates transport along microtubules in peripheral nerves; role in prevention of neurodegeneration
IGHMBP2	dHMN VI (SMARD1)	Widespread tissue distribution; RNA processing

AR=autosomal recessive. BSCL2=Berardinelli-Seip congenital lipodystrophy type 2. CHN=congenital hypomyelinating neuropathy. CMT=Charcot–Marie–Tooth disease. DCTN1=dynactin. dHMN=distal hereditary motor neuronopathy. DI=dominant intermediate. DNM2=dynamin 2. DSN=Déjèrine-Sottas neuropathy. EGR2=early-growth-response 2. FGD4=FGD1-related F-actin binding protein. FIG4=FIG4 homologue of Saccharomyces cerevisiae. GARS=glycil-tRNA synthetase. GDAP1=ganglioside-induced differentiation-associated protein 1. GJB1/Cx32=gap junction B1/connexin 32. HNPP=hereditary neuropathy with liability to pressure palsies. HSPB1/HSP27=heat shock 27-kDa protein 1. HSPB8/ HSP22=heat shock 22-kDa protein 8. IGHMBP2=immunoglobulin mu binding protein 2. KIAA1985/SH3TC2=SH3 domain and tetratricopeptide repeat domain 2. LMNA=lamin A/C nuclear envelope protein. MED25=mediator of RNA polymerase II transcription, subunit 25. MFN2=mitofusin 2. MPZ=myelin protein zero. MTMR2=myotubularin-related protein 2. NDRG1=N-myc downstream-regulated gene 1. NEFL=neurofilament light chain. PMP22=peripheral myelin protein 22. PRPS1=phosphoribosylpyrophosphate synthetase 1. PRX=periaxin. RAB7=small GTPase late endosomal protein RAB7. SBF2/MTMR13=set-binding factor 2/myotubularin-related protein 13. SIMPLE/LITAF=small integral membrane protein of lysosome/late endosome; lipopolysaccharide-induced tumour necrosis factor-alpha factor. SMARD1=spinal muscular atrophy with respiratory distress 1. YARS=tyrosyl-tRNA synthetase.

Table 3: Mutated genes, associated phenotypes, and mutated protein locations and functions in CMT neuropathies (Adapted from Pareyson, D. 2009).

4.2 *MPZ*-RELATED CMTs

Mutations in human *MPZ* gene result mainly in autosomal dominant neuropathies and are estimate to account for ~5% of all CMT cases. Currently, more than 200 different *MPZ* mutations have been identified (http://www.molgen.ua.ac.be/CMTMutations/default.cfm), the majority of which are located in the extracellular domain (Figure 9) [121, 122].

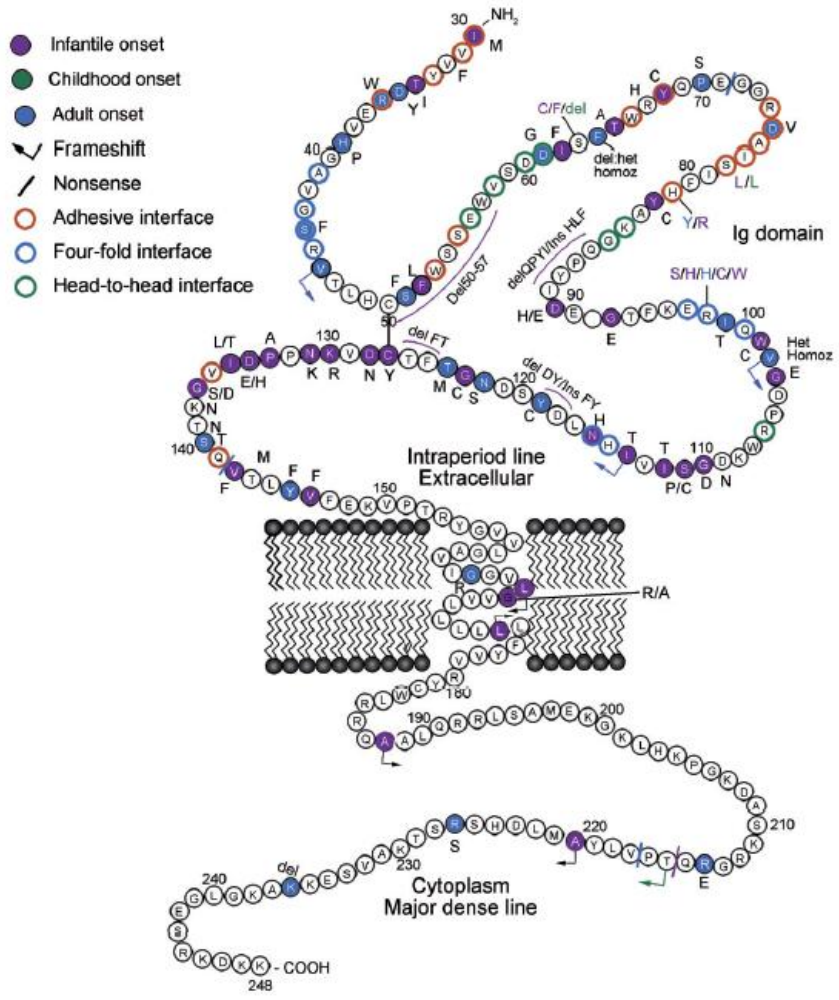

Figure 9: Mutations in the *MPZ* gene associated with inherited neuropathies.
The numbering system for *MPZ* mutations includes the 29 amino acid leader peptide cleaved before insertion in the myelin sheath. Arrows represent frameshift mutations, lines represent nonsense mutation and letters represent aa change. Adhesive interface, 4-fold interface and head-to-head interface refer to amino acid residues deemed essential for adhesion between adjacent myelin wraps (Sanmaneechai, O. 2015).

MPZ mutations can give rise to different phenotypes: an early-onset phenotype, with onset of the disease during the 1st decade of life and characterized by very slow Motor Nerve Conduction Velocity (MNCV), a late-onset phenotype, with onset from the 2nd decades of life and with a normal or minimally impaired MNCV, or a childhood-adolescent-onset, with motor and sensory symptoms during the 2nd decades of life, and showing a slowly progressive course, with MNCV of intermediate range [123]. Collectively *MPZ* related mutations are usually referred as CMT1B. Also the way by which distinct *MPZ* mutations cause different phenotypes is different: mutations that cause infantile phenotype tend to disrupt the developmental process of myelination, while in cases of late-onset disease, myelin sheaths are formed but are slightly impaired and during aging this leads to an axonal degeneration that cause the neuropathy [121]. But why particular mutations cause so different phenotypes is not completely understood. Several *MPZ* mutations cause the mutated protein being retained in the ER instead of being transported to the myelin sheaths; in that way, the protein cannot be properly folded and lead to the activation of the Unfolded Protein Response (UPR). Other proposed pathomechanisms include the disruption of the intracellular adhesion properties [124] and misglycosylation of P0: in this latter case, there can be the loss of native glycosylation site, or the gain of a new glycosylation site [125, 126].

5. GLYCOSYLATION

Glycosylation defines the reaction in which glycans are attached to proteins or lipids. Ten monosaccharides are used in the enzymatic process of glycosylation in mammals: fucose (Fuc), galactose (Gal), glucose (Glc), *N*-acetylgalactosamine (GalNAc), *N*-acetylglucosamine (GlcNAc), glucuronic acid (GlcA), iuduronic acid (IdoA), mannose (Man), sialic acid (SA) and xylose (Xyl) [127]. Glycan structures attached to proteins can be highly complex, due to multiple enzymatic site preferences, as well as the use of stereochemical α or β conjunctions. Structural diversity is mainly produced through the secretory pathway of cells; the glycosylation of proteins and lipids occurs in the ER and Golgi apparatus, with

most of the final processing occurring in the *cis*-, *medial*- and *trans*- Golgi compartment [128]. Protein glycosylation includes:

***N*-glycosylation:** consist of *N*-acetylglucosamine (GlcNAc) attached by a β1-glycosidic linkage to the nitrogen atom of the amino group of Asn (*N*) at the consensus glycosylation motif Asn-X-Ser/Thr (in which X denotes any amino acid except for Pro).

***O*-glycosylation:** glycans are attached to the oxygen atom of the hydroxyl groups of Ser (S) or Thr (T) residues. *O*-glycans can be further subclassified on the basis of the initial sugar attached to the protein and the additional sugar structures added to the initial glycan.

Glycosaminoglycans (frequently termed proteoglycans)**:** represent a major class of glycoproteins that are defined by long glycosaminoglycan (GAG) chains attached to proteins through a tetrasaccharide core consisting of glucuronic acid (GlcA)–galactose (Gal)–Gal–xylose (Xyl); this carbohydrate core is attached to the hydroxyl group of Ser at Ser-Gly-X-Gly amino acid motifs.

C-mannosylation: glycans are attached through C-C linkage to the C2 position of Trp in the sequence W–X–X–W (W indicates tryptophan; X is any amino acid).

Glypiation: glycosylphosphatidylinositol (GPI)-anchored glycoproteins represent another major class of glycoconjugates. These glycoproteins are linked at the carboxyl terminus through a phosphodiester linkage to phosphoethanolamine attached to a trimannosyl-nonacetylated glucosamine (Man3-GlcN) core; the GlcN residue is linked to phosphatidylinositol, which is embedded in the cell membrane.

The addiction of sugar to lipids formed glycolipids and, between this types of glycoconjugates, there are glycosphingolipids (Figure 10) [127-130].

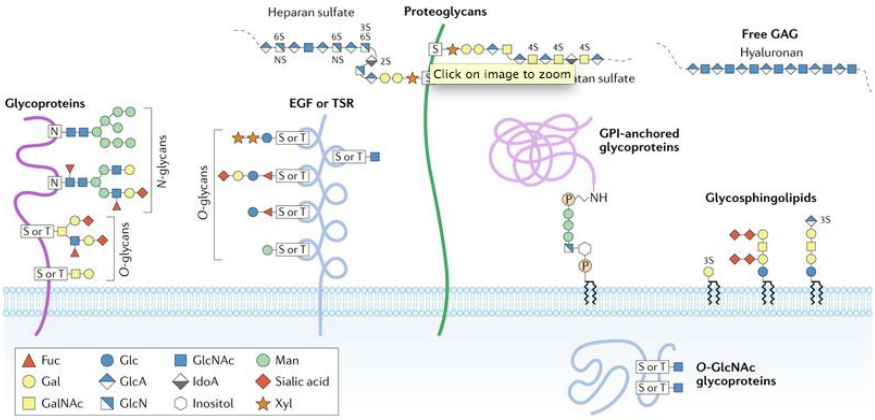

Figure 10: Major types of glycosylation in humans.

Glycans can be covalently attached to proteins and lipids to form glycoconjugates. Glycoproteins consist of glycans and glycan chains linked to nitrogen and oxygen atoms of amino acid residues and are thus termed *N*-glycans and *O*-glycans, respectively. Other two major class of glycoproteins are proteoglycans and glycosylphosphatidylinositol (GPI)-anchored glycoproteins. Finally, glycosphingolipids are a class of glycoconjugates in which glycans are attached to cellular membrane lipids (Reily, C. 2019).

Glycan moieties participate in multiple mechanisms: glycans associated with cell surface receptors and proteins directly modulate protein function and signalling, alter the dynamics of glycoprotein endocytosis and cell surface half-life by binding to multivalent lectins. Glycans structure is also fundamental for protein secretion and folding, contribute to quality control surveillance in the ER and mediate transit and selective protein targeting throughout the secretary pathway. In general, principal functions of glycans are the regulation of cytosolic and nuclear functions, immune surveillance, inflammatory reactions, autoimmunity, hormone action and tumor metastasis, cell adhesion and receptor activation [131, 132].

5.1 *N*-GLYCOSYLATION

N-glycosylation comprises an assembly part and a processing part that are extended over three cellular compartments: the cytosol, the ER and the Golgi. The biosynthesis of the oligosaccharide initiates at the cytoplasmic side of the ER

membrane with the transfer of *N*-acetylglucosamine (GlcNAc) phosphate from UDP-GlcNAc to membrane-bound carrier dolichyl monophosphate (Dol-P), forming GlcNAc-pyrophosphatedolichol (GlcNac-PP-Dol). Subsequently, one GlcNAc and five mannose (Man) residues are attached to this dolichol-linked monosaccharide; the lipid-linked $Man_5GlcNac_2$ is translocated across the ER membrane and is elongated at the lumen side by attachment of others four mannose and three glucose residues. The completed $Glc_3Man_9GlcNAc_2$ oligosaccharide is then transferred to specific asparagine residues of nascent proteins by the oligosaccharyl-transferase complex. The asparagine residues are specified by the consensus sequence N-X-S/T. The processing part of the *N*-glycosylation starts in the ER, where glucose residues are removed as part of quality-control process; the structure than moves to the *cis*-Golgi, where the carbohydrate structures are further trimmed by a series of specific mannosidases before being transferred to *medial*-Golgi for maturation. It is within the *medial*- and *trans*-Golgi compartment that *N*-glycans are produced through the addition of GlcNAc, galactose, sialic acid and fucose sugars (Figure 11) [128, 133-135].

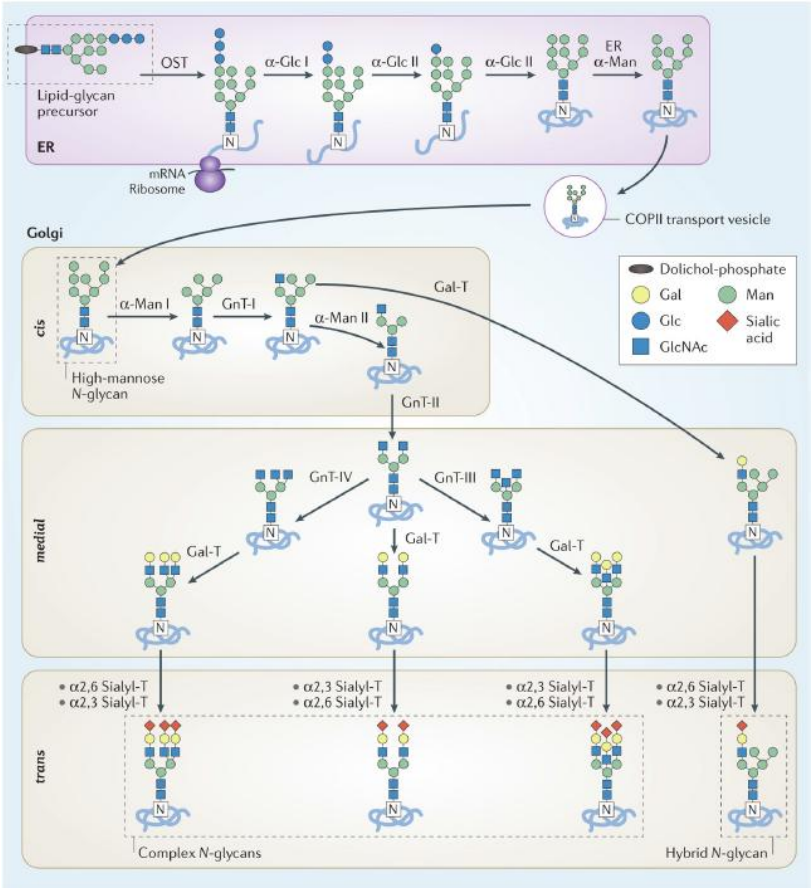

Figure 11: *N*-glycan biosynthesis in the secretory pathway.

N-glycan synthesis is initiated in the ER by the transfer of a lipid-glycan precursor to an asparagine. After a quality-control checkpoint, the glycoprotein moves to the Golgi apparatus for additional trimming and further glycan modifications. The expression levels of glycosyltransferases, the accessibility of the glycoprotein glycosylation sites and the length of time during which the glycoprotein remains in the ER and Golgi apparatus all affect the final site-specific *N*-glycan composition (Reily, C. 2019).

5.2 DEFECTS IN GLYCOSYLATION

Genetic defects in glycosylation are often embryonic lethal, underlying the vital role of glycans [136, 137]. The disorders of glycosylation are classified in type I, when the disorder is caused by abnormalities in the formation of the oligosaccharide structure on the glycolipid precursor before the attachment to the Asp residue of the protein, or type II, if the defects are in the control of the *N*-linked branching structure of the nascent glycoprotein [138]. As reported in Online Mendelian Inheritance in Man [OMIM] (http://www.ncbi.nlm.nih.gov/entrez/query.fcgi?db=OMIM), disorders of glycosylation include at least 21 disorders of protein *N*-glycosylation, 12 disorders of *O*-glycosylation and two disorders of the glycolipid synthesis pathway [139]. The mutated genes encode enzymes involved in glycosylation, either in the cytosol or in the secretory pathway. Other pathogenic mutations have been described that lead to a loss- or gain- of glycosylation of specific proteins encoded by the mutated genes, indicating the importance of glycosylation in human physiology [140-145].

In the Human Gene Mutation Database (HGMD) are reported a total of 20667 pathogenic missense mutation affecting 1325 genes; between these genes, 577 encodes proteins that are predicted to enter the ER and that are therefore likely to be exposed to the *N*-glycosylation machinery, while the remaining 748 genes encode proteins that are not predicted to enter the secretory pathway (the prediction if the proteins enter the secretory pathway or not is based on *in silico* identification of a signal peptide with a cleavage site or a signal anchor without a cleavage site, or the lack of signal peptide). Vogt and colleagues searched in HGMD for potential gain- or loss- of glycosylation missense mutations and,

among 577 genes encoding for proteins that migrate through the secretory pathway, they founded that up to 77 (~13,3%) may be subjected to potential gain of glycosylation (corresponding to ~1,4% of pathogenic missense mutations found in the 577 genes), indicating that this kind of mutations are more frequent that expected. Conversely, the loss of glycosylation sites was both less frequent and usually less severe, suggesting that the introduction of a new glycan might have a more disruptive effect on protein function than the loss of a glycan (Table 4) [98, 146, 147].

	Total missense mutations			Predicted gain-of-glycosylation missense mutations (%)			Predicted loss-of-glycosylation missense mutations (%)		
	1,325	577	748	1,325	577	748	1,325	577	748
Documented in HGMD	20,667	10,047	10,620	246 (1.19%)	142 (1.41%)	104 (0.98%)	164 (0.79%)	82 (0.82%)	82 (0.77%)
Possible *in silico*	5,949,671	2,418,935	3,530,736	45,299 (0.76%)	17,410 (0.72%)	27,889 (0.79%)	94,194 (1.58%)	47,430 (1.95%)	46,764 (1.32%)
P value	–	–	–	7×10^{-12}	8×10^{-16}	0.04	4×10^{-20}	9×10^{-17}	5×10^{-7}

Table 4: Predicted gain and losses of consensus *N*-glycosylation site associated with missense mutations in the HGMD. A total of 20667 pathogenic missense mutations affecting 1325 genes have been logged in the HGMD. Of these genes, 577 encode proteins that are predicted to be exposed to the *N*-glycosylation machinery; the remaining 748 genes encode proteins that are not predicted to enter the secretory pathway. The numbers of documented pathogenic missense mutations, including those that lead to a potential gain or loss of *N*-glycosylation (based on the creation or removal of a consensus site for *N*-glycosylation), with the corresponding total number of possible missense mutations (created *in silico*) for each of these three groups are compared (Vogt, G. 2005).

P0 protein has a single glycosylation site in position 122 where there is present the sequence Asp122-X-Thr124; during post-translational modification, the carbohydrate is *N*-glycosidically linked to asparagine 122. For that reason, also the P0 protein is subjected to mutations that cause the gain- or the loss- of glycosylation. Different mutations in P0 protein causing loss of glycosylation have been reported: the substitution $N^{122}\rightarrow S$ generate the sequence S^{122}-X-T^{124} that lead to the loss of the glycosylation site, resulting in a late-onset neuropathy [148]. The very common mutation $T^{124}\rightarrow M$, that lead to the loss of glycosylation site, is associated with a late-onset axonal neuropathy with sensory involvement [149]. Other mutations involving the threonine in position 124 include $T^{124}\rightarrow K$

[150] and T^{124}→A [151] have been reported and both of them correspond to unglycosylated proteins. Interestingly, also mutations causing gain of glycosylation have been reported: the mutation D^{61}→N resulted in a hyperglycosylated form of P0, causing an early-onset demyelinating neuropathy [126, 152]. Analyzing the Inherited Peripheral Nervous System Mutation Database, there are other three P0 mutations such as D^{109}→N [153], D^{118}→N [154] and K^{138}→N [155] that potentially introduce a new glycosylation sequon, even if the gain of glycosylation was not further studied. Also for P0 mutations, most mutations causing a loss of glycosylation are associated with a late-onset phenotype, whereas the majority of mutations associated with a gain of glycosylation, cause a severe, early-onset neuropathy, supporting the idea that loose a glycosylation site is less important than acquiring one.

6. CLINICAL CASES OF PATIENTS WITH D^{61}→N MUTATION

Literature reports two distinct patients affected by CMT1B that present the amino acidic substitution D^{61}→N that introduces a new glycosylation site in the P0 protein [126, 152].

Case 1 [126]

The patient is a 46-year-old Italian woman, with no family history of neuromuscular disease. She did not begin walking until two years of age. In the childhood, she fell frequently and was severely impaired in running and climbing. During her second decade she developed prominent wasting and weakness of both hands and legs. Because of severe *pes equinovarus* she underwent surgery at 24 years of age. On neurological examination she presented bilateral claw hand deformity and foot drop, with moderate proximal wasting and weakness (4/5 MRC) of the lower limbs. Vibration sense was decreased at the lower limbs. Deep tendon reflexes were diffusely absent and a stepping gait was observed. Both motor and sensory action potentials were unrecordable. A sural nerve biopsy, performed when she was 20 years old, showed a severe loss of myelinated fibers with some residual fibers containing myelin outfoldings (Figure 12).

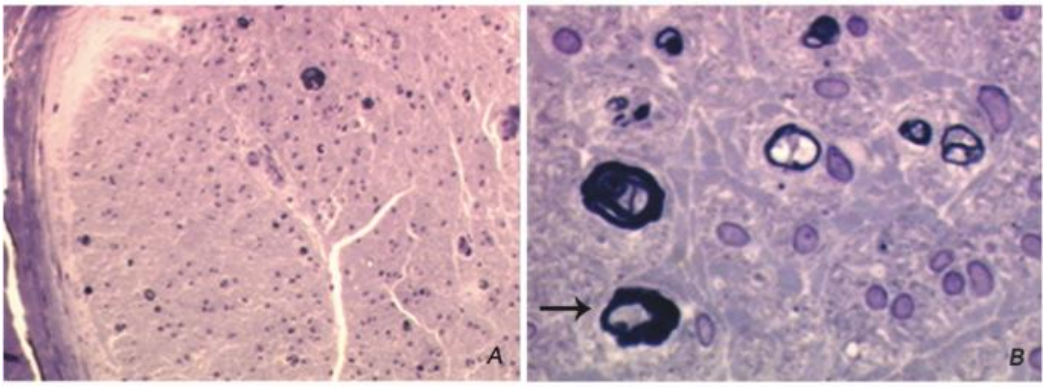

Figure 12: Images of the sural nerve biopsy from the patient of the case 1.
Sural nerve biopsy of the patient carrying the *MPZ* mutation D61N.
A) Toluidine Blue, 25X.
B) Toluidine Blue, 100X. A severe loss of myelinated fibers can be observed, with some residual fibers containing myelin outfoldings (thin arrow) (Prada, V. 2012).

Case 2 [152]

A boy aged 2 years and 11 months was evaluated for gross motor delay and generalized hypotonia. No family history of neuromuscular disease was reported. He sat independently at age 8 months, but was unable to stand with support at 12 months of age. He began crawling at age 15 months, and walked independently at age 2 years and 3 months. He was alert and bright, but his face appeared myopathic. Physical examination revealed a mildly high-arched palate, but neither thenar plus hypothenar atrophy nor *pes cavus*. A cranial nerve examination revealed normal ocular movements and pupillary responses to light. Mild facial muscle weakness was evident. Tongue fasciculations were absent. He was hypotonic, but his muscle strength was only mildly reduced in the four extremities. Hyperextension was observed in the finger, wrist, and knee joints. His muscle bulk was normal. Deep tendon reflexes were absent at the biceps, triceps, patella, and ankles. No sensory disturbance was evident. He was able to stand up from a supine position using a modified Gowers maneuver. His gait, with bilateral genu recurvatum, was wide-based and ataxic. Cranial magnetic resonance imaging indicated no intracranial abnormalities. A nerve conduction study revealed very prolonged distal latencies, markedly reduced motor conduction velocities (3.0-4.0 m/second), and the temporal dispersion of compound muscle action potentials

from his upper and lower extremities. To evoke motor nerve responses, electrical stimuli greater than 50 mA were necessary. Sensory responses were not evoked. Magnetic resonance imaging of the lumbar plexus demonstrated no enlarged nerve roots. A sural nerve biopsy revealed a severe loss of large myelinated fibers in all fascicles. Well-organized onion-bulb formations were not evident. No inflammatory infiltrates, edema, or storage materials were observed. Intramuscular nerves rarely included large myelinated fibers. A teased fiber analysis demonstrated thin, myelinated segments and tomacula-like structures. Electron microscopic examination revealed occasional onion- bulb formations consisting of multilayered empty basal lamina. Occasional fibers with thin or abnormally compacted myelin were also observed. Unmyelinated fibers were well preserved (Figure 13).

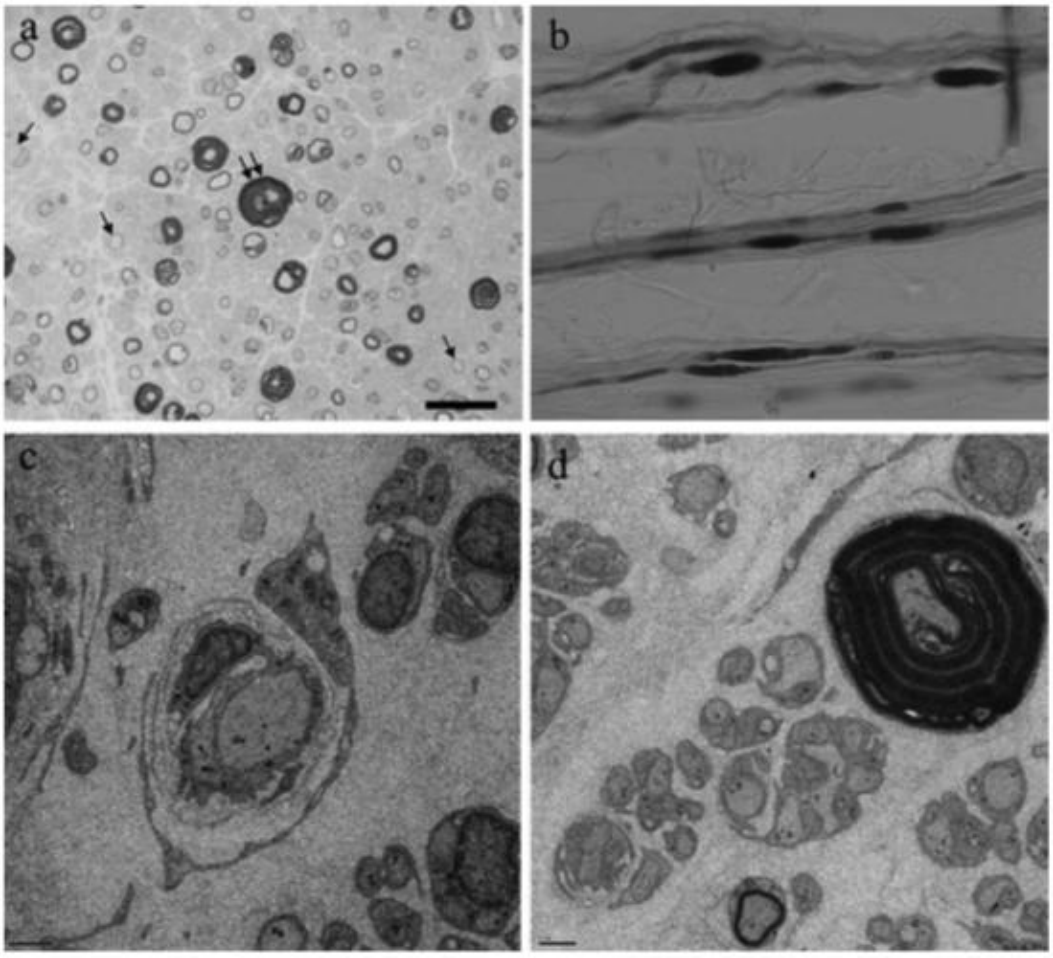

Figure 13: Images of the sural nerve biopsy from the patient of the case 2.

A) Epoxy-embedded and toluidine blue-stained semithin section of the sural nerve reveals the endoneurium, including nonmyelinated (arrows), hypomyelinated, and hypermyelinated (double arrows) fibers. Bar, 20 mm.

B) Teased fiber analysis demonstrates thin, myelinated segments and tomacula- like structures. A lack of myelination is evident in the nerves.

C) Electron microscopy reveals an absence of myelin and onion-bulb formations consisting of multilayered empty basal lamina. Bar, 2 mm.

D) Electron microscopy indicates abnormally compacted myelin. Bar, 2 mm (Yonekawa, T. 2013).

AIM OF THE PROJECT

The aim of this project was to investigate how peripheral myelination is affected by P0 misglycosylation. We used two different strategies:

1) Characterize, in different *in vitro* models, the effects of P0 mutants causing gain- or loss- of glycosylation. In particular, we evaluated if the mutations predicted to cause a gain- or loss- of glycosylation corresponded to hyper or unglycosylated P0 mutants and if this mutations were able to interfere with the sorting to the cell membrane and with the adhesive function of P0. Indeed, since a group of molecules, defined imino-sugars, might complement hyperglycosylation, we decided to evaluate if NB-DNJ (Miglustat), a molecule belonging to this group of compound, was able to rescue *in vitro* the effects of one mutation causing hyperglycosylation.

2) Establish a murine model of MPZ^{D61N} mutation to evaluate *in vivo* the effects of hyperglycosylation. We evaluated if the "knock in" mouse model carrying the amino acidic substitution $D^{61}\rightarrow N$ developed a demyelinating neuropathy, providing a model of CMT1B due to hyperglycosylation of P0; finally, we obtained from WT and MPZ^{D61N} mice a model of *ex-vivo* myelination to dissect axonal-glia interplay and to test imino-sugars as potential therapies for hyperglycosylation.

The importance of this study is due to the fact that, while peripheral myelin is largely composed by glycoproteins, misglycosylation has never been investigated as a cause of peripheral neuropathies. Misglycosylation is a novel pathomechanism that may occur in P0 related neuropathies which deserves a complete characterization. To our knowledge the MPZ^{D61N} mouse model is the first transgenic mouse expressing a gain-of-glycosylation mutant, with relevant implications for other diseases caused by hyperglycosylation such as rare mutations causing Cystic Fibrosis, different immunodeficiencies [146] and myoclonus-dystonia, due to a gain-of-glycosylation mutation in ε-sarcoglycan [156].

MATERIALS AND METHODS

Plasmids generation and site-directed mutagenesis

The full-length human cDNA of wild-type *MPZ* gene has been cloned into the expression vector for mammalian cells pEGFP–N1 (Figure 1) as previously described [125].

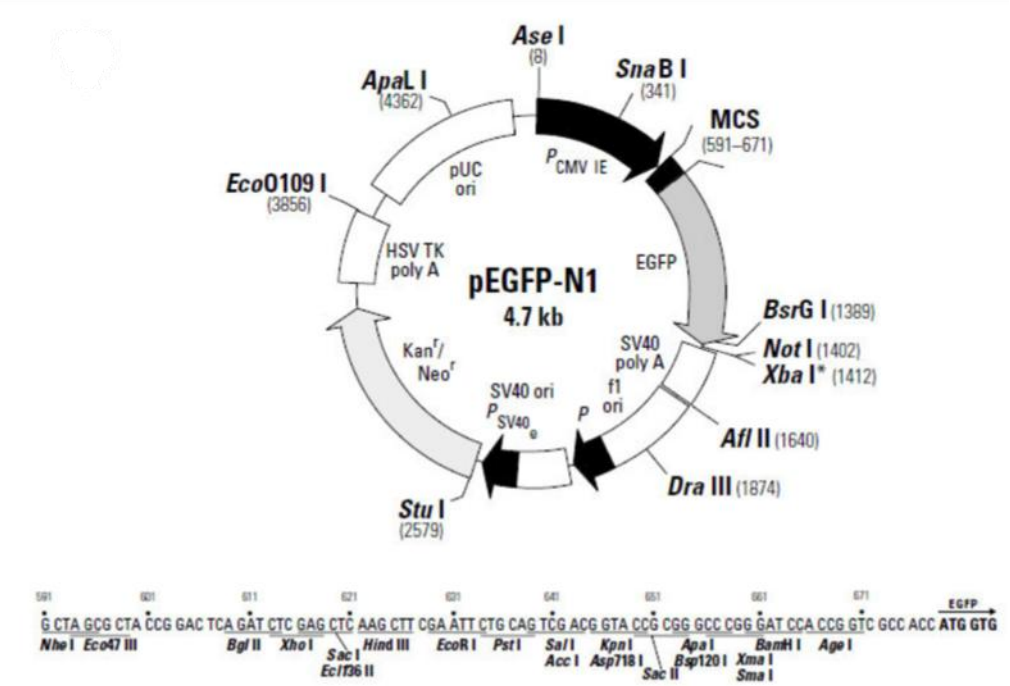

Figure 1: Schematic representation of the pEGFP-N1 expression vector with detail of the multiple Cloning Site (MCS). P0wt and selected mutations were cloned using EcoRI and BamHI restriction enzymes.

Through site-directed mutagenesis (QuikChange II XL Site-Directed Mutagenesis Kit, Stratagene), different plasmids coding for all the mutations in fusion with EGFP vector (pEGFP from Clonetech) have been generated, using specific primers containing the nucleotide changes (Table 1), according to manufacturer's protocol. The mutated cDNAs were amplified by PCR using primers containing restriction enzyme sites for EcoRI and BamHI, and then fused in-frame into the expression vectors for mammalian cells pEGFP–N1 (Clontech, Mountain View).

Mutation	Position	Primers Sequence
D61N	g181a_	5'-aggtgaaggagatgttatctgagacccactcact-3' 5'-agtgagtgggtctcagataacatctccttcacct-3'
D61N+N122A	g181a_ a364g_a365c_	5'-gtcacaagtgaacgtgccagcgtcactgtagtctaggttg-3' 5'-caacctagactacagtgacgctggcacgttcacttgtgac-3'
D109N	g325a_	5'-tgacaatggagccattcttccagcgagggtc-3' 5'-gaccctcgctggaagaatggctccattgtca-3'
D109N+N122A	g325a_ a364g_a365c_	5'-gtcacaagtgaacgtgccagcgtcactgtagtctaggttg-3' 5'-caacctagactacagtgacgctggcacgttcacttgtgac-3'
D118N	g352a_	5'-gccattgtcactgtagtttaggttgtgtatgacaatgg-3' 5'-ccattgtcatacacaacctaaactacagtgacaatggc-3'
D118N+N122A	g352a_ a364g_a365c_	5'-gtcacaagtgaacgtgccagcgtcactgtagtctaggttg-3' 5'-caacctagactacagtgacgctggcacgttcacttgtgac-3'
K138N	g414t_	5'-gtgacctgagaggtattgcccactatgtctgga-3' 5'-tccagacatagtgggcaatacctctcaggtcac-3'
K138N+N122A	g414t_ a364g_a365c_	5'-gtcacaagtgaacgtgccagcgtcactgtagtctaggttg-3' 5'-caacctagactacagtgacgctggcacgttcacttgtgac-3'
T124M	c371t_	5'-tgacgtcacaagtgaacatgccattgtcactgtag-3' 5'-ctacagtgacaatggcatgttcacttgtgacgtca-3'
T124A	a370g_	5'-gacgtcacaagtgaacgcgccattgtcactgtagt-3' 5'-actacagtgacaatggcgcgttcacttgtgacgtc-3'
T124K	c371a_	5'-ctacagtgacaatggcaagttcacttgtgacgtca-3' 5'-tgacgtcacaagtgaacttgccattgtcactgtag-3'
N122S	a365g_	5'-gtgaacgtgccactgtcactgtagtctaggttgtgt-3' 5'-acacaacctagactacagtgacagtggcacgttcac-3'

Table 1: List of mutations that have been cloned in pEGFP-N1 vector; the position of the mutation and sequence of the primers are reported.

Cellular cultures

HeLa cell and Schwannoma *RT4*-D6P2T lines were maintained in Dulbecco's Modified Eagle's Medium (Gibco, Invitrogen) supplemented with 10% fetal bovine serum, 2 mM L-glutamine and 1% penicillin/ streptomycin at 37°C, in a humidified incubator with 5% CO_2.

Transient transfection and protein localization

HeLa and Schwannoma cells were transiently transfected with each mutant-EGFP construct, by single transfection using Lipofectamine 2000 according to manufacturer's protocol (Invitrogen).

To study the expression of P0wt and its mutations on the cell surface, HeLa and Schwannoma cells were transfected with both P0wt and mutated P0 linked to EGFP, allowed to grow for 24 hours in a chamber slide (Nalge Nunc International), washed with PBS and fixed in 4% paraformaldehyde for 10 minutes, washed and mounted.

Biotinylation and endocytic assay

Transiently transfected cells (P0wt-EGFP and mutants-EGFP) were subjected to two washings with cold PBS, containing calcium and magnesium at a concentration of 1 mM of $MgCl_2$ and 0.1 mM of $CaCl_2$ (PBS Ca/Mg) and then were treated with sulfosuccinimide-NHS-biotin (1.5 mg/ml; Pierce, Rockford) in PBS Ca/Mg at 4°C for 1 h. Biotinylating reagents were removed by washing with PBS Ca/Mg twice and by further quenching with 100 mM glycine for 30 min. Cells were then lysed with RIPA buffer (50 mM Tris pH 7.4, 150 mM NaCl, 1 mM EDTA, 0,1% SDS, 1% Triton X-100, 0,5% sodium deoxycholate and Protease Inhibitor (4693132001, Sigma)). After a centrifuge of 45 min at 4°C, supernatants were incubated with streptavidin magnetic beads (2 mg of beads/500 ml of supernatant; New England Biolabs) for 1 h at RT. Beads were washed three times with RIPA buffer, and adsorbed proteins were eluted with 100 μl of Laemmli loading buffer for 5 min at 95°C. Equal amounts of proteins were separated by SDS-PAGE and immunoblotted with anti-EGFP antibody and with HRP-conjugated secondary antibody. Immunoreactive bands were visualized by ECL on hypersensitive ECL film (Amersham, GE Healthcare). Trafficking was evaluated also with endocytic assay [157]: after the treatment with sulfosuccinimido-NHS-biotin, cells were incubated at 37°C for 5 min to induce endocytosis and then tranfered at 4°C to stop the reaction. With the addition of L-glutathione (GSH solution) (50 mM GSH, 75 mM NaCl, 1 mM $MgCl_2$, 0.1 mM $CaCl_2$, 80 mM NaOH, 10% FBS) at 4°C for 15 min (repeated three times) disulfide bond in biotin covalently attached to plasma membrane proteins have

been reduced. Following those treatments, cells have been lysed, biotinylated proteins have been isolated by streptavidin, eluted into SDS sample buffer and separated by SDS-PAGE.

Adhesion test

After 24h from transient transfection, HeLa cells were washed with PBS and incubated with Cell Dissociation Buffer (Invitrogen, San Giuliano Milanese, MI, Italy), for 3 min at RT, counted in Bürker chambers and resuspended to a final concentration of $1.5x10^6$ cells/ml in DMEM containing 10% FBS and 25 mM of Hepes (Sigma) to maintain the cellular pH. By three passages through an 18-gauge syringe, we obtained a single cell suspension. Suspensions, containing a minimum of 95% single cells, were allowed to aggregate at 37°C with gentle rocking at 5 rpm. After 3 h, the tubes were gently inverted and aliquots of 10 µl were removed, put on a microscope slide without using fixatives and immediately examined under the microscope (Olympus AX60). From each slide, 30 frames, randomly selected at 20X magnification, were digitalized and stored, using the Pro Plus Imaging System (Immagini e Computer). The area of cellular aggregates (>4 cells) were measured with Pro Plus Imaging System (Immagini e Computer) and the average area of aggregates formed by HeLa cells transfected with each mutant was calculated and normalized to the average area of aggregates produced by cells expressing P0wt.

Animals

All experiments involving animals were performed in accordance with Italian national regulations and in accord with experimental protocols approved by the San Raffaele Scientific Institute Animal Care and Use Committees.

MPZ^{D61N} mice were generated by Core Facilities for Conditional Mutagenesis (CFCM) using the CRISPR/Cas9 technology. The CRISPR/Cas9 system used for gene editing takes advantage of a guide RNA that detects the specific sequence in the genome and the Cas9 enzyme that binds to the single guide RNA and cleaves the DNA at the target site. In the case where a specific mutation is to be introduced at the cut site, a repair template DNA carrying the mutation is also

needed. The CRISPR/Cas9 components can be introduced into one-cell staged mouse embryo to generate offspring that contains the desired knock-in mutation. The process involves four steps: designing of CRISPR targets; synthesis and purification of RNA and DNA components; isolation of one-cell staged mouse embryos, micro-injection of CRISPR/Cas9 components and transfer of injected embryos into pseudopregnant mice; genotyping of offspring to identify the mutation [158]. The generation of the *MPZ*^{D61N} mouse model was performed in collaboration with Sigma-Aldrich that designed molecular component.

The donor oligo contains:

1. G>A snp conversion that introduce the desired mutation;
2. A>G snp conversion that is necessary to prevent gRNA binding and re-cleavage possibility;
3. A>T snp conversion that eliminates the DdeI restriction enzyme site.

For genotyping, genomic DNA was extracted from tail biopsies. All PCR products were stained with SYBR Safe DNA Gel Stain (Invitrogen), run in 3% agarose gels and detected with UVP GelDOC-It Imaging System.

D61N PCR primers:

D61N sense: 5’ TGCTCTCTCCAGCCCTGG 3’

D61N antisense: 5’ GGAGCCATCCTTCCAGCGA 3’

PCR program:

95°C 10’

95°C 30’’
60°C 30’’ } 30 cycles
72°C 1’

72°C 10’

4°C

Digestion program:

37°C 30’

Expected band size:

Before digestion: 491 bp

After digestion: WT: 110, 168, 213 bp

D61N/+: 110, 168, 213, 323 bp

Morphological and morphometric analysis

Sciatic nerves were freshly dissected, fixed in 2% glutaraldehyde in phosphate buffer, osmicated in 1% OsO_4, alcohol dehydrated, infiltrated with propylene oxide and embedded in Epon. Transverse semithin sections and ultrathin sections were cut with an Ultracut microtome. Semithin sections were stained with toluidine blue and acquired with a Leica DM5000 microscope equipped with a DFC480 digital camera, whereas ultrathin sections were stained with lead citrate and photographed with a Zeiss (Oberkochen, Germany) EM10 electron microscope. g-ratio (axon diameter/fiber diameter) was measured on semithin sections using ImageJ software; four-six images per nerve were acquired with a 100X objective; ~800–2000 fibers per condition were measured. The proportion of fibers with myelin outfoldings was also determined [159].

Electrophysiology

8 *MPZ*$^{D61N/+}$ and 8 control mice were analyzed at 1 month and 3 months old. Electrophysiological tests were performed using an EMG system (NeuroMep Micro, Neurosoft, Russia). Mice were anesthetized with trichloroethanol, 0,3 mg/g of body weight, and placed under a heating lamp to maintain a constant body temperature. Monopolar needle electrodes were inserted subcutaneously to stimulate the tibial nerve at the ankle and, subsequently, the sciatic nerve at the sciatic notch; the cathode was placed close to the nerve and the anode was inserted proximally to the cathode. The stimulation consisted of single 100 μs, 1Hz supramaximal pulses. The muscular response was recorded by inserting the active electrode into muscles in the middle of the paw and the reference electrode in the skin between the first and second digit. NCV (m/s), peak-to-peak cMAP amplitude (mV) and F-Wave Latency (FWL) (ms) were measured. FWL measurement was obtained stimulating the tibial nerve at the ankle and recording the responses in the paw muscles, using the same pair of needle electrodes used for the nerve conduction study.

Behavioral analysis

Tremor was estimated visually on a + to ++++ scale.

Rotarod test

Motor ability was assessed using the accelerating Rotarod (Ugo Basile, Comerio, Italy). Groups of 3 months old transgenic and control littermates were tested in two sessions of three trials each per day (6 h rest between the two daily sessions) for 3 consecutive days. During the test, the rod accelerated from 4 to 40 rotations per minute, and the time that the animal remained on the rod (maximum 900 s) was measured.

Grip strength test

The grip strength test is a simple non-invasive method designed to evaluate mouse muscle force and hind limb strength. Grip strength test was performed on a group of 9 *MPZ*$^{D61N/+}$ and 10 WT mice at 3 months of age using a grip strength meter (Grip-Strength Meter, 47200, Ugo Basile, Italy) to determine hind limbs muscle strength. The grip strength meter was arranged horizontally on the table. While holding the tails, the mice were lowered towards the grip strength meter to enable to grasp the T-shaped bar with the hindpaws. After grasping the bar, the mice were pulled backwards till the grasp was released. The test was repeated six consecutive time. For each session the average value of the peak force (in gf) was calculated [160].

TaqMan quantitative PCR analysis

Total RNA was extracted with Trizol (Roche Diagnostic GmbH, Germany) and retrotranscribed as previously described [124]. TaqMan assays were performed following manufacturer's instructions (TaqMan, PE Applied Biosystems Instruments) on an ABI PRISM 7700 sequence detection system (Applied Biosystems Instruments). Normalization was performed using 18S rRNA as reference gene. Target and reference genes PCR amplification were performed in separate tubes with Assay on Demand (Applied Biosystems Instruments): 18S assay, Hs99999901_s1; Ddit3/Chop assay, Mm00492097_m1; Xbp-1s assay, Mm03464496_m1; Hspa5/BiP assay, Mm00517691_m1; MPZ assay, Mm00485141_g1; MBP assay, Mm01266402_m1; PMP22 assay, Mm01333393_m1.

Western blot analysis

Sciatic nerves were dissected and frozen in liquid nitrogen. Frozen nerves were pulverized on dry ice and proteins were extracted in denaturing lysis buffer (Tris-HCl 50 mM pH 7.5, NaCl 150 mM, EDTA 10 mM, 2% SDS) containing protease inhibitor cocktail (PIC 100X, Roche) and phosphatase inhibitors (Roche). Total protein concentration was determined by BCA assay (Pierce) following manufacturer's instructions. Equal amounts of proteins were separated by SDS-PAGE (Biorad) and gels were transferred onto nitrocellulose membrane (GE Healthcare). Membranes were blocked with 5% milk (milk powder/ 1X PBS-Tween 0.1%) or 5% BSA (BSA powder/ 1X PBS-Tween 0.1%) and incubated with primary antibodies diluted in 1% milk or 1% BSA/ 1X PBS-Tween 0.1% at 4°C overnight. HRP-conjugated antibodies were diluted in 1% milk or 1% BSA/ 1X PBS-Tween 0.1% and incubated 1 h at RT. Signals were detected by ECL method. Densitometric analysis was performed with NIH-Image-J software.

PNGaseF treatment

For the digestion with PNGaseF, an amidase that cleaves N-glycans, proteins were extracted from sciatic nerves or from Hela cells as previous described for the western blot analysis, but using the RIPA buffer, digested for 1 h at 37°C with PNGaseF, according to manufacturer's protocol (NEB), separated by SDS-PAGE and immunoblotted.

Teased fibers preparation

Sciatic nerves were freshly dissected, fixed in 2% glutaraldehyde in phosphate buffer, osmicated in 1% OsO_4 in triethyl phosphate and placed in glycerol. Single fibers were separated with fine needles, placed on slides and analyzed with a light microscope (Leica DM5000).

Myelinating Dorsal Root Ganglia (DRG) explant cultures

DRG explants were isolated from E13.5 WT and D61N/+ embryos, seeded on rat collagen I-coated coverslip and maintained in cultures as previously described

[33]. Myelination was induced by supplementing media with 50 μg/ml ascorbic acid (Sigma-Aldrich) for 14 days. Culture medium was refreshed every two days. Samples were fixed and prepared for immunofluorescence.

Immunohistochemistry and analysis of myelination

Schwann cell/DRG neuron co-cultures were fixed for 15 min in 4% paraformaldehyde, permeabilized for 3 min in ice-cold methanol, blocked for 1 h with 1% BSA + 10% NGS in PBS, and incubated at 4°C overnight with primary antibody. After washing, the coverslips were incubated 1 h at room temperature in the dark with secondary antibody, washed, incubated for 5 min in the dark with Hoechst solution for nuclei staining, washed and mounted with Vectashield. To quantify the amount of myelin, 8 non-overlapping images per DRG were acquired with a Leica DM5000 microscope (10X and 20X objectives) equipped with a Leica DFC480 digital camera and the number of MBP-positive myelinated fibers were counted. The percentage of MBP-positive fibers showing myelin abnormalities among the total number of MBP-positive fibers was indicated. At least 3 independent dissections were performed.

Antibodies

For western blot the following primary antibodies were used: chicken anti-myelin protein zero (P0) (PZO; Aves); mouse anti-myelin basic protein (MAB 382; Chemicon); rabbit anti-PMP22 (AB211052; ABCAM); rabbit anti-eIF2α (D7D3) XP (5324; Cell Signaling); rabbit anti-phospho-eIF2α (Ser51) (D9G8) XP (3398; Cell Signaling); rabbit anti-p44/42 (ERK1/2) (9102; Cell Signaling); rabbit anti-phospho-p44/42 (Thr202/Tyr204) (4370; Cell Signaling); rabbit anti-AKT (9272; Cell Signaling); rabbit anti-phospho-AKT (Ser473) (9271; Cell Signaling); rabbit anti-GRP78 (BiP) (NB 300520; Novus Biological); mouse anti-β-tubulin (T4026; Sigma); rabbit anti-Calnexin (C4731; Sigma); mouse anti-GFP tag (GF28R) (MA515256; Thermo Fisher).

For immunofluorescence the following primary antibody was used: rat anti-MBP.

Secondary antibodies included donkey anti chicken-HRP (AB 16349; ABCAM); horseradish peroxidase (HRP)-conjugated goat anti rabbit (P0448; Dako); anti-

mouse IgG Peroxidase (A3682; Sigma Aldrich) and Mouse IgG HRP-linked whole Ab (10196124; Fisher Scientific). For immunofluorescence, secondary antibody included Cy3-conjugated goat anti-rat (112166062; Jackson ImmunoResearch), Alexa Fluor 546 goat anti-mouse IgG (A11030; Thermo Fisher). For immuno-EM the following antibodies were used: monoclonal anti-P0 protein were donated by Dr. JJ Archelos (Karl Franzen universität, Graz, Austria); secondary goat anti-mouse conjugated to 6-, 12-, or 18- nm gold particles were obtained from Jackson ImmunoResearch Laboratories, Inc (Montluçon, France).

RESULTS

In silico prediction of gain/loss of N- and O-linkage sites in *MPZ* gene

Protein misglycosylation following a missense mutation denotes the introduction of a new glycosylation site or the removal of a constitutive one; this mechanism is more frequent than expected [146, 147] and it is has been described also for *MPZ* mutation [98, 126, 149, 152]. The Mutation Database of Inherited Peripheral Neuropathies (http://www.molgen.ua.ac.be/CMTMutations/default.cfm) shows 126 mutations in the *MPZ* gene. If we consider the missense mutations affecting amino acids within P0ECD, the reported mutations are 84. With the help of two free, dedicated softwares, NetNGlyc 1.0 Server and NetOGlyc 3.1 Server [161], we have introduced in the *MPZ* sequence all the amino acid changes reported in the database and identified four more *MPZ* mutations, all in the extracellular domain, potentially able to produce hyperglycosylated forms of P0: D61N [126]; D109N [153]; D118N [154] and K138N [155]. The N-glycosylation efficiency of a N-X-S/T sequon depends on multiple factors, including the proximity to the C-terminal of the protein and the presence of particular amino acids in close proximity to the glycosylation site, being some of them favorable to glycosylation, whereas others render the modification unlikely [162]. The four mutations already listed are all far from the C-terminal and none of them presents unfavorable amino acids. Interestingly, the new glycosylation sequence of K138N, is preceded by a glycine which render effective glycosylation a likely event [162]. However, the D118N mutation is very close to the wild type acceptor sequon, which is in position 122. The existence of a minimal distance between consecutive N-glycosylation sequences has been debated, but theoretically N-glycosylation may occur also for overlapping glycosites [163]. Differently, none of the described *MPZ* mutations reached a score over the threshold of NetOGlyc 3.1 Server, meaning that a gain-of-O-glycosylation is unlikely. The analysis of the database highlighted also three *MPZ* mutations preventing the native glycosylation acceptor site: N122S [148], T124M [149], T124K [150]. Our group has described a fourth mutation, T124A [151], also affecting the unique P0 glycosylation site. The percentage of predicted misglycosylated P0 mutants is

6,3% if considering all mutations and 9,5% if restricting the analysis to the missense substitutions within P0ECD, thus representing a potentially relevant pathomecanism.

Generation of *MPZ* mutations *in vitro*

Through site-directed mutagenesis, we generated different constructs coding EGFP-tagged versions of all the mutant proteins and expressed them in Schwannoma cell line. Western blot analysis showed that the predicted hyperglycosylated mutants displayed a molecular weight (MW) always higher than that of P0wt, even if it varied from the highest MW of K138N to the lowest MW of D118N (Figure 1A), whereas the predicted hypoglycosylated proteins presented a MW lower than P0wt (Figure 1B).

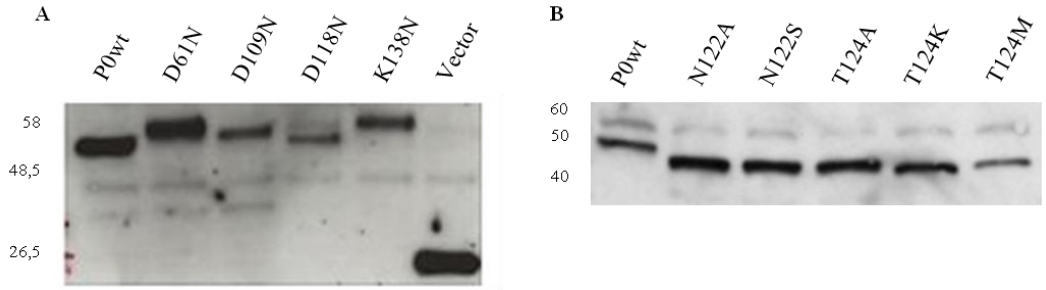

Figure 1: *MPZ* mutation *in vitro*: differences in molecular weight

Western blot of Schwannoma cells transiently transfected with the different *MPZ* plasmids:

A) the MW of fusion proteins predicted to be hyperglycosylated is higher compared to the MW of P0wt, varying from the highest MW of K138N to the lowest MW of D118N.

B) the MW of proteins predicted to be hypoglycosylated appears to be lower than the MW of P0wt.

Next, to test whether the higher MW of D61N, D109N, D118N and K138N was due to extra glycans, we treated protein extracts from transfected cells with PNGaseF, an amidase that cleaves N-glycans. This assay showed that after treatment, the MW of all mutant proteins decreased to the same level of P0wt treated with the same amidase, thus demonstrating that the higher MW of these mutant proteins was due to additional oligosaccharides. Conversely, none of the

P0 variants predicted to be non-glycosylated were sensitive to PNGaseF, thus confirming that they lack glycans (Figure 2A). To further demonstrate the hyperglycosylation and that the increase of the MW was really due to the second oligosaccharide, we generated constructs carrying each predicted gain-of-glycosylation *MPZ* mutation together with the N122A mutation, to produce P0 variants with the unique novel glycosylation site but without the wild type N-sequon N122. Again, all of these mutant proteins presented a higher MW compared to the P0wt and all these proteins were sensitive to PNGaseF treatment, further proving that they all have a second glycosylation site (Figure 2B, C, D).

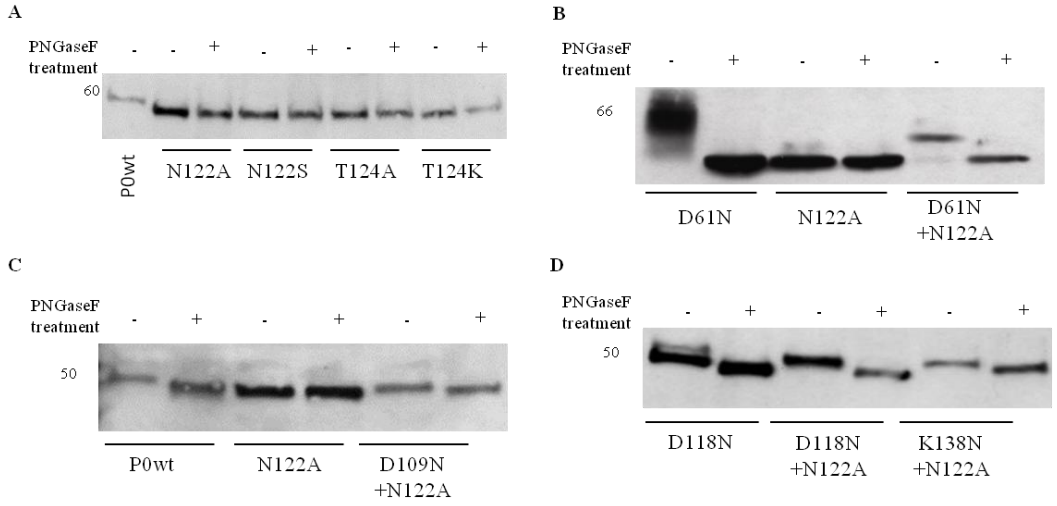

Figure 2: Treatment with PNGaseF of *MPZ* mutations *in vitro*

Schwannoma cells have been transiently transfected with the different *MPZ* plasmids: **A-D)** Western blot of hyperglycosylated and hypoglycosylated proteins treated with PNGaseF; all the predicted hyperglycosylated proteins were sensitive to PNGaseF, while the predicted hypoglycosylated were not. Concerning the hyperglycosylated mutations, we studied also the double mutants carrying the additional N122A mutation that eliminates the constitutive glycosylation site. All double mutants were sensitive to PNGaseF, thus proving that the novel glycosylation sites are glycosylated.

Evaluation of protein localization and intracellular adhesion of *MPZ* mutations *in vitro*

To verify whether P0 misglycosylation was altering P0 trafficking and localization, we transfected different cell lines (HeLa and Schwannoma *RT4*-D6P2T) with EGFP-tagged mutant proteins. Immunofluorescence analysis

showed that whereas P0wt reached the cell membrane, the hyperglycosylated proteins D61N, D109N and K138N were partially retained intracellularly (Figure 3A). Conversely, the D118N hyperglycosylated mutant and all the hypoglycosylated mutant proteins normally reached the plasma membrane (Figure 3A and data not shown).

To further investigate the trafficking of the hyperglycosylated mutant proteins, we performed also a biotinylation/endocytic assay [157]; this assay allows to understand if a protein reaches the plasma membrane and if it is recycled by the endosomes, indicating a rapid internalization of the protein. This analysis suggested that all the hyperglycosylated proteins were biotinylated, consistent with membrane protein insertion; however, mutant variants are more endocytosed, supporting the hypothesis of an increased instability compared with wild type protein (Figure 3B).

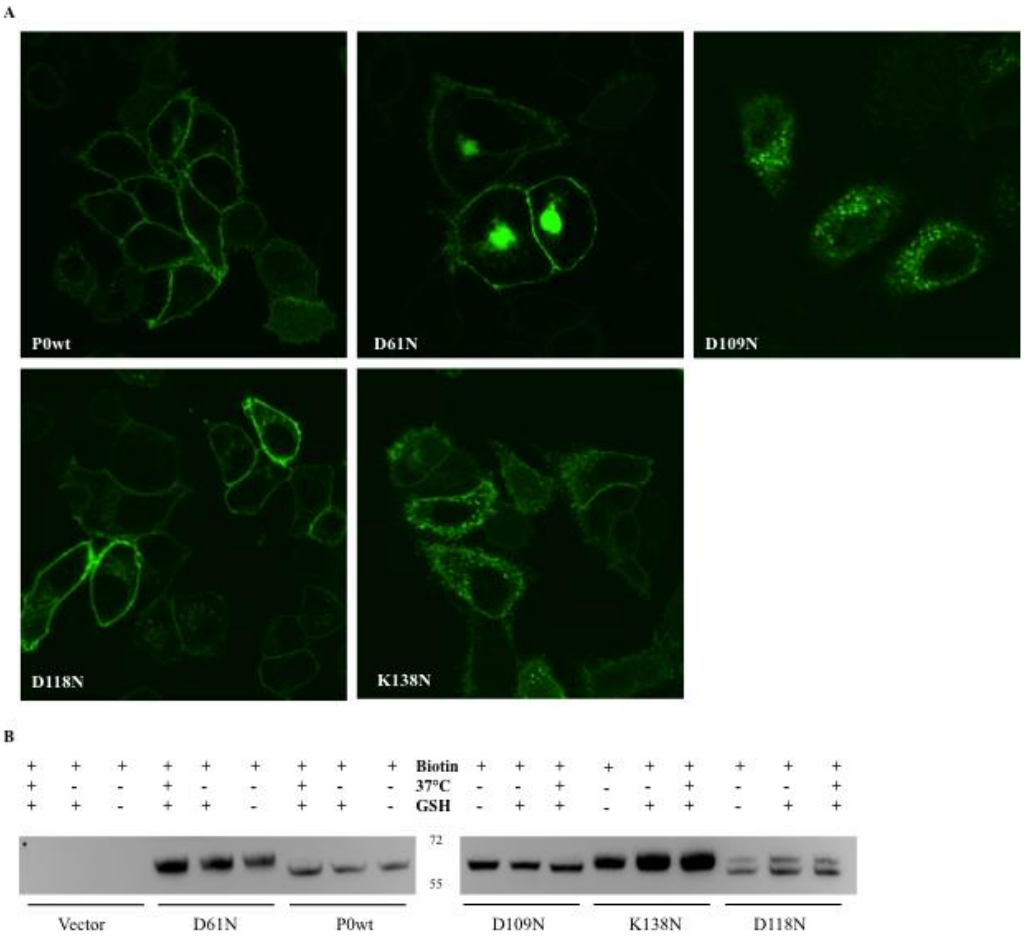

Figure 3: Protein localization *in vitro*

A) Confocal microscopy of Hela cells transiently transfected with EGFP-tagged hyperglycosylated proteins; the mutant proteins D61N, D109N and K138N are partially retained intracellularly, whereas D118N appears to be normally trafficked.

B) Biotinylation-endocytic assay: +-- indicate proteins that are only biotinylated, +-+ proteins that are biotinylated and treated with GSH solution to reduce disulfide bonds, +++ proteins that are biotinylated, in which endocytosis has been induced and the disulfide bond are reduced with GSH solution; the WB showed that the signal produced by mutated proteins in which the endocytosis has been induced (+++ bands) is higher than the signal produced by P0wt subjected to the same treatment, indicating that these proteins are more endocytosed. As expected, the empty vector didn't reach the plasma membrane and consequently, no signal is produced.

In myelin, P0 protein has an essential role in the adhesion of adjacent membrane wraps, through the formation of functional tetramers. To test whether the misglycosylating mutations interfered with this function, we performed an aggregation assay in transiently transfected HeLa cells [125]. The size of aggregates formed by cells expressing P0wt protein were indicated as 100% and were used as reference value; cells expressing hyperglycosylated P0 proteins formed aggregates which were smaller as compared to P0wt: the size of D61N aggregates were 67%, those of D109N were 54%, those of D118N were 70% and those of K138N were 67%; these results supported the hypothesis that hyperglycosylated variants impair the adhesion property (Figure 4A). Instead, cells expressing hypoglycosylated P0 proteins formed aggregates similar to those formed by the cells expressing P0wt, with the exception of T124K that formed smaller aggregates (the size was 59% compared to the size of P0wt aggregates) (Figure 4B). In both the adhesion test were measured also the aggregates formed by cells transfected with the empty vector using it as a negative control.

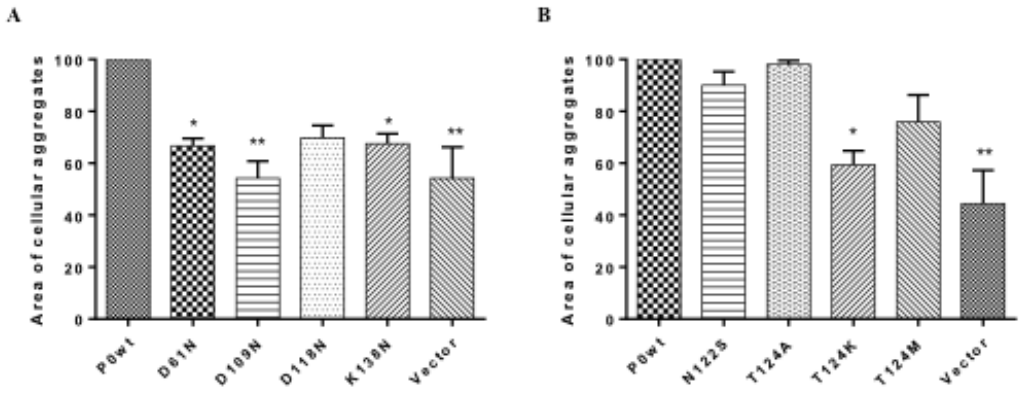

Figure 4: Adhesion properties of mutated proteins

A) Adhesion test on HeLa cells transfected with P0wt and the hyperglycosylated proteins. The graph shows the area of aggregates formed by the cells transfected with the different proteins: the majority of the hyperglycosylated proteins formed smaller aggregates compared to the aggregates formed by P0wt, indicating a decrease in adhesion ability (One-way ANOVA corrected for multiple comparison using statistical Tukey test).

B) Adhesion test on HeLa cells transfected with P0wt and hypoglycosylated proteins; all the hypoglycosylated protein, except for the T124K, formed aggregates similar to that formed by the P0wt (One-way ANOVA corrected for multiple comparison using statistical Tukey test).

Altogether these data indicate that the hyperglycosylated mutations, but not the hypoglycosylated ones, interfered with protein localization and protein adhesion properties, confirming the general rule that gain-of-glycosylation is more disruptive compared with loss-of-glycosylation [146, 147] and suggesting to further investigate hyperglycosylation.

Generation of *Mpz*$^{D61N/+}$ mice, a model for the hyperglycosylation

To evaluate *in vivo* the effects of hyperglycosylation, we established a transgenic mouse model for the *Mpz*^{D61N} mutation using the genome-editing tool CRISPR-associated protein 9 (Cas9) nuclease. The CRISPR/Cas9 system in fact allows the precise editing of the mouse genome to introduce specific nucleotide changes [164], thus perfectly mimicking human disease mutations. In particular, for the

generation of the *Mpz*^{D61N} model, three different snp conversions were introduced: a G>A conversion (position 181) that introduced the desired D to N amino acidic change, a A>G conversion (position 168) that prevent gRNA binding and recleavage possibility and a A>T conversion (position 177) that eliminates the DdeI restriction enzyme site (Figure 5A); the latter conversion allowed us to discriminate between WT and mutant mice (Figure 5B). The A>G and A>T conversions were designed not to cause any amino acidic change, so that the only difference in amino acid sequence as compared to P0wt is the D to N in position 61. To confirm that the mutant P0D61N protein is hyperglycosylated *in vivo*, we performed a PNGaseF assay on protein extracts from sciatic nerves of WT and mutant *Mpz*$^{D61N/+}$ mice at one month. The untreated WT lanes are characterized by a single band (29kDa), while the mutant extracts present two distinct bands, one corresponding to the WT and a second one with a higher MW. After PNGaseF treatment, the MW of P0 in the *Mpz*$^{D61N/+}$ extracts collapses to a single lower band of the same MW as the WT, demonstrating that the increased MW of the upper band is entirely due to extra glycan residues (Figure 5C).

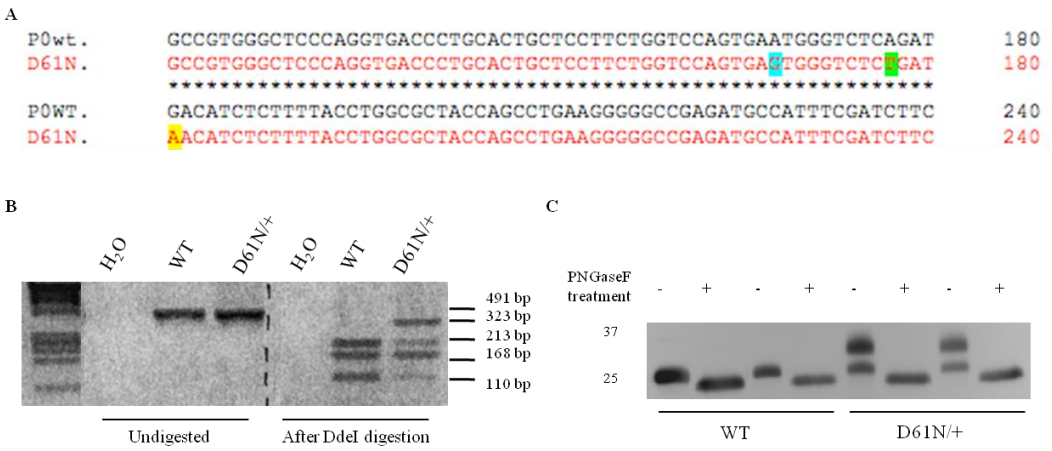

Figure 5: Mouse model generation

A) Comparison between P0 protein sequence before and after the introduction of snp conversion to generate the *Mpz*^{D61N} model: in blue the snp conversion to prevent gRNA binding and recleavage possibility, in green the snp conversion that eliminates the DdeI restriction enzyme site and in yellow the snp conversion that introduces the desired mutation.

B) PCR products before and after digestion with DdeI enzyme: before digestion the PCR product is 491 bp; after digestion, there are three bands of 110 bp, 168 bp and 213 bp in wild-type animals, while, in mutant mice, there are two bands of 168 bp and 323 bp, so that the Mpz$^{D61N/+}$ mice display a total of 4 bands.

C) Proteins extracted from sciatic nerves of WT and *Mpz*$^{D61N/+}$ animals were treated with PNGaseF; before PNGase digestion, P0wt runs as a single band while P0D61N/+ extract shows a double band. After treatment with PNGaseF, the MW of P0 in *Mpz*$^{D61N/+}$ samples decreases to a single band of the same MW of control proteins treated with the same enzyme.

Mpz$^{D61N/+}$ mice present severe impairment in motor capacity and neurophysiology

Mice heterozygous for *Mpz* variant D61N (*Mpz*$^{D61N/+}$) were viable, bred normally and pups were born with the expected mendelian ratio and were initially indistinguishable from WT littermates. *Mpz*$^{D61N/+}$ mice started manifesting a tremoring phenotype around postnatal day 15 (P15). The tremor was visually estimated on a + to ++++ scale and it worsened with ageing, but without impairing life expectancy (Figure 6A).

To test whether this tremor would affect motor ability we evaluated the latency to fall on the accelerating Rotarod [124] in mice at three month of age. The mean latency to fall off the rotarod over the 3-day trial period was 184,7 ± 14,21 s for *Mpz*$^{D61N/+}$ mice, as compared to 329,7 ± 23,24 s for WT (P value < 0,0001) (Figure 6B). We performed another behavioral test to evaluate the force and hind limb strength of *Mpz*$^{D61N/+}$ mice compared to WT mice at three months of age: the grip strength test. We measured the maximal force produced during the pull in six different trials and we obtained that the mean force in WT animals was 97,19 ± 4,4 gr, while in *Mpz*$^{D61N/+}$ mice the mean force was 82,68 ± 4,1 gr (P value

0,0246) (Figure 6C). With this two tests, we demonstrated that *Mpz*$^{D61N/+}$ mice presented motor impairment and reduced muscular strength.

A

	15 days	1 month	6 months
WT	No tremor	No tremor	No tremor
D61N/+	Tremor 1+	Tremor 3+	Tremor 4+

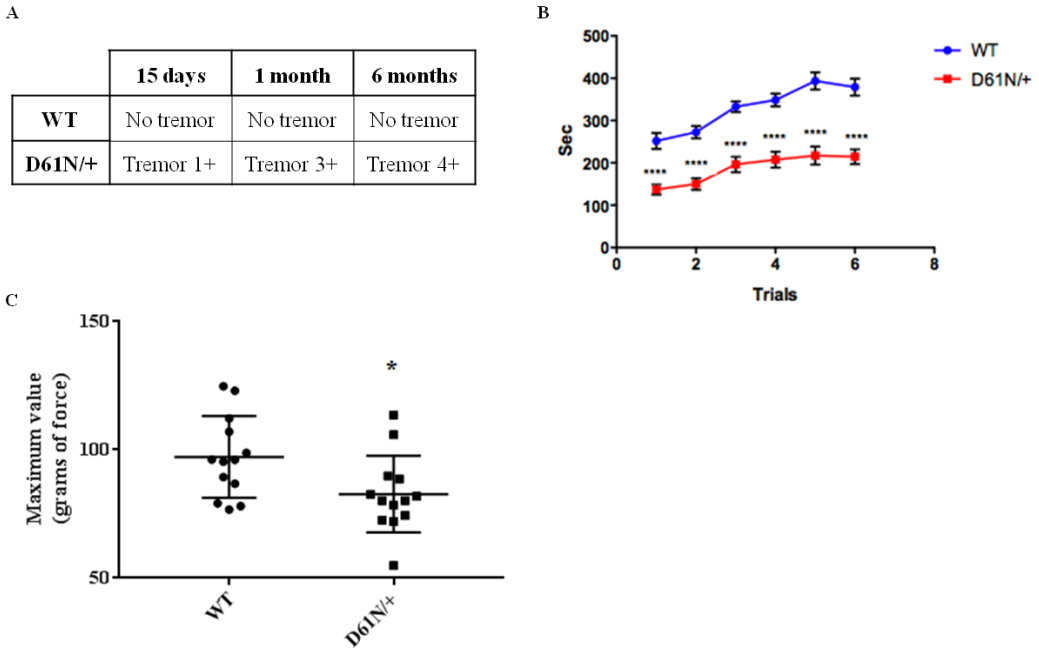

Figure 6: *Mpz*$^{D61N/+}$ mice present motor impairment

A) Table describing the features of WT and *Mpz*$^{D61N/+}$ mice at different time points; the scale of tremor is visual and goes from + to ++++.

B) Rotarod analysis, performed at 3 months of age, shows that *Mpz*$^{D61N/+}$ mice have a latency to fall of 184,7 s ± 14,21, compared to 329,7 s ± 23,24 for WT (Two-way ANOVA corrected for multiple comparison using statistical Sidak test; P value < 0,0001).

C) Grip strength test, performed at 3 month of age, shows that *Mpz*$^{D61N/+}$ mice have less strength in hind limbs. In particular the force needed to win their grasp is 82,68 ± 4,1 gr compared to 97,19 ± 4,4 gr for WT mice (Unpaired t-test; P value 0,0708).

Next, we performed electrophysiological analysis on mutant and control animals at one and three months of age; we evaluated the sciatic nerve motor conduction velocity (MCV), the F-wave latency, the distal and proximal latency and the distal and proximal amplitude. At one month of age, all the parameters were significantly altered in *Mpz*$^{D61N/+}$ as compared to WT. In particular, MCV was significantly lower (12,05 ± 1,22 m/s) as compared to controls (33,02 ± 1,622 m/s), with prolonged latencies and a severe decrease of cMAPs (Figure 7).

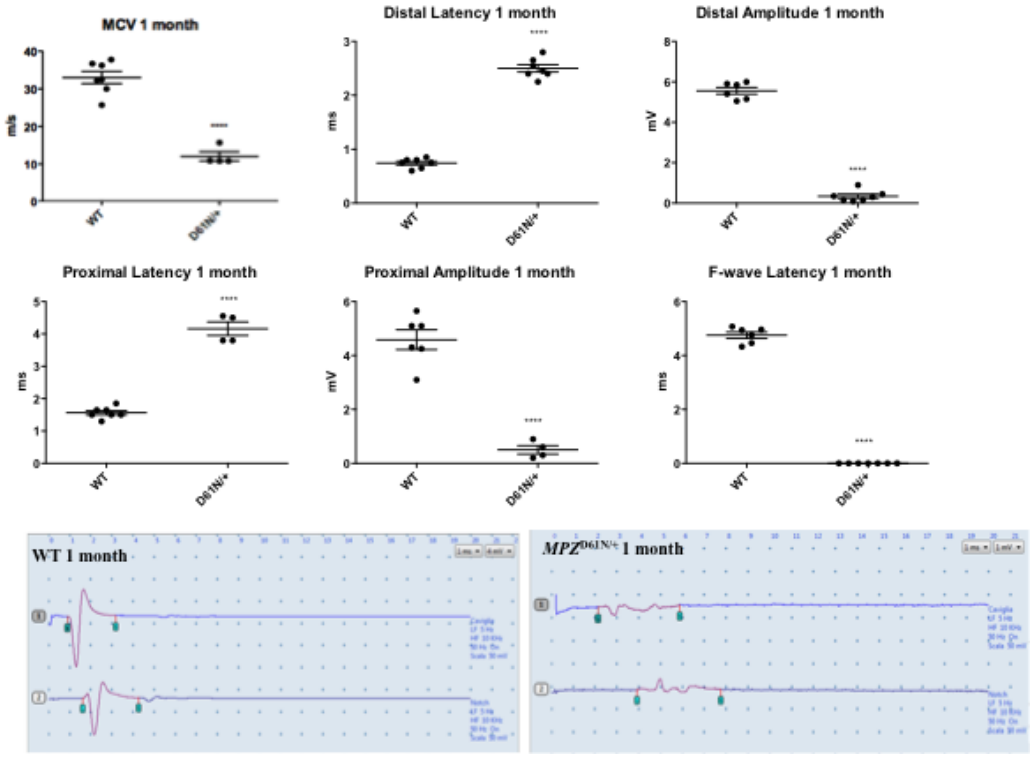

Figure 7: Electrophysiological parameters in WT and *Mpz*$^{D61N/+}$ mice at 1 month

Electrophysiological recordings from 1 month WT and *Mpz*$^{D61N/+}$ mice: all the electrophysiological parameters recorded were significantly different between the two groups (Unpaired t-test; P value < 0,0001) In the lower part are presented the original recordings: flags indicate the onset and end of the cMAPs; *Mpz*$^{D61N/+}$ mice showed a dispersed morphology, a prolonged latency of both distal and proximal cMAP with a significant reduction of the nerve conduction velocities, , as well as a reduced cMAP amplitude compared to controls.

Moreover, by three months of age, all the electrophysiological parameters were unrecordable in most neuropathic mice suggesting a severe conduction block; the few parameters recorded were significantly impaired: for examples, the MCV was 39,34 ± 0,26 m/s in WT mice and 13,2 ±1,8 m/s in the only two *Mpz*$^{D61N/+}$ mice in which the parameter was recordable (Figure 8).

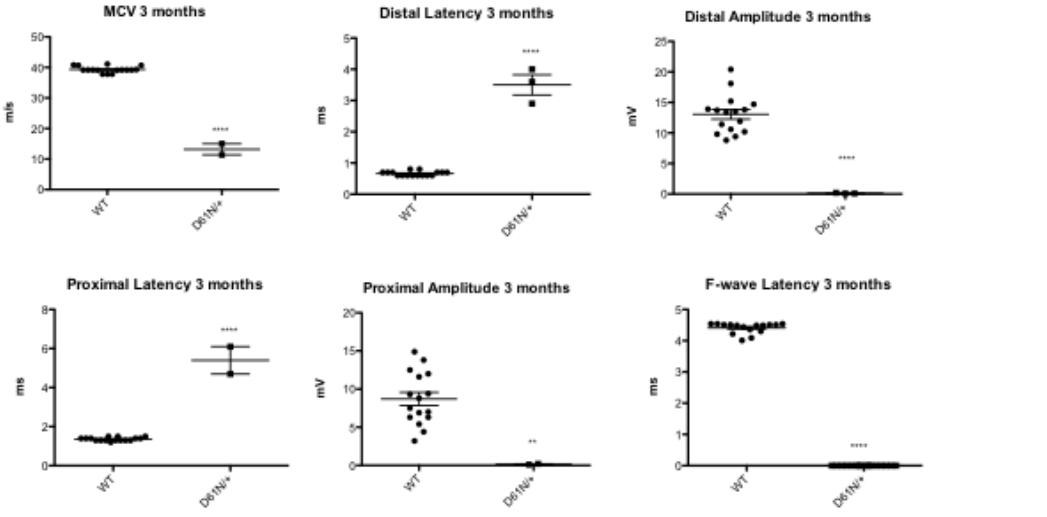

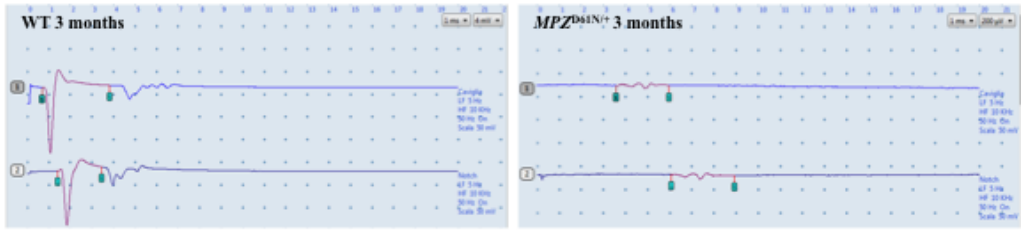

	3 MONTHS	
	WT	*MPZ*$^{D61N/+}$
Sciatic nerve motor conduction velocity (m/s)	39,3±(0,74)	86% Absent
F-wave latency (ms)	4,4±(0,14)	100% Absent
Distal latency (ms)	0,66±(0,05)	79% Absent
Proximal latency (ms)	1,36±(0,08)	86% Absent
Distal amplitude (mV)	13,06±(2,3)	79% Absent
Proximal amplitude (mV)	8,7±(2,9)	86% Absent

Figure 8: Electrophysiological parameters in WT and *Mpz*$^{D61N/+}$ mice at 3 months
Electrophysiological recordings from 3 months WT and *Mpz*$^{D61N/+}$ mice: all the electrophysiological parameters recorded were significant different between the two groups (Unpaired t-test; P value < 0,0001) The original redrawn recordings are presented and the trend of the tracks is similar to that recorded when they were 1 month old. The table in the lower part showed the value of the different electrophysiological parameters in WT animals, while for *Mpz*$^{D61N/+}$ mice is indicated the percentage of animals in which the different parameters were unrecordable.

Mpz$^{D61N/+}$ show a severe de/dysmyelinating phenotype

The behavioral and neurophysiological analysis outlined above suggested that the *Mpz*$^{D61N/+}$ mutation determined a dramatic impairment of nerve functionality. To further corroborate this, we performed morphological analysis on semi-thin

section from 1 month sciatic nerves stained with toluidine blue (Figure 9A). Mutant fibers showed a decrease of myelin thickness, typical of a de/dysmyelinating phenotype, as measured by g-ratio analysis, (g-ratio 0,72 ± 0,01 in *Mpz*$^{D61N/+}$ mice vs 0,65 ± 0,01 in controls; P value 0,0027) (Figure 9B); moreover, we also noticed a reduction in myelinated axon diameter in *Mpz*$^{D61N/+}$ nerves as compared to WT control (Figure 9C), despite no differences in the overall number of myelinated fibers (Figure 9D).

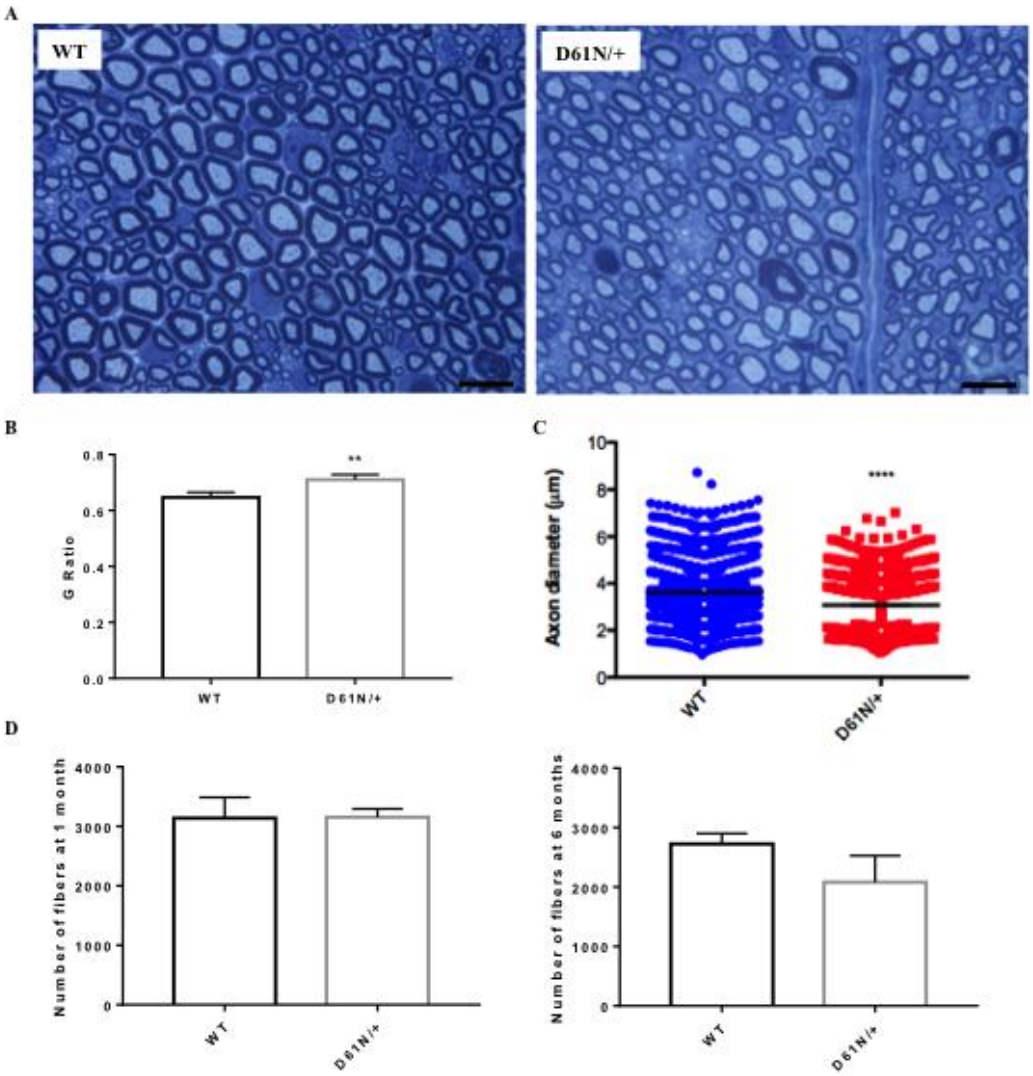

Figure 9: Morphological analysis of WT and *Mpz*$^{D61N/+}$ sciatic nerves

A) Images of semithin section of sciatic nerves from WT and *Mpz*$^{D61N/+}$ mice at 1 month (Magnification: 100X; Scale bar: 5 μm).

B) G-Ratio of WT and *Mpz*$^{D61N/+}$ fibers was analyzed (Error bars, SEM; unpaired, 2-tails, Student's *t* test; P value 0,0027).

C) Comparison between axon diameter of WT and *Mpz*$^{D61N/+}$ fibers (Unpaired, 2-tails, Student's *t* test; P value < 0,0001).

D) Number of fibers in WT and *Mpz*$^{D61N/+}$ sciatic nerves at 1 month and 6 months (Unpaired, 2-tails, Student's *t* test; P value 0,93 and 0,08 respectively).

Of note, *Mpz*$^{D61N/+}$ nerves were also characterized by the presence of tomacula like structures, basically absent in WT controls, that increase with time, from 80 ± 24,19 to 222 ± 12,49 per nerve section (Figure 10A, B), supporting the progressive worsening of the phenotype already noted in the behavioral and neurophysiological tests.

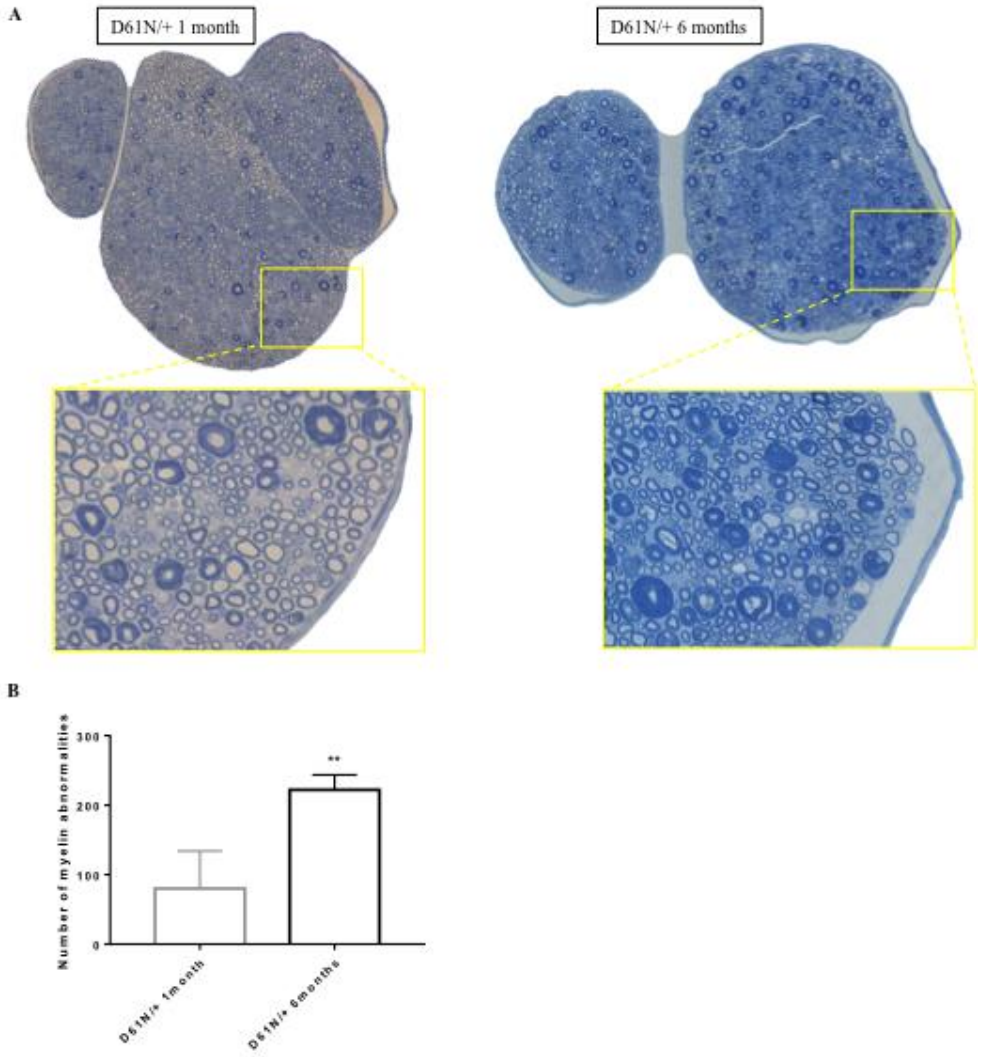

Figure 10: *Mpz*$^{D61N/+}$ myelin abnormalities

A) Reconstruction of a *Mpz*$^{D61N/+}$ 1 month and 6 months sciatic nerve; a magnification is present to better visualize the increase of tomacula-like structures.

B) Number of myelin abnormalities in *Mpz*$^{D61N/+}$ sciatic nerves at 1 month and 6 months (Unpaired, 2-tails, Student's *t* test; P value 0,055).

The analysis of osmicated teased fibers revealed that these myelin abnormalities are not restricted to paranodal areas, but distributed along the entire internode (Figure 11).

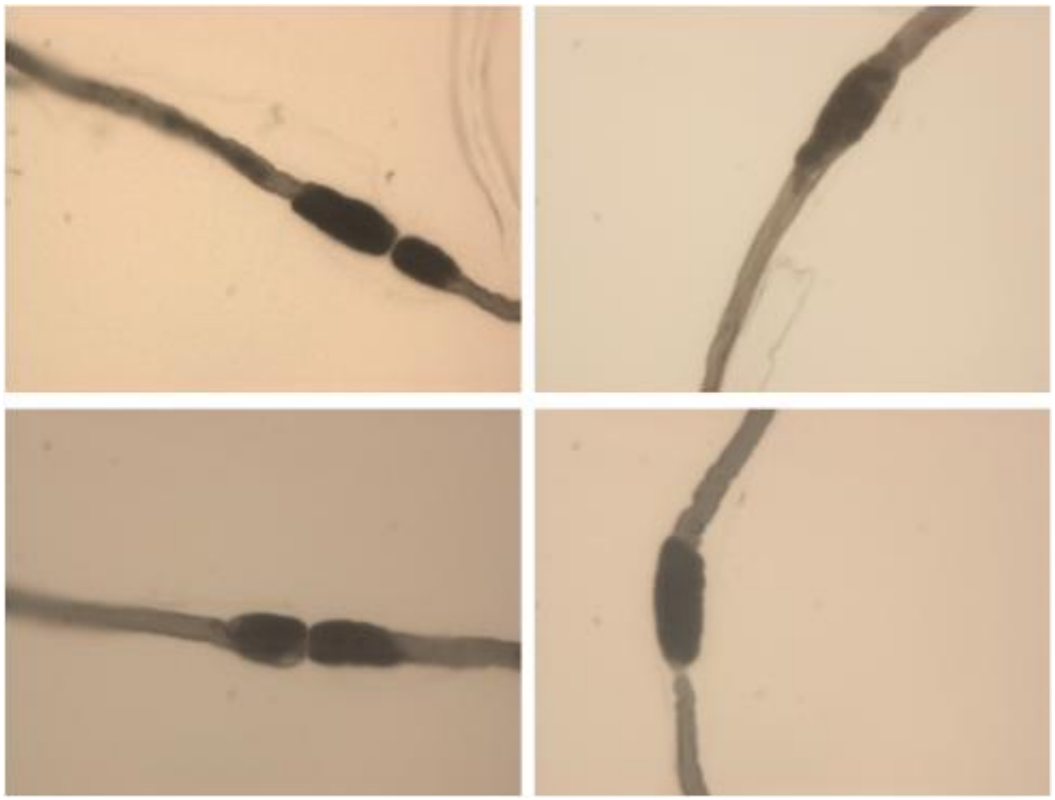

Figure 11: Analysis of *Mpz*$^{D61N/+}$ osmicated fibers

Osmicated teased nerve fibers from a *Mpz*$^{D61N/+}$ mouse. Focal myelin thickenings originate both at paranodal regions and at internodal regions (Magnification 40X).

Mpz$^{D61N/+}$ present defects in myelin compaction

To further characterize myelin abnormalities and myelin compaction, we performed electron microscopy analysis on transverse and longitudinal section of WT and *Mpz*$^{D61N/+}$ sciatic nerves. On transverse section, mutant nerves displayed frequent abnormal thickening of the myelin sheath that appeared to compress the axon; in longitudinal section of mutant nerves were evident several foldings and hypermyelinating aspects of one myelinated axon (white star) (Figure 12A). Moreover, high magnification analysis revealed that in many of the mutant fibers myelin periodicity was altered. In fact, whereas WT fibers showed a consistent frequency in major dense line and intraperiod line, in *Mpz*$^{D61N/+}$ nerves some myelin lamellae looked normally compacted (black bar), while other showed uncompaction and widening of the intraperiod line (white bar) (Figure 12B).

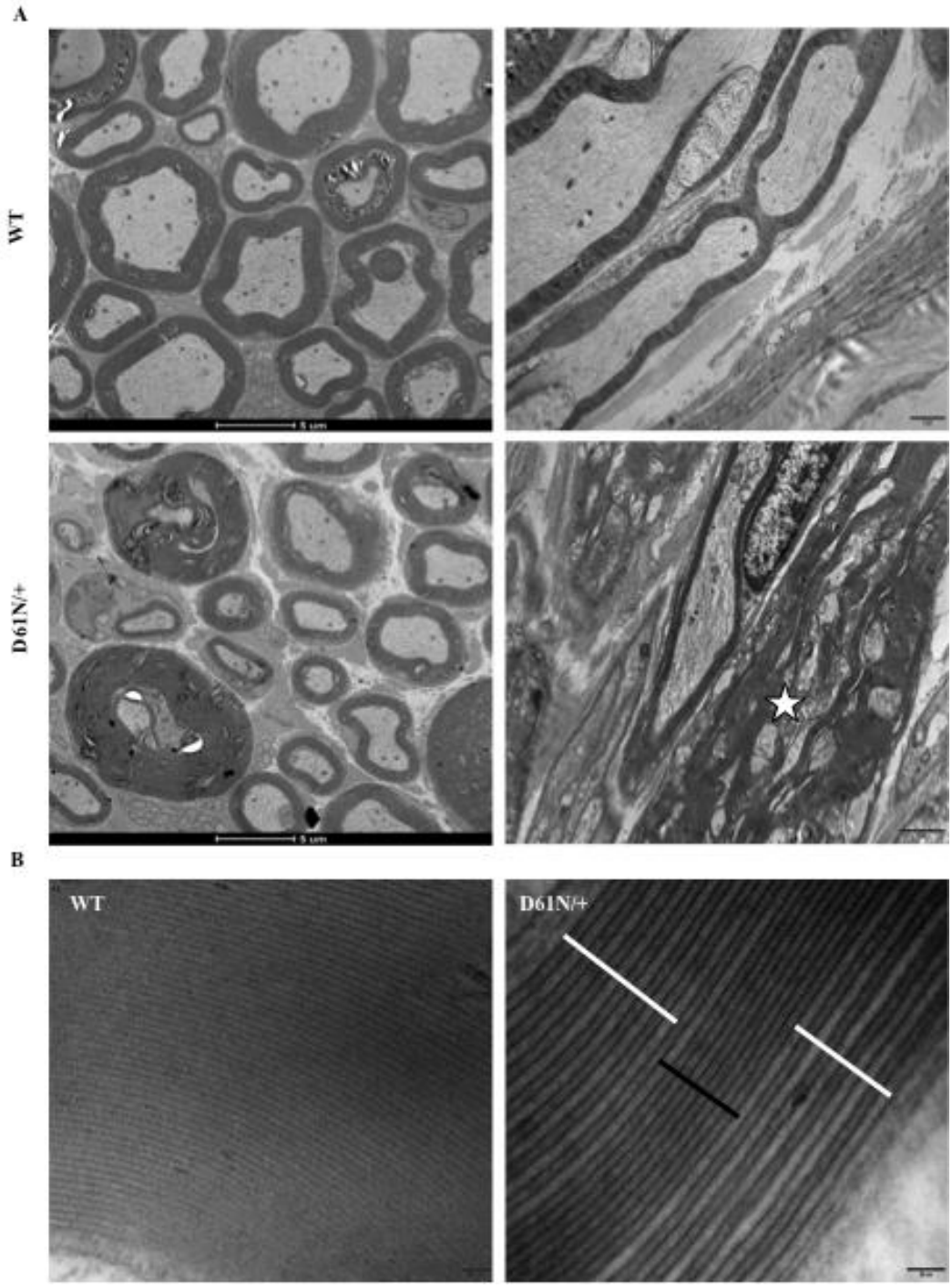

Figure 12: Electron microscopy of WT and mutant sciatic nerves

A) Transverse and longitudinal section of a WT and *Mpz*$^{D61N/+}$ sciatic nerves. White star indicate a myelinated axon with hypermyelinating aspects. Scale Bar: 5µm in transverse section, 2µm in longitudinal section.

B) Transverse section of a WT and *Mpz*$^{D61N/+}$ sciatic nerves. Black bar indicate myelin lamellae normally compacted, white bar indicate uncompaction and widening of the intraperiod line. Scale bar: 500nm.

Finally, by immuno-EM, using an anti-P0 antibody, we evaluated the amount of P0 expressed on the cell membrane in normal myelin as compared with the pathological samples (Figure 13A). This analysis suggested a reduction in the density of P0 molecules (ratio between the number of gold particles and the membrane surface) in the myelin of *Mpz*$^{D61N/+}$ mice, decreasing from 33,07 ± 1,469 in WT to 17,91 ± 1,219 particles per square micron in mutant nerves (Figure 13B). This reduction could be due to a reduction of myelin compaction or to a reduction of P0 that can reach the cell membrane.

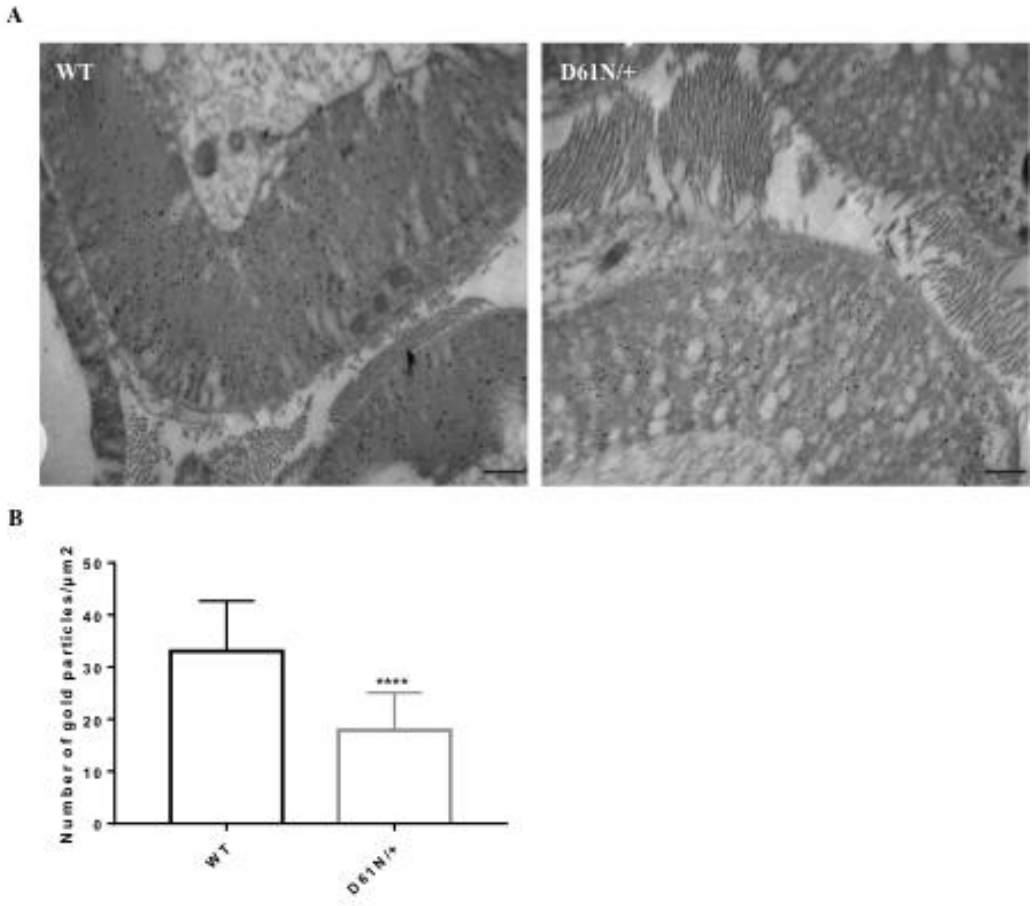

Figure 13: Immuno electron microscopy of WT and mutant sciatic nerves

A) Transverse section of a WT and *Mpz*$^{D61N/+}$ sciatic nerve. The amount of P0 on the cell membrane has been visualized using an anti-P0 antibody. Scale bar: 500nm.

B) Density of P0 molecules calculated as ratio between the number of gold particles and the membrane surface (Unpaired t test. P value < 0,0001).

Analysis of myelin proteins in WT and *Mpz*$^{D61N/+}$ mice

The 20-30% of the peripheral myelin is composed by proteins; in addition to the P0 protein, the other two most abundant proteins in the peripheral myelin are Peripheral Myelin Protein 22 (PMP22) and Myelin Basic Protein (MBP). PMP22 is involved in the determination of myelin thickness and in the maintenance of the compaction of myelin sheaths, while MBP participate in the maintenance of the major dense line [15]. Given the defects in myelin structure and myelin compaction of the model, we analyzed the quantity of the principal myelin proteins extracting total proteins from 1 month and 6 months sciatic nerves of WT and mutant mice; we also analyzed mRNA levels of MPZ, MBP and PMP22 at 1 month of age. As shown in western blots and in the quantification of protein levels, at 1 month MBP (even if not significantly) and PMP22 resulted decreased in mutant nerves, coherently with myelin defects previously shown, while MPZ levels didn't change; there were no significant differences in mRNA levels (Figure 14A, B, C). At 6 months of age, protein levels analysis confirmed the reduction in MBP and PMP22 (Figure 14D).

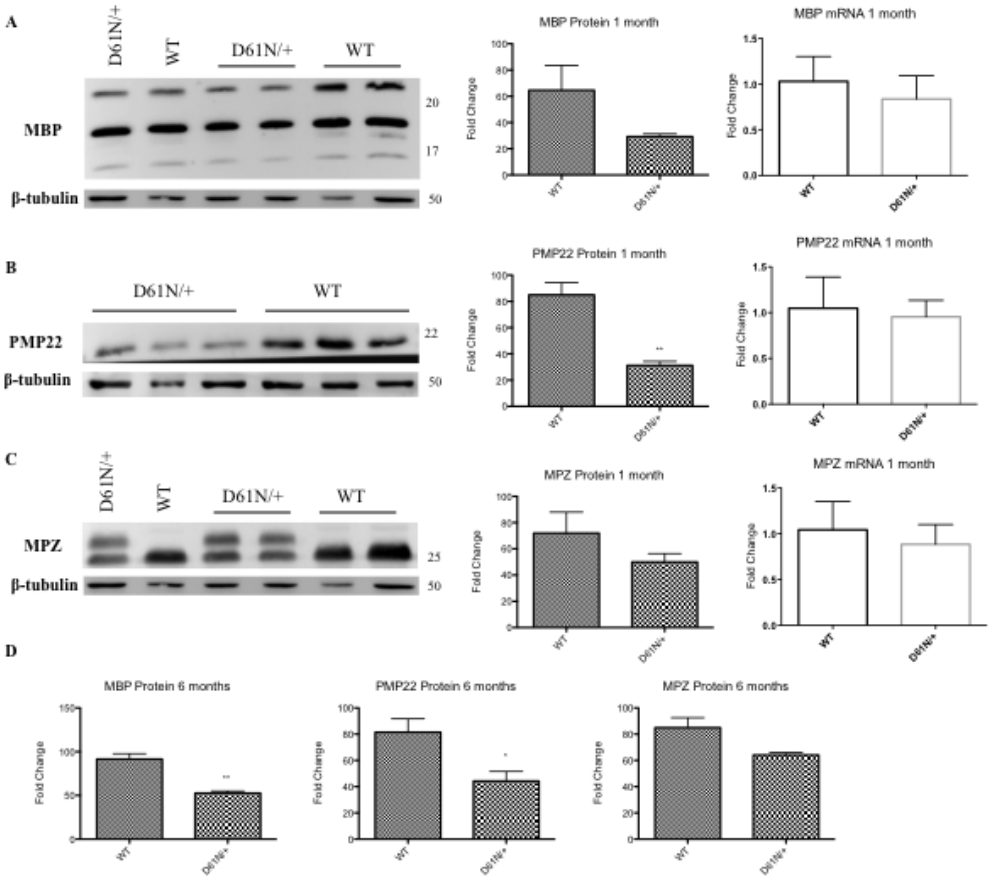

Figure 14: Analysis of myelin proteins

A) Western blot, protein quantification and mRNA level of MBP in sciatic nerves of 1 month WT and *Mpz*$^{D61N/+}$ animals (Error bars, SEM; unpaired, 2-tails, Student's *t* test; P value 0,1357 and 0,2779 respectively).

B) Western blot, protein quantification and mRNA level of PMP22 in sciatic nerves of 1 month WT and *Mpz*$^{D61N/+}$ animals (Error bars, SEM; unpaired, 2-tails, Student's *t* test; P value 0,0055 and 0,5991 respectively).

C) Western blot, protein quantification and mRNA level of MPZ in sciatic nerves of 1 month WT and *Mpz*$^{D61N/+}$ animals (Error bars, SEM; unpaired, 2-tails, Student's *t* test; P value 0,2702 and 0,3723 respectively).

D) Protein quantification for MPB, PMP22 and MPZ in sciatic nerves of 6 months WT and *Mpz*$^{D61N/+}$ animals (Error bars, SEM; unpaired, 2-tails, Student's *t* test; P value 0,0041; 0,0412 and 0,0555respectively).

β-tubulin was used as loading control for protein analysis.

Analysis of myelin pathways in WT and *Mpz*$^{D61N/+}$ mice

Schwann cell myelination is regulated by different players, downstream of which there are important signaling pathways, such as the PI-3 Kinase/AKT/mTOR pathway and the ERK/MAPK pathway. We evaluated the phosphorylation of AKT and ERK in WT and *Mpz*$^{D61N/+}$ mice at 1 month of age. Both p-AKT and p-ERK resulted decrease in *Mpz*$^{D61N/+}$ mice, indicating a defect in myelination (Figure 15A, B)

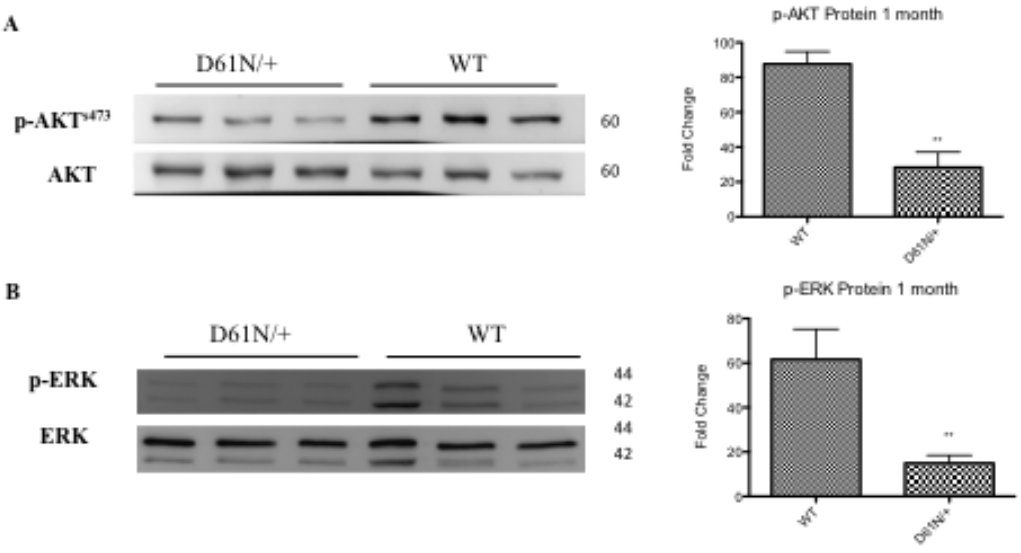

Figure 15: Analysis of two different myelination pathways in WT and mutant sciatic nerves

A) Western blot analysis and protein quantification of phospho-AKT in sciatic nerves of WT and *Mpz*$^{D61N/+}$ animals at 1 month (Error bars, SEM; unpaired, 2-tails, Student's *t* test; P value 0,0062).

B) Western blot analysis and protein quantification of phospho-ERK in sciatic nerves of WT and *Mpz*$^{D61N/+}$ animals at 1 month (Error bars, SEM; by unpaired, 2-tails, Student's *t* test; P value 0,0078).

Analysis of UPR activation in WT and *Mpz*$^{D61N/+}$ mice

Several *MPZ* mutations cause the mutant protein to be retained in the endoplasmic reticulum (ER), activating a canonical Unfolded Protein Response (UPR) [124, 165-167]; the partial intracellular retention of mutant protein *in vitro,* led us to evaluate if the mutation *Mpz*$^{D61N/+}$ caused the activation of these mechanisms. We measured the expression of ER stress/UPR markers such as BiP, C/EBP-Homologous Protein (CHOP), phosphorylated eukaryotic Initiation Factor 2 α (P-eIF2α) and spliced X-box Binding Protein 1 (Xbp1s) in sciatic nerves at 1 month. *Mpz*$^{D61N/+}$ nerves showed a trend towards higher levels for all the markers analysed as compared with WT nerves, suggesting an activation of UPR in mutant nerves (Figure 16A, B). However, by 6 months of age there is no more activation of BiP and P-eIF2α markers (Figure 16C), suggesting that this activation is a transient event present only during the active phase of myelination.

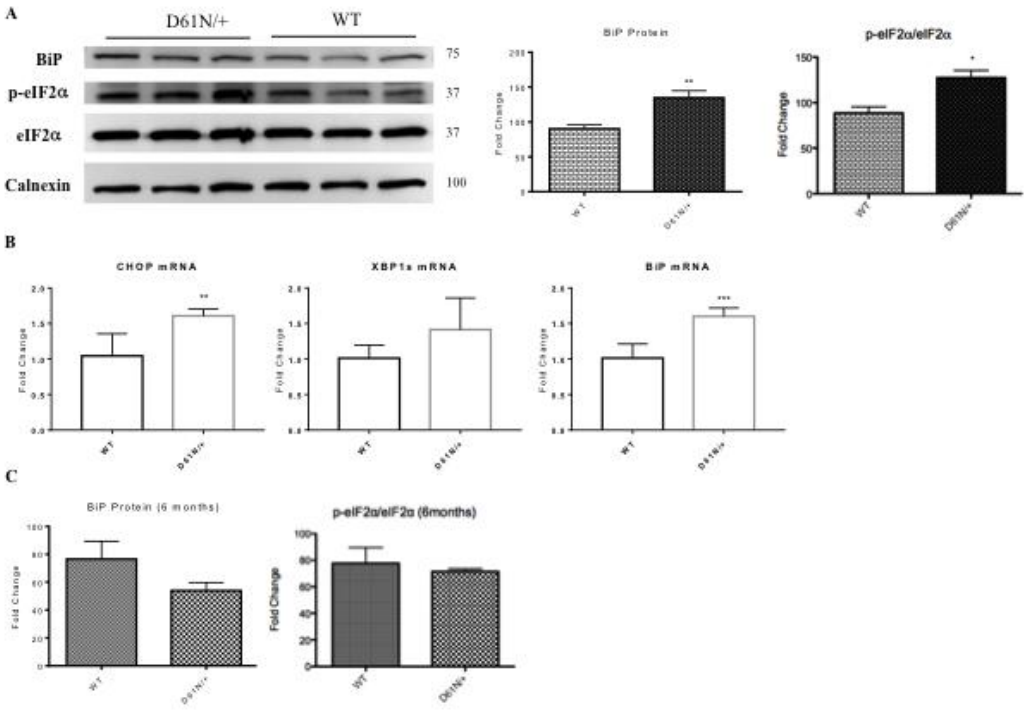

Figure 16: Analysis of ER stress/UPR levels

A) Western blot analysis and protein level for the UPR markers BiP and p-eIF2α/eIF2α in WT and *Mpz*$^{D61N/+}$ sciatic nerves at 1 month; calnexin was used as loading control (Error bars, SEM; unpaired, 2-tails, Student's *t* test; P value 0,0028 and 0,0203 respectively).

B) qRT-PCR analysis on 1 month sciatic nerve extracts for CHOP, spliced Xbp1 and BiP. (Error bars, SEM; unpaired, 2-tails, Student's *t* test; P value 0,0047; 0,0983 and 0,0005 respectively)

C) Protein levels of BiP and p-eIF2α/eIF2α in WT and *Mpz*$^{D61N/+}$ sciatic nerves at 6 months measured by densiometric analysis (Error bars, SEM; unpaired, 2-tails, Student's *t* test; P value 0,1824 and 0,6476 respectively).

NB-DNJ: a possible benefit for hyperglycosylated mutations *in vitro* and *ex vivo* models

Recent papers [146] [168] suggested that gain-of-glycosylation mutations may benefit from imino-sugars administration, a class of compound potentially able to modify N-glycosylation of proteins. Therefore, we treated Hela cells expressing the D61N mutation with 750 µM NB-DNJ to assess if this compound was able to complement *in vitro* the phenotype, by improving the trafficking of the mutant

protein and cell adhesion. Immunofluorescence analysis suggested that the treatment ameliorated P0D61N protein trafficking, reduced its intracellular retention and improved adhesion, without affecting WT protein trafficking; interestingly, the treatment of cells with the compound seems to reduced the MW of mutant protein, as though there was a modification in glycosylation (Figure 17 A, B, C).

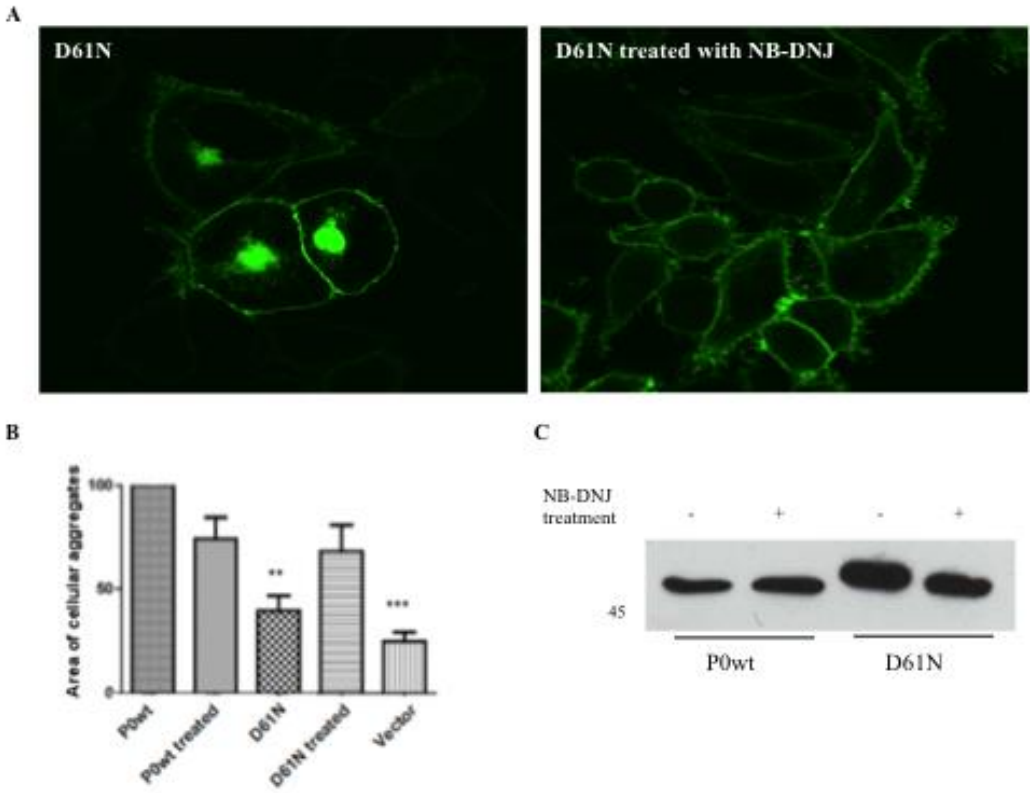

Figure 17: Treatment with NB-DNJ in *in vitro*

A) Confocal images of HeLa cells expressing the mutant protein D61N before and after the treatment with NB-DNJ; the treatment ameliorates protein trafficking.

B) Adhesion assay performed on HeLa cells treated with NB-DNJ, the non treated protein have been used as control (One-way ANOVA corrected for multiple comparison using statistical Tukey test).

C) Western blot analysis of HeLa cells expressing the P0wt protein and the mutant protein D61N treated with NB-DNJ; the treatment reduced the MW of mutant protein.

Based on these results, we tested NB-DNJ in an *ex vivo* system, by establishing myelinating organotypic DRG cultures from wild-type and *Mpz*$^{D61N/+}$ 13,5-day-old embryos (Figure 18). In mutant DRGs cultures, the number of myelinated internodes tend to be reduced; mutant DRGs also presented frequent myelin swellings reminiscent of the tomacula-like structures we saw in nerves.

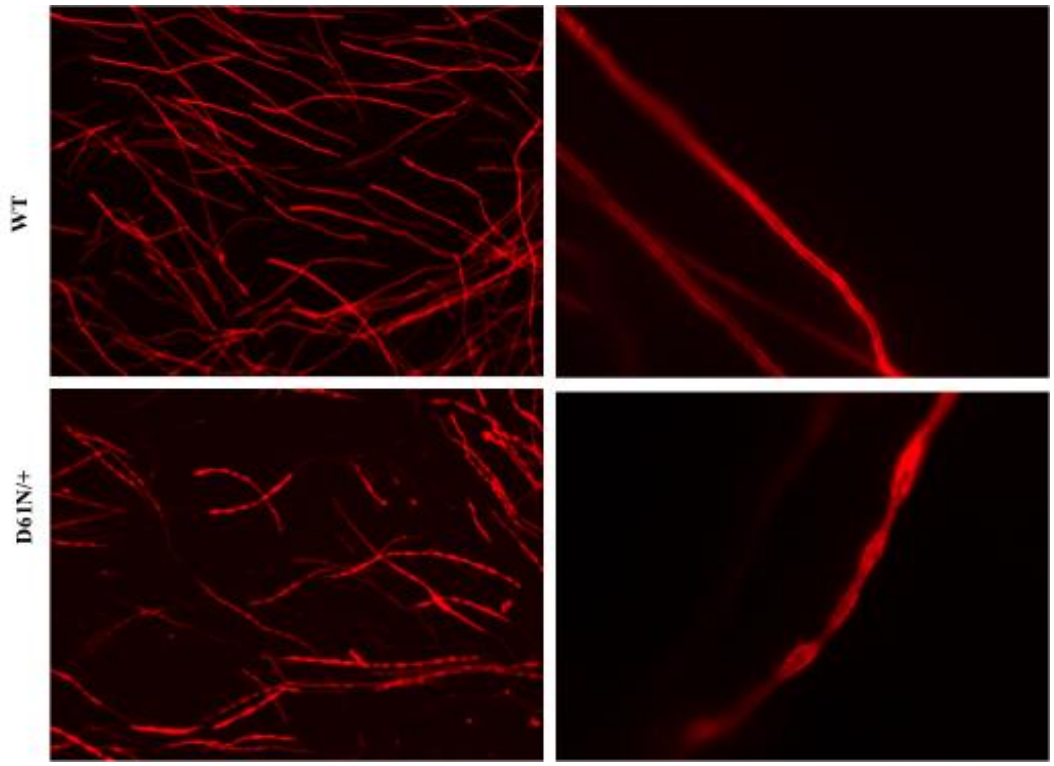

Figure 18: DRG coculture from WT and *Mpz*$^{D61N/+}$ embryos

Images of WT and *Mpz*$^{D61N/+}$ DRGs stained for MBP. In mutant cultures there are fewer and often abnormal myelinated internodes.

Magnification: 20X; 100X

We reasoned that NB-DNJ, by modulating N-glycosylation, could ameliorate the morphology of myelinated internodes; we treated WT and *Mpz*$^{D61N/+}$ DRGs with 50 µM and 100 µM NB-DNJ; DRGs treated only with ascorbic acid were used as control. Two weeks treatment with NB-DNJ appeared to partially rescue myelin abnormalities in a dose dependent way: myelin defects were reduced by 25% after the treatment with 50 µM, and by 50% with the higher dosage (Figure 19A).

To better investigate this myelin abnormalities reduction, we performed a western

blot analysis on DRGs in the three different conditions (treated only with ascorbic acid or treated with 50 µM and 100 µM NB-DNJ). However, what we founded is that, after the treatment with NB-DNJ, the proteins P0 and MBP appeared reduced, suggesting that a partial reduction of total myelin proteins might contribute to the amelioration of myelin morphology (Figure 19B).

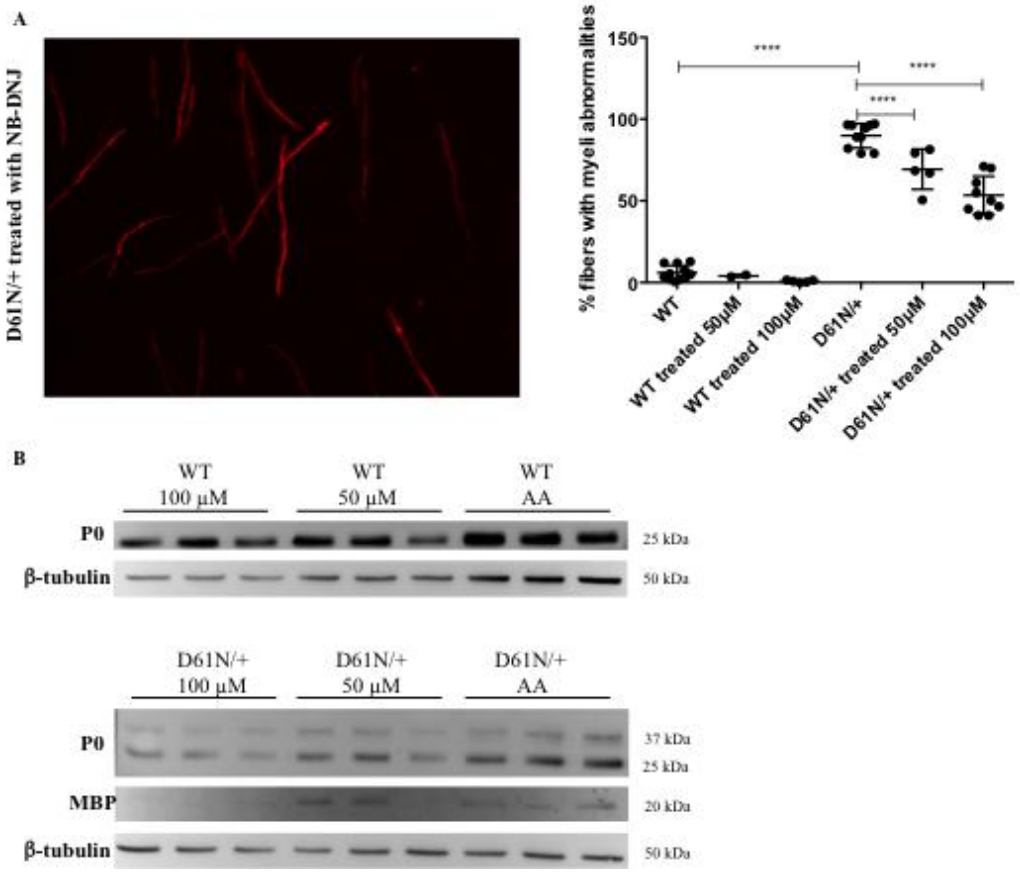

Figure 19: Treatment with NB-DNJ in *ex vivo* models

A) DRG cultures from WT and *Mpz*$^{D61N/+}$ embryos treated with 50 µM or 100 µM NB-DNJ; myelin abnormalities seem to decrease. Quantification of myelin abnormalities before and after the treatment with NB-DNJ (One-way ANOVA corrected for multiple comparison using statistical Holm-Sidak test; P value < 0,0001).

B) Western blot analysis of DRG from WT and *Mpz*$^{D61N/+}$ embryos treated with only ascorbic acid (AA) or also with NB-DNJ for 14 days. P0 and MBP were analyzed and β-tubulin was used as loading control.

DISCUSSION

Motor, sensory and cognitive functions of the nervous system require a rapid and precise impulse propagation; to allow this, in vertebrates, axons are surrounded by the myelin sheath. In the PNS, the plasma membrane of SCs forms consecutive wrappings around the axons to form myelin. In order to achieve this goal, SCs synthesize a huge amount of lipids and proteins. This event is strictly regulated, as alterations in the amount or in the (genomic) sequence of myelin proteins cause, in humans, peripheral neuropathies, known as Charcot-Marie-Tooth (CMT) disease. CMT represent a heterogeneous group of hereditary disorders and, with a prevalence of around 1:2500, is the most common inherited neurological condition. CMT is caused by mutations in genes that encode for different proteins with different functions, such as myelin compaction and maintenance or cytoskeleton formation, axonal transport or mitochondrial metabolism. The most common CMT type, accounting for ~50% of all CMTs, is CMT1A caused by duplication on chromosome 17p11.2, a region that includes the *PMP22* gene; CMT1X is the second most common CMT type and is caused by mutations in the *GJB1* gene. Finally, mutations in *MPZ* gene are estimated to account for ~5% of all CMT cases. Clinical manifestations of CMTs are heterogeneous, suggesting that multiple and different pathogenic mechanisms [169] are involved, rendering the finding of effective therapies very hard. Great advances in understanding the patho-biology of CMTs have been made, but to date no cure is available [109, 169]. In particular, more than 200 different mutations in the sequence of P0, mostly in the extracellular domain, are associated with diverse phenotypic manifestations [121]. *MPZ* mutations, in fact, can give rise to different phenotypes: an early-onset phenotype, with onset of the disease during the 1st decade of life and characterized by very slow MNCV, a late-onset phenotype, with onset from the 2nd decades of life and with a normal or minimally impaired MNCV, or a childhood-adolescent-onset, with motor and sensory symptoms during the 2nd decades of life, and showing a slowly progressive course, with MNCV of intermediate range [123]. Among the different pathogenetic mechanisms, the activation of the Unfolded Protein Response is the most

extensively studied: this mechanism occurs when a mutated protein is retained into the ER and it has been estimated that it could play a role in about one half of CMT1B neuropathies [108, 170]. This also means that there are other mechanisms responsible for CMT. Indeed, another mechanism could be misglycosylation, that can cause the loss of the native glycosylation site, or the gain of a new glycosylation site [125, 126].

Misglycosylation, not only for CMTs, is an increasingly recognized pathomechanism: in fact, important papers [146, 147] have demonstrated that the generation of new glycosylation sites or the removal of constitutive ones are phenomena more frequent than expected. In particular, the analysis of mutation in 577 genes coding for membrane proteins revealed that mutations causing a gain of glycosylation account for about 1,4% of all missense mutations [146]. While peripheral myelin is largely composed by glycoproteins, misglycosylation has never been investigated as cause of peripheral neuropathies; for this reason, we decided to fully investigate how peripheral myelination is affected by P0 misglycosylation using *in vitro* and *in vivo* systems.

In vitro analysis of hyperglycosylated and hypoglycosylated mutations

We characterized the effects of P0 mutants predicted to cause loss- or gain- of glycosylation in different *in vitro* models.

We studied different mutations that can be divided in two groups:

- the mutations that create a second Asp122-X-Thr124 sequence and generate proteins with a double glycosylation site: $D^{61}\rightarrow N$, $D^{109}\rightarrow N$, $D^{118}\rightarrow N$ and $K^{138}\rightarrow N$
- the mutations located in the Asp122-X-Thr124 consensus sequence that generate mutant proteins predicted to be unglyglycosylated: $T^{124}\rightarrow M$, $T^{124}\rightarrow K$, $T^{124}\rightarrow A$, $N^{122}\rightarrow A$ and $N^{122}\rightarrow S$.

All these mutation had been already reported in literature [126, 148-155], but in most of them misglycosylation was not really proven, as well as the consequences of this event have not been fully investigated.

Through transient transfections of HeLa and Schwannoma rat cells, we studied mutant proteins tagged with EGFP: we demonstrated that the mutations that were

predicted to introduce a new glycosylation site generated proteins with a higher MW as compared to the P0wt, whereas the proteins predicted to lose the constitutive glycosylation site had a lower MW; we demonstrated also that in both cases the difference in MW was indeed due to the acquisition or loss of oligosaccharides. Another important difference founded between the two groups of mutant proteins were the localization: all the unglycosylated proteins reached the plasma membrane as the P0wt protein; instead, the hyperglycosylated proteins were partially retained intracellularly. The partial retention could be due to the steric hindrance caused by the second oligosaccharide that increase the MW compared to the P0wt and that could slow down the normal protein trafficking. As matter of fact, the correct trafficking of P0 is fundamental: in fact, only when the protein reaches the plasma membrane it can perform its adhesive function, while a mislocalized protein will severely impair its function and potentially cause a cellular toxicity. This impairment has been highlighted with the adhesion test: the hyperglycosylated proteins that are partially retained intracellularly showed a reduced adhesion capacity if compared to both P0wt and the unglycosylated proteins. The latter instead normally reached the plasma membrane and, in almost all cases, display a normal adhesion capacity, confirming the importance of a proper protein trafficking for the P0 protein. Moreover, the slowdown in protein trafficking is associated with an increased endocytosis of hyperglycosylated proteins, supporting the hypothesis of a greater instability of mutant proteins compared to the P0wt.

Interestingly, the two groups of mutations in patients give rise to different phenotypes: it was reported that most the unglycosylated mutations were associated with a late-onset neuropathy in which there was a clear axonal involvement; instead, the hyperglycosylated mutations correlated with an early-onset neuropathy, characterized by a demyelinating phenotype [126, 148-155]. However, two exceptions were reported: the $D^{118}\rightarrow N$ amino acidic substitution, that give rise to a mild hyperglycosylation, was founded in a family affected by CMT2 [154], while the $T^{124}\rightarrow K$ was founded in a patient with congenital hypomyelination neuropathy [150]; in this latter case, it was hypothesized that the mutated allele of the *MPZ* gene could have a dominant-negative effect. The

divergent phenotypes are the consequence of different mutations that modify P0 protein function in different manners: the hypoglycosylated mutations do not impair directly the P0 function but probably interfere with the correct SC-axon interaction, unlike to what hyperglycosylated mutations do, that is to distort the P0 structure and interfere with the correct myelination during the development.

MPZ^{D61N}, a knock-in model of CMT1B and hyperglycosylation

Several animal models of CMT have been developed, some of them extremely close to the human pathology [171]. However, at the moment there are no animal models of hyperglycosylation available; so, we decided to generate a full knock-in mouse model carrying the hyperglycosylated mutation *MPZ*^{D61N}. The model was generated by the Core Facility for Conditional Mutagenesis (CFCM) at the San Raffaele Scientific Institute, using the CRISPR/Cas9 technology. The *MPZ*^{D61N} mouse model represent the first knock-in model of CMT generated using these technique. Thanks to the technology used for the generation, only the desired amino acidic substitution $D^{61}\rightarrow N$ has been introduced. Biochemical analysis of the P0 protein revealed the presence of the amino acidic substitution that introduce the second glycosylation site.

The mice showed neuropathological evidence as early as P15: even if the mutant mice were viable and grew similarly to the WT, *MPZ*$^{D61N/+}$ mice presented an evident tremor that interfered with their motor capacity which was reduced as compared to WT mice. Also from an electrophysiological point of view they appeared severely compromised: at 1 month of age, a dramatic reduction in nerve conduction velocity and in the cMAP were evident; the same analysis repeated at 3 months of age showed a further worsening since the electrophysiological parameters were unrecordable in mutant mice.

Morphological evidence in *Mpz*$^{D61N/+}$ mice

Dysmyelination and/or demyelination is an hallmark of CMTs caused by mutations in *MPZ* gene. The behavioural and neurophysiological analysis outlined above suggested that the *Mpz*$^{D61N/+}$ mutation indeed determined a dramatic impairment of nerve structure. Accordingly, sciatic nerve morphology from

Mpz$^{D61N/+}$ mice showed de/dysmyelination: myelin thickness is reduced as compared to WT nerves and also axons diameter appeared reduced, confirming that the introduced mutation modified the correct structure and function of the protein. Another peculiarity of the nerves of these mice is the presence of tomacula-like structures, represented by axons on which myelin lamellae are repeatedly and redundantly wrapped causing focal myelin swellings. Interestingly, these structures increased in number with the age of mice, which could explain the dramatic worsening of the neurophysiology at 3 months and the motor impairment, since it is conceivable that all these abnormalities might interfere with the correct nerve conduction and, consequently, functionality. It is important to emphasize that these mice faithfully recapitulate the human pathology: in fact, in both patients carrying the $D^{61}\rightarrow N$ amino acidic substitution, sural nerves presented fibers surrounded by thin myelin sheaths, tomacula-like structures and also fibers with abnormally compacted myelin [126, 152]. It might seems paradoxical that the same mutation can give rise to different phenotypes: demyelination on one side, and redundant myelin on the other. As already reported in literature [172, 173] the presence of both pathological features could suggest that the pathomechanism underlying the loss of myelin compaction and the myelin redundancy may be the same; alternatively it is possible that the amount of mutant protein reaching the cell membrane could cause myelin uncompaction, while the retained amount could cause a misregulation in myelin protein expression leading to demyelination.

Tomacula-like structures, together with outfoldings or infoldings, have been already described in other CMT models [159, 174, 175], and are considered pathognomonic in CMT4B, a severe recessive form of CMT, caused by mutations in genes coding for Myotubularin 2 or 13. However, the pathogenic mechanism that cause this myelin abnormalities is still unknown. Tomacula-like structures are characterized by myelin that, in addition to being redundant, is also uncompacted. P0 contributes to form the intracellular “major dense line”; to fulfil this function, the extracellular domain contains a conserved sequence that has a role in mediating homophilic P0 interaction. However, crystal structure analysis of P0 indicates that this region is also implicated in the formation of P0 homotetramers

in trans, keeping together the adjacent wraps of myelin. The presence of an extra glycan, with its steric hindrance, could interfere with myelin compaction and this could cause the uncompaction observed in the myelin in nerves of *Mpz*$^{D61N/+}$ mice. Differently from other mice model [174], we founded that this tomacula-like structures are not prevalently present at the paranodal regions, but they are distributed along the entire internode. By immuno-EM we measured the amount of P0 expressed on the cell membrane and we found that the quantity of P0 in mutant nerves was reduced as compared to the amount of P0 in WT myelin. This could be due to the reduction of myelin compaction (that would increase the surface) or to the reduction of P0 that can reach the plasma membrane: in fact, either the increase in myelin lamellae distance, or the partial retention of the P0 might explain this reduction. However, the fact that the mice carry both the P0wt and the *MPZ* mutation, did not allow us to better dissect the *in vivo* trafficking of the mutated protein.

Myelin in PNS contains a huge amount of proteins: the principal two proteins, in addition to P0, are MBP and PMP22 that, even if in a different way, are both involved in the formation and/or maintenance of the myelin. MBP, that is localized in the major dense line of compact myelin, has an important role in the compaction and maintenance of myelin and it interacts with lipids of the membrane [15]. However, in the PNS MBP is not necessary for the formation of myelin lamellae while in CNS, mice lacking MBP showed defects in myelin compaction [176]. PMP22 is localized in compact myelin and has a role in myelin formation and maintenance; it mediates both homophilic interaction between PMP22 molecules and heterophilic interaction with P0. The defects in myelin compaction found in our model led us to analyze also these two proteins: despite no differences in mRNA levels, the overall amount of proteins from mutant nerves appeared reduced as compared to WT nerves. It was already reported that both P0 and PMP22 proteins are targeted to the plasma membrane in which they are inserted into the same sites, providing a possible explanation why mutations in either one of these genes share common phenotypes: in some patients, heterozygotes for the mutated gene, the myelin is initially formed, but later loss of compaction and demyelination proceeds, indicating that a lower amount of

functional protein is not sufficient to sustain a compact myelin sheath [177]. Indeed, mutations in P0 and PMP22 could also produce congenital hypomyelination neuropathy [178, 179]. This correlation between P0 and PMP22 might explain why also in our model in which the mutation is in P0, we observed a large reduction also of PMP22. Interestingly, it was reported that *PMP22/+* mice, that are models for the inherited human peripheral neuropathy HNPP, are characterized by tomaculous neuropathy with multifocal thickenings of the myelin sheaths, with evidence of para- and internodal tomacula in teased fibers [70]. The morphological similarities between *PMP22/+* mice and $Mpz^{D61N/+}$ mice sustain the hypothesis that the decrease in PMP22 protein levels that we observed in sciatic nerves of $Mpz^{D61N/+}$ mice could be one of the factors causing morphological defects described above. Another interesting similarity between P0 and PMP22 is that both proteins have a single L2/HNK1 epitope, which is known to participate in adhesive interactions. Indeed, even if the glycosylation is functionally important [180], it does not seem to be essential for either the homophilic P0-P0 [181] or heterophilic P0-PMP22 interactions; thus, the precise function of this sugar moiety is still unclear.

Analysis of different pathways present in $Mpz^{D61N/+}$ model

PNS myelination is tightly regulated by NRG1 type III and by different pathways that are activated downstream of NRG1 type III such as PI-3 Kinase/AKT/mTOR pathway [39], the ERK/MAPK pathway [42], the cAMP signalling [43] and the Calcineurin/NFAT signalling [44]; however, the precise mechanism that drives myelination and differentiation is not completely understood. The PI3-kinase pathway activates two different responses in SCs: the first depends upon NRG1 type III activation and induces myelination, whereas the second may negatively influence myelination [39]. Another pathway that participate to PNS myelination is ERK1/2 signaling, but also in this case with a dual role: ERK1/2 ablation during development was shown to impair SC differentiation and myelination [42], while the activation of the pathway led to increased myelin growth [182, 183]. In our mouse model, the phosphorilation of AKT and ERK, and so their activation, is decreased in respect to the WT; this suggest that the mutation somehow

determines a dysregulation of the pathways that control myelination.

The partial intracellular retention of the mutated protein led us to also evaluate the activation of the Unfolded Protein Response (UPR). This pathway is of particular interest because recently different molecules that can attenuate the protein retention in the ER and the subsequent activation of the UPR have been identified [50, 184-186], pointing at the modulation of the UPR as a possible therapeutic avenue; as such it was important to understand if the pathway was active in our mouse model. We evaluated the protein levels of two component of the UPR pathway, as BiP and phospho-eiF2α at 1 month and 6 months of age in WT and mutant mice: at 1 month protein levels were mildly increased in mutant mice, indicating the activation of the pathway; however, at 6 months of age, protein levels were comparable with WT, suggesting that this pathway is only transiently activated. Normally the activation of the UPR is much stronger than what we observed in the *Mpz*$^{D61N/+}$ model and appears to be constant during time [50, 166, 167], indicating that UPR is probably not the principal mechanism that causes the pathology.

NB-DNJ: a possible treatment for hyperglycosylation?

The current lack of effective therapies always leads us to seek new strategies for the treatment of CMT. The use of a class of compounds belonging to the imino-sugar category was proposed as a potential treatment for gain of glycosylation mutations [168, 187]. These molecules would be able to interfere with specific enzymes involved in the protein glycosylation chain, such as Golgi and endoplasmic reticulum glycosydases [188]. Among these molecules, N-butyl-deoxynojirimycin (NB-DNJ) is a very interesting drug that has already been used for different disorders with a good safety profile in humans. Miglustat, the commercial name of the molecule, is used for the treatment of cyctic fibrosis [189], Gaucher disease [190] and Niemann-Pick disease, a lysosomal storage pathology [191]. Miglustat prevents the enzyme glucosylceramide synthase, involved in the first step of the production of glycosphingolipids, thus reducing the synthesis of glycosphingolipids in cells. Moreover, Miglustat inhibits the N-glycan processing enzyme α-glucosydases I and II, localized in the ER.

The treatment with Miglustat of cells transfected with the mutated protein revealed an amelioration of the protein trafficking that appeared to be less intracellular retained. Further experiments showed also that cell transfected with the mutant protein showed a partial rescue of adhesive capacity after Miglustat treatment; importantly, also the MW of the protein after treatment was decreased, indicating that probably the treatment was effectively acting on the glycan composition, restoring the normal structure of the protein.

To better evaluate the effect of this treatment and before using Miglustat for the treatment of *Mpz*$^{D61N/+}$ mice, we tested this drug on organotypic Dorsal Root Ganglion (DRG) coculture, a system in which SCs and neurons are both present, thus better modeling the human disease. We established DRGs cocultures from WT and mutant embryos and we observed that in mutant DRGs the myelinated tracts were less in number; interestingly, we also confirmed in this system the morphological defects typical of this mouse model: in fact, the myelinated tracts of DRGs from mutant embryos present many myelin abnormalities and appeared like a "string of pearls", due to the presence of focal enlargements of the myelin. So both features appear to be maintained, confirming us that this is indeed a good system on which testing potential treatments. After treatment with Miglustat, the morphology of mutant organotypic DRG cocultures did change significantly since the number of myelin tracts presenting myelin abnormalities was reduced by 25% after the treatment with the lower concentration of NB-DNJ, and by 50% with the higher dosage. This first results made us hope to have found a potential drug for the treatment of hyperglycosylation. However, WB analysis revealed that in DRGs, Miglustat did not appear to modify the glycosylation of P0, since the MW of the mutant P0 did not change after the treatment. Indeed, we also found that the quantity of another myelin protein such as MBP was reduced with the treatment; we therefore reasoned that the overall reduction in myelin proteins could explain the morphological rescue, likely due to a decrease in myelin production rather than to a correction of glycosylation.

Therefore, we think that it would be important to perform a mass spectrometry experiment to characterize the extra glycan introduced with the mutation and also the native oligosaccharide. Only in that way, we could better understand how to

act in a targeted manner.

In conclusion: we investigated *in vitro* the effects of P0 mutants causing gain- or loss- of glycosylation and confirmed that mutations predicted to cause a gain- or loss- of glycosylation corresponded to hyper or unglycosylated P0 mutants. Further, we studied for each P0 variant the trafficking through the secretory pathway and the effect of the changed amino acid on the adhesive function of P0, thus establishing a precise genotype-phenotype correlation. Indeed, most mutations causing a loss of glycosylation were associated with a late-onset phenotype and a mild cellular phenotype, whereas the majority of mutations associated with a gain of glycosylation, caused a severe, early-onset neuropathy with significant consequences on P0 trafficking and adhesive properties; these data confirm previous observations that, in general, losing a glycosylation site is less harmful than acquiring a new one.

Then we established a murine model of MPZ^{D61N} mutation to evaluate *in vivo* the effects of hyperglycosylation. This is the first transgenic mouse, obtained with the CRISPR/Cas9 technique, expressing a gain-of-glycosylation mutant, providing a model of CMT1B due to hyperglycosylation of P0.

Therefore, through *in vitro*, *in vivo* and *ex vivo* experiments, we established the ultimate link between P0 misglycosylation and peripheral nerve impairment and we performed preliminary experiments to evaluate a specific therapy for this pathomechanism. All our results may have implications for other diseases caused by hyperglycosylation such as rare mutations causing Cystic Fibrosis, different immunodeficiencies [146] and myoclonus-dystonia, due to a gain-of-glycosylation mutation in ε-sarcoglycan [156].

BIBLIOGRAPHY

1. Scherer, S.S., *Nodes, paranodes, and incisures: from form to function.* Ann N Y Acad Sci, 1999. **883**: p. 131-42.
2. Arroyo, E.J. and S.S. Scherer, *On the molecular architecture of myelinated fibers.* Histochem Cell Biol, 2000. **113**(1): p. 1-18.
3. Salzer, J.L., P.J. Brophy, and E. Peles, *Molecular domains of myelinated axons in the peripheral nervous system.* Glia, 2008. **56**(14): p. 1532-40.
4. Buttermore, E.D., C.L. Thaxton, and M.A. Bhat, *Organization and maintenance of molecular domains in myelinated axons.* J Neurosci Res, 2013. **91**(5): p. 603-22.
5. Poliak, S. and E. Peles, *The local differentiation of myelinated axons at nodes of Ranvier.* Nat Rev Neurosci, 2003. **4**(12): p. 968-80.
6. Bunge, M.B., R.P. Bunge, and G.D. Pappas, *Electron microscopic demonstration of connections between glia and myelin sheaths in the developing mammalian central nervous system.* J Cell Biol, 1962. **12**: p. 448-53.
7. Geren, B.B. and F.O. Schmitt, *THE STRUCTURE OF THE SCHWANN CELL AND ITS RELATION TO THE AXON IN CERTAIN INVERTEBRATE NERVE FIBERS.* Proc Natl Acad Sci U S A, 1954. **40**(9): p. 863-70.
8. Nave, K.A. and H.B. Werner, *Myelination of the nervous system: mechanisms and functions.* Annu Rev Cell Dev Biol, 2014. **30**: p. 503-33.
9. Balice-Gordon, R.J., L.J. Bone, and S.S. Scherer, *Functional gap junctions in the schwann cell myelin sheath.* J Cell Biol, 1998. **142**(4): p. 1095-104.
10. Court, F.A., et al., *Restricted growth of Schwann cells lacking Cajal bands slows conduction in myelinated nerves.* Nature, 2004. **431**(7005): p. 191-5.
11. Sherman, D.L., et al., *Drp2 and periaxin form Cajal bands with dystroglycan but have distinct roles in Schwann cell growth.* J Neurosci, 2012. **32**(27): p. 9419-28.

12. Saito, F., et al., *Unique role of dystroglycan in peripheral nerve myelination, nodal structure, and sodium channel stabilization.* Neuron, 2003. **38**(5): p. 747-58.
13. Deerinck, T.J., et al., *Clustering of voltage-sensitive sodium channels on axons is independent of direct Schwann cell contact in the dystrophic mouse.* J Neurosci, 1997. **17**(13): p. 5080-8.
14. Salzer, J.L., *Clustering sodium channels at the node of Ranvier: close encounters of the axon-glia kind.* Neuron, 1997. **18**(6): p. 843-6.
15. Garbay, B., et al., *Myelin synthesis in the peripheral nervous system.* Prog Neurobiol, 2000. **61**(3): p. 267-304.
16. Woodhoo, A. and L. Sommer, *Development of the Schwann cell lineage: from the neural crest to the myelinated nerve.* Glia, 2008. **56**(14): p. 1481-90.
17. Jessen, K.R. and R. Mirsky, *Schwann cells and their precursors emerge as major regulators of nerve development.* Trends Neurosci, 1999. **22**(9): p. 402-10.
18. Jessen, K.R. and R. Mirsky, *Signals that determine Schwann cell identity.* J Anat, 2002. **200**(4): p. 367-76.
19. Voyvodic, J.T., *Target size regulates calibre and myelination of sympathetic axons.* Nature, 1989. **342**(6248): p. 430-3.
20. Gershon, M.D., *V. Genes, lineages, and tissue interactions in the development of the enteric nervous system.* Am J Physiol, 1998. **275**(5): p. G869-73.
21. Feltri, M.L., Y. Poitelon, and S.C. Previtali, *How Schwann Cells Sort Axons: New Concepts.* Neuroscientist, 2016. **22**(3): p. 252-65.
22. Monk, K.R., M.L. Feltri, and C. Taveggia, *New insights on Schwann cell development.* Glia, 2015. **63**(8): p. 1376-93.
23. Martini, R., *The effect of myelinating Schwann cells on axons.* Muscle Nerve, 2001. **24**(4): p. 456-66.
24. Pereira, J.A., F. Lebrun-Julien, and U. Suter, *Molecular mechanisms regulating myelination in the peripheral nervous system.* Trends Neurosci, 2012. **35**(2): p. 123-34.

25. Mirsky, R., et al., *Novel signals controlling embryonic Schwann cell development, myelination and dedifferentiation.* J Peripher Nerv Syst, 2008. **13**(2): p. 122-35.
26. Parkinson, D.B., et al., *c-Jun is a negative regulator of myelination.* J Cell Biol, 2008. **181**(4): p. 625-37.
27. Jessen, K.R. and R. Mirsky, *The origin and development of glial cells in peripheral nerves.* Nat Rev Neurosci, 2005. **6**(9): p. 671-82.
28. Castelnovo, L.F., et al., *Schwann cell development, maturation and regeneration: a focus on classic and emerging intracellular signaling pathways.* 2017. **12**(7): p. 1013-1023.
29. Birchmeier, C. and K.A. Nave, *Neuregulin-1, a key axonal signal that drives Schwann cell growth and differentiation.* Glia, 2008. **56**(14): p. 1491-7.
30. Garratt, A.N., S. Britsch, and C. Birchmeier, *Neuregulin, a factor with many functions in the life of a schwann cell.* Bioessays, 2000. **22**(11): p. 987-96.
31. Nave, K.A. and J.L. Salzer, *Axonal regulation of myelination by neuregulin 1.* Curr Opin Neurobiol, 2006. **16**(5): p. 492-500.
32. Michailov, G.V., et al., *Axonal neuregulin-1 regulates myelin sheath thickness.* Science, 2004. **304**(5671): p. 700-3.
33. Taveggia, C., et al., *Neuregulin-1 type III determines the ensheathment fate of axons.* Neuron, 2005. **47**(5): p. 681-94.
34. Woodhoo, A., et al., *Notch controls embryonic Schwann cell differentiation, postnatal myelination and adult plasticity.* Nat Neurosci, 2009. **12**(7): p. 839-47.
35. Rosenberg, S.S., B.K. Ng, and J.R. Chan, *The quest for remyelination: a new role for neurotrophins and their receptors.* Brain Pathol, 2006. **16**(4): p. 288-94.
36. Golan, N., et al., *Genetic deletion of Cadm4 results in myelin abnormalities resembling Charcot-Marie-Tooth neuropathy.* J Neurosci, 2013. **33**(27): p. 10950-61.

37. Mogha, A., et al., *Gpr126 functions in Schwann cells to control differentiation and myelination via G-protein activation.* J Neurosci, 2013. **33**(46): p. 17976-85.
38. Trimarco, A., et al., *Prostaglandin D2 synthase/GPR44: a signaling axis in PNS myelination.* Nat Neurosci, 2014. **17**(12): p. 1682-92.
39. Heller, B.A., et al., *Functionally distinct PI 3-kinase pathways regulate myelination in the peripheral nervous system.* J Cell Biol, 2014. **204**(7): p. 1219-36.
40. Domenech-Estevez, E., et al., *Akt Regulates Axon Wrapping and Myelin Sheath Thickness in the PNS.* 2016. **36**(16): p. 4506-21.
41. Napoli, I., et al., *A central role for the ERK-signaling pathway in controlling Schwann cell plasticity and peripheral nerve regeneration in vivo.* Neuron, 2012. **73**(4): p. 729-42.
42. Newbern, J.M., et al., *Specific functions for ERK/MAPK signaling during PNS development.* Neuron, 2011. **69**(1): p. 91-105.
43. Glenn, T.D. and W.S. Talbot, *Signals regulating myelination in peripheral nerves and the Schwann cell response to injury.* Curr Opin Neurobiol, 2013. **23**(6): p. 1041-8.
44. Kao, S.C., et al., *Calcineurin/NFAT signaling is required for neuregulin-regulated Schwann cell differentiation.* Science, 2009. **323**(5914): p. 651-4.
45. Jessen, K.R. and R. Mirsky, *Negative regulation of myelination: relevance for development, injury, and demyelinating disease.* Glia, 2008. **56**(14): p. 1552-65.
46. Britsch, S., et al., *The transcription factor Sox10 is a key regulator of peripheral glial development.* Genes Dev, 2001. **15**(1): p. 66-78.
47. Finzsch, M., et al., *Sox10 is required for Schwann cell identity and progression beyond the immature Schwann cell stage.* J Cell Biol, 2010. **189**(4): p. 701-12.
48. Jaegle, M., et al., *The POU proteins Brn-2 and Oct-6 share important functions in Schwann cell development.* Genes Dev, 2003. **17**(11): p. 1380-91.

49. Parkinson, D.B., et al., *Krox-20 inhibits Jun-NH2-terminal kinase/c-Jun to control Schwann cell proliferation and death.* J Cell Biol, 2004. **164**(3): p. 385-94.
50. D'Antonio, M., et al., *Resetting translational homeostasis restores myelination in Charcot-Marie-Tooth disease type 1B mice.* J Exp Med, 2013. **210**(4): p. 821-38.
51. Heape, A., et al., *A quantitative developmental study of the peripheral nerve lipid composition during myelinogenesis in normal and trembler mice.* Brain Res, 1986. **390**(2): p. 181-9.
52. Yates, A.J. and J.R. Wherrett, *Changes in the sciatic nerve of the rabbit and its tissue constituents during development.* J Neurochem, 1974. **23**(5): p. 993-1003.
53. Saher, G., et al., *High cholesterol level is essential for myelin membrane growth.* Nat Neurosci, 2005. **8**(4): p. 468-75.
54. Baumann, N. and D. Pham-Dinh, *Biology of oligodendrocyte and myelin in the mammalian central nervous system.* Physiol Rev, 2001. **81**(2): p. 871-927.
55. Zeller, N.K., et al., *Characterization of mouse myelin basic protein messenger RNAs with a myelin basic protein cDNA clone.* Proc Natl Acad Sci U S A, 1984. **81**(1): p. 18-22.
56. de Ferra, F., et al., *Alternative splicing accounts for the four forms of myelin basic protein.* Cell, 1985. **43**(3 Pt 2): p. 721-7.
57. Barbarese, E., P.E. Braun, and J.H. Carson, *Identification of prelarge and presmall basic proteins in mouse myelin and their structural relationship to large and small basic proteins.* Proc Natl Acad Sci U S A, 1977. **74**(8): p. 3360-4.
58. Martini, R. and M. Schachner, *Molecular bases of myelin formation as revealed by investigations on mice deficient in glial cell surface molecules.* Glia, 1997. **19**(4): p. 298-310.
59. Privat, A., et al., *Absence of the major dense line in myelin of the mutant mouse "shiverer".* Neurosci Lett, 1979. **12**(1): p. 107-12.

60. Dupouey, P., et al., *Immunochemical studies of myelin basic protein in shiverer mouse devoid of major dense line of myelin.* Neurosci Lett, 1979. **12**(1): p. 113-8.
61. Li, J., et al., *The PMP22 gene and its related diseases.* Mol Neurobiol, 2013. **47**(2): p. 673-98.
62. Jetten, A.M. and U. Suter, *The peripheral myelin protein 22 and epithelial membrane protein family.* Prog Nucleic Acid Res Mol Biol, 2000. **64**: p. 97-129.
63. Pareek, S., et al., *Neurons promote the translocation of peripheral myelin protein 22 into myelin.* J Neurosci, 1997. **17**(20): p. 7754-62.
64. Pareek, S., et al., *Detection and processing of peripheral myelin protein PMP22 in cultured Schwann cells.* J Biol Chem, 1993. **268**(14): p. 10372-9.
65. Snipes, G.J., et al., *Characterization of a novel peripheral nervous system myelin protein (PMP-22/SR13).* J Cell Biol, 1992. **117**(1): p. 225-38.
66. Suter, U. and S.S. Scherer, *Disease mechanisms in inherited neuropathies.* Nat Rev Neurosci, 2003. **4**(9): p. 714-26.
67. D'Urso, D. and H.W. Muller, *Ins and outs of peripheral myelin protein-22: mapping transmembrane topology and intracellular sorting.* J Neurosci Res, 1997. **49**(5): p. 551-62.
68. Hasse, B., et al., *Peripheral myelin protein 22 kDa and protein zero: domain specific trans-interactions.* Mol Cell Neurosci, 2004. **27**(4): p. 370-8.
69. Notterpek, L., et al., *Peripheral myelin protein 22 is a constituent of intercellular junctions in epithelia.* Proc Natl Acad Sci U S A, 2001. **98**(25): p. 14404-9.
70. Adlkofer, K., et al., *Heterozygous peripheral myelin protein 22-deficient mice are affected by a progressive demyelinating tomaculous neuropathy.* J Neurosci, 1997. **17**(12): p. 4662-71.
71. Adlkofer, K., et al., *Hypermyelination and demyelinating peripheral neuropathy in Pmp22-deficient mice.* Nat Genet, 1995. **11**(3): p. 274-80.

72. van Paassen, B.W., et al., *PMP22 related neuropathies: Charcot-Marie-Tooth disease type 1A and Hereditary Neuropathy with liability to Pressure Palsies.* Orphanet J Rare Dis, 2014. **9**: p. 38.
73. Patzig, J., et al., *Quantitative and integrative proteome analysis of peripheral nerve myelin identifies novel myelin proteins and candidate neuropathy loci.* J Neurosci, 2011. **31**(45): p. 16369-86.
74. Lemke, G., E. Lamar, and J. Patterson, *Isolation and analysis of the gene encoding peripheral myelin protein zero.* Neuron, 1988. **1**(1): p. 73-83.
75. You, K.H., et al., *DNA sequence, genomic organization, and chromosomal localization of the mouse peripheral myelin protein zero gene: identification of polymorphic alleles.* Genomics, 1991. **9**(4): p. 751-7.
76. Hayasaka, K., et al., *Structure and chromosomal localization of the gene encoding the human myelin protein zero (MPZ).* Genomics, 1993. **17**(3): p. 755-8.
77. Lee, M., et al., *P0 is constitutively expressed in the rat neural crest and embryonic nerves and is negatively and positively regulated by axons to generate non-myelin-forming and myelin-forming Schwann cells, respectively.* Mol Cell Neurosci, 1997. **8**(5): p. 336-50.
78. Baron, P., et al., *Developmental expression of P0 mRNA and P0 protein in the sciatic nerve and the spinal nerve roots of the rat.* J Neurocytol, 1994. **23**(4): p. 249-57.
79. Stahl, N., J. Harry, and B. Popko, *Quantitative analysis of myelin protein gene expression during development in the rat sciatic nerve.* Brain Res Mol Brain Res, 1990. **8**(3): p. 209-12.
80. Trapp, B.D., *Distribution of the myelin-associated glycoprotein and P0 protein during myelin compaction in quaking mouse peripheral nerve.* J Cell Biol, 1988. **107**(2): p. 675-85.
81. Morgan, L., K.R. Jessen, and R. Mirsky, *The effects of cAMP on differentiation of cultured Schwann cells: progression from an early phenotype (04+) to a myelin phenotype (P0+, GFAP-, N-CAM-, NGF-receptor-) depends on growth inhibition.* J Cell Biol, 1991. **112**(3): p. 457-67.

82. Fernandez-Valle, C., et al., *Expression of the protein zero myelin gene in axon-related Schwann cells is linked to basal lamina formation.* Development, 1993. **119**(3): p. 867-80.
83. Melcangi, R.C., et al., *Age-induced decrease of glycoprotein Po and myelin basic protein gene expression in the rat sciatic nerve. Repair by steroid derivatives.* Neuroscience, 1998. **85**(2): p. 569-78.
84. Morgan, L., K.R. Jessen, and R. Mirsky, *Negative regulation of the P0 gene in Schwann cells: suppression of P0 mRNA and protein induction in cultured Schwann cells by FGF2 and TGF beta 1, TGF beta 2 and TGF beta 3.* Development, 1994. **120**(6): p. 1399-409.
85. Cheng, L. and A.W. Mudge, *Cultured Schwann cells constitutively express the myelin protein P0.* Neuron, 1996. **16**(2): p. 309-19.
86. Scherer, S.S., et al., *Differential regulation of the 2',3'-cyclic nucleotide 3'-phosphodiesterase gene during oligodendrocyte development.* Neuron, 1994. **12**(6): p. 1363-75.
87. Ghislain, J. and P. Charnay, *Control of myelination in Schwann cells: a Krox20 cis-regulatory element integrates Oct6, Brn2 and Sox10 activities.* EMBO Rep, 2006. **7**(1): p. 52-8.
88. Peirano, R.I., et al., *Protein zero gene expression is regulated by the glial transcription factor Sox10.* Mol Cell Biol, 2000. **20**(9): p. 3198-209.
89. Schreiner, S., et al., *Hypomorphic Sox10 alleles reveal novel protein functions and unravel developmental differences in glial lineages.* Development, 2007. **134**(18): p. 3271-81.
90. D'Urso, D., et al., *Protein zero of peripheral nerve myelin: biosynthesis, membrane insertion, and evidence for homotypic interaction.* Neuron, 1990. **4**(3): p. 449-60.
91. Yazaki, T., et al., *Glycopeptide of P0 protein inhibits homophilic cell adhesion. Competition assay with transformants and peptides.* FEBS Lett, 1992. **307**(3): p. 361-6.
92. Makowska, A., et al., *Immune responses to myelin proteins in Guillain-Barre syndrome.* J Neurol Neurosurg Psychiatry, 2008. **79**(6): p. 664-71.

93. Trapp, B.D., et al., *Immunocytochemical localization of P0 protein in Golgi complex membranes and myelin of developing rat Schwann cells.* J Cell Biol, 1981. **90**(1): p. 1-6.
94. Shapiro, L., et al., *Crystal structure of the extracellular domain from P0, the major structural protein of peripheral nerve myelin.* Neuron, 1996. **17**(3): p. 435-49.
95. Zhang, K. and M.T. Filbin, *Formation of a disulfide bond in the immunoglobulin domain of the myelin P0 protein is essential for its adhesion.* J Neurochem, 1994. **63**(1): p. 367-70.
96. Ishaque, A., et al., *The PO glycoprotein of peripheral nerve myelin.* Can J Biochem, 1980. **58**(10): p. 913-21.
97. Roomi, M.W., et al., *The PO protein. The major glycoprotein of peripheral nerve myelin.* Biochim Biophys Acta, 1978. **536**(1): p. 112-21.
98. Sedzik, J., J.P. Jastrzebski, and M. Grandis, *Glycans of myelin proteins.* J Neurosci Res, 2015. **93**(1): p. 1-18.
99. Eichberg, J., *Myelin P0: new knowledge and new roles.* Neurochem Res, 2002. **27**(11): p. 1331-40.
100. Hilmi, S., et al., *Myelin P0 glycoprotein: identification of the site phosphorylated in vitro and in vivo by endogenous protein kinases.* J Neurochem, 1995. **64**(2): p. 902-7.
101. Filbin, M.T., et al., *Role of myelin P0 protein as a homophilic adhesion molecule.* Nature, 1990. **344**(6269): p. 871-2.
102. Giese, K.P., et al., *Mouse P0 gene disruption leads to hypomyelination, abnormal expression of recognition molecules, and degeneration of myelin and axons.* Cell, 1992. **71**(4): p. 565-76.
103. Martini, R., et al., *Protein zero (P0)-deficient mice show myelin degeneration in peripheral nerves characteristic of inherited human neuropathies.* Nat Genet, 1995. **11**(3): p. 281-6.
104. Shy, M.E., et al., *Heterozygous P0 knockout mice develop a peripheral neuropathy that resembles chronic inflammatory demyelinating polyneuropathy (CIDP).* J Neuropathol Exp Neurol, 1997. **56**(7): p. 811-21.

105. Xu, W., et al., *Absence of P0 leads to the dysregulation of myelin gene expression and myelin morphogenesis.* J Neurosci Res, 2000. **60**(6): p. 714-24.
106. Menichella, D.M., et al., *Protein zero is necessary for E-cadherin-mediated adherens junction formation in Schwann cells.* Mol Cell Neurosci, 2001. **18**(6): p. 606-18.
107. Skre, H., *Genetic and clinical aspects of Charcot-Marie-Tooth's disease.* Clin Genet, 1974. **6**(2): p. 98-118.
108. Brennan, K.M., Y. Bai, and M.E. Shy, *Demyelinating CMT--what's known, what's new and what's in store?* Neurosci Lett, 2015. **596**: p. 14-26.
109. Baets, J., P. De Jonghe, and V. Timmerman, *Recent advances in Charcot-Marie-Tooth disease.* Curr Opin Neurol, 2014. **27**(5): p. 532-40.
110. Saporta, M.A. and M.E. Shy, *Inherited peripheral neuropathies.* Neurol Clin, 2013. **31**(2): p. 597-619.
111. Jani-Acsadi, A., K. Krajewski, and M.E. Shy, *Charcot-Marie-Tooth neuropathies: diagnosis and management.* Semin Neurol, 2008. **28**(2): p. 185-94.
112. Pareyson, D., V. Scaioli, and M. Laura, *Clinical and electrophysiological aspects of Charcot-Marie-Tooth disease.* Neuromolecular Med, 2006. **8**(1-2): p. 3-22.
113. Saporta, M.A., *Charcot-Marie-Tooth disease and other inherited neuropathies.* Continuum (Minneap Minn), 2014. **20**(5 Peripheral Nervous System Disorders): p. 1208-25.
114. Barisic, N., et al., *Charcot-Marie-Tooth disease: a clinico-genetic confrontation.* Ann Hum Genet, 2008. **72**(Pt 3): p. 416-41.
115. Scherer, S.S. and L. Wrabetz, *Molecular mechanisms of inherited demyelinating neuropathies.* Glia, 2008. **56**(14): p. 1578-89.
116. Pareyson, D., P. Saveri, and C. Pisciotta, *New developments in Charcot-Marie-Tooth neuropathy and related diseases.* Curr Opin Neurol, 2017. **30**(5): p. 471-480.

117. Boerkoel, C.F., et al., *Charcot-Marie-Tooth disease and related neuropathies: mutation distribution and genotype-phenotype correlation.* Ann Neurol, 2002. **51**(2): p. 190-201.
118. Szigeti, K., C.A. Garcia, and J.R. Lupski, *Charcot-Marie-Tooth disease and related hereditary polyneuropathies: molecular diagnostics determine aspects of medical management.* Genet Med, 2006. **8**(2): p. 86-92.
119. Dubourg, O., et al., *The frequency of 17p11.2 duplication and Connexin 32 mutations in 282 Charcot-Marie-Tooth families in relation to the mode of inheritance and motor nerve conduction velocity.* Neuromuscul Disord, 2001. **11**(5): p. 458-63.
120. Verhoeven, K., et al., *MFN2 mutation distribution and genotype/phenotype correlation in Charcot-Marie-Tooth type 2.* Brain, 2006. **129**(Pt 8): p. 2093-102.
121. Sanmaneechai, O., et al., *Genotype-phenotype characteristics and baseline natural history of heritable neuropathies caused by mutations in the MPZ gene.* Brain, 2015. **138**(Pt 11): p. 3180-92.
122. Shy, M.E., et al., *Phenotypic clustering in MPZ mutations.* Brain, 2004. **127**(Pt 2): p. 371-84.
123. Callegari, I., et al., *Mutation update for myelin protein zero-related neuropathies and the increasing role of variants causing a late-onset phenotype.* J Neurol, 2019.
124. Wrabetz, L., et al., *Different intracellular pathomechanisms produce diverse Myelin Protein Zero neuropathies in transgenic mice.* J Neurosci, 2006. **26**(8): p. 2358-68.
125. Grandis, M., et al., *Different cellular and molecular mechanisms for early and late-onset myelin protein zero mutations.* Hum Mol Genet, 2008. **17**(13): p. 1877-89.
126. Prada, V., et al., *Gain of glycosylation: a new pathomechanism of myelin protein zero mutations.* Ann Neurol, 2012. **71**(3): p. 427-31.
127. Moremen, K.W., M. Tiemeyer, and A.V. Nairn, *Vertebrate protein glycosylation: diversity, synthesis and function.* Nat Rev Mol Cell Biol, 2012. **13**(7): p. 448-62.

128. Reily, C., et al., *Glycosylation in health and disease.* Nat Rev Nephrol, 2019. **15**(6): p. 346-366.
129. Ohtsubo, K. and J.D. Marth, *Glycosylation in cellular mechanisms of health and disease.* Cell, 2006. **126**(5): p. 855-67.
130. Spiro, R.G., *Protein glycosylation: nature, distribution, enzymatic formation, and disease implications of glycopeptide bonds.* Glycobiology, 2002. **12**(4): p. 43R-56R.
131. Haltiwanger, R.S. and J.B. Lowe, *Role of glycosylation in development.* Annu Rev Biochem, 2004. **73**: p. 491-537.
132. Varki, A., *Biological roles of oligosaccharides: all of the theories are correct.* Glycobiology, 1993. **3**(2): p. 97-130.
133. Aebi, M., *N-linked protein glycosylation in the ER.* Biochim Biophys Acta, 2013. **1833**(11): p. 2430-7.
134. Aebi, M., et al., *N-glycan structures: recognition and processing in the ER.* Trends Biochem Sci, 2010. **35**(2): p. 74-82.
135. Jaeken, J., *Congenital disorders of glycosylation.* Ann N Y Acad Sci, 2010. **1214**: p. 190-8.
136. Freeze, H.H., et al., *Neurology of inherited glycosylation disorders.* Lancet Neurol, 2012. **11**(5): p. 453-66.
137. Monticelli, M., et al., *Immunological aspects of congenital disorders of glycosylation (CDG): a review.* J Inherit Metab Dis, 2016. **39**(6): p. 765-780.
138. Al Teneiji, A., et al., *Phenotypic and genotypic spectrum of congenital disorders of glycosylation type I and type II.* Mol Genet Metab, 2017. **120**(3): p. 235-242.
139. Freeze, H.H., *Genetic defects in the human glycome.* Nat Rev Genet, 2006. **7**(7): p. 537-51.
140. Aly, A.M., et al., *Hemophilia A due to mutations that create new N-glycosylation sites.* Proc Natl Acad Sci U S A, 1992. **89**(11): p. 4933-7.
141. Brennan, S.O., et al., *New carbohydrate site in mutant antithrombin (7 Ile---Asn) with decreased heparin affinity.* FEBS Lett, 1988. **237**(1-2): p. 118-22.

142. Grasbon-Frodl, E., et al., *Loss of glycosylation associated with the T183A mutation in human prion disease.* Acta Neuropathol, 2004. **108**(6): p. 476-84.

143. Kretz, K.A., et al., *Characterization of a mutation in a family with saposin B deficiency: a glycosylation site defect.* Proc Natl Acad Sci U S A, 1990. **87**(7): p. 2541-4.

144. Parad, R.B., et al., *Dysfunctional C1 inhibitor Ta: deletion of Lys-251 results in acquisition of an N-glycosylation site.* Proc Natl Acad Sci U S A, 1990. **87**(17): p. 6786-90.

145. Regis, S., et al., *An Asn > Lys substitution in saposin B involving a conserved amino acidic residue and leading to the loss of the single N-glycosylation site in a patient with metachromatic leukodystrophy and normal arylsulphatase A activity.* Eur J Hum Genet, 1999. **7**(2): p. 125-30.

146. Vogt, G., et al., *Gains of glycosylation comprise an unexpectedly large group of pathogenic mutations.* Nat Genet, 2005. **37**(7): p. 692-700.

147. Vogt, G., et al., *Gain-of-glycosylation mutations.* Curr Opin Genet Dev, 2007. **17**(3): p. 245-51.

148. Blanquet-Grossard, F., et al., *Charcot-Marie-Tooth type 1B neuropathy: a mutation at the single glycosylation site in the major peripheral myelin glycoprotein Po.* Hum Mutat, 1996. **8**(2): p. 185-6.

149. De Jonghe, P., et al., *The Thr124Met mutation in the peripheral myelin protein zero (MPZ) gene is associated with a clinically distinct Charcot-Marie-Tooth phenotype.* Brain, 1999. **122 (Pt 2)**: p. 281-90.

150. Kochanski, A., et al., *A novel MPZ gene mutation in congenital neuropathy with hypomyelination.* Neurology, 2004. **62**(11): p. 2122-3.

151. Mandich, P., et al., *Clinical features and molecular modelling of novel MPZ mutations in demyelinating and axonal neuropathies.* Eur J Hum Genet, 2009. **17**(9): p. 1129-34.

152. Yonekawa, T., et al., *Congenital hypomyelinating neuropathy attributable to a de novo p.Asp61Asn mutation of the myelin protein zero gene.* Pediatr Neurol, 2013. **48**(1): p. 59-62.

153. Lagueny, A., et al., *Peripheral myelin modification in CMT1B correlates with MPZ gene mutations.* Neuromuscul Disord, 1999. **9**(6-7): p. 361-7.
154. Choi, B.O., et al., *Mutational analysis of PMP22, MPZ, GJB1, EGR2 and NEFL in Korean Charcot-Marie-Tooth neuropathy patients.* Hum Mutat, 2004. **24**(2): p. 185-6.
155. Mersiyanova, I.V., et al., *Screening for mutations in the peripheral myelin genes PMP22, MPZ and Cx32 (GJB1) in Russian Charcot-Marie-Tooth neuropathy patients.* Hum Mutat, 2000. **15**(4): p. 340-7.
156. Waite, A., et al., *A gain-of-glycosylation mutation associated with myoclonus-dystonia syndrome affects trafficking and processing of mouse epsilon-sarcoglycan in the late secretory pathway.* Hum Mutat, 2011. **32**(11): p. 1246-58.
157. Cihil, K.M. and A. Swiatecka-Urban, *The cell-based L-glutathione protection assays to study endocytosis and recycling of plasma membrane proteins.* J Vis Exp, 2013(82): p. e50867.
158. Harms, D.W., et al., *Mouse Genome Editing Using the CRISPR/Cas System.* Curr Protoc Hum Genet, 2014. **83**: p. 15.7.1-27.
159. Bolino, A., et al., *Disruption of Mtmr2 produces CMT4B1-like neuropathy with myelin outfolding and impaired spermatogenesis.* J Cell Biol, 2004. **167**(4): p. 711-21.
160. Wiesmann, M., et al., *Effect of a multinutrient intervention after ischemic stroke in female C57Bl/6 mice.* 2018. **144**(5): p. 549-564.
161. Julenius, K., et al., *Prediction, conservation analysis, and structural characterization of mammalian mucin-type O-glycosylation sites.* Glycobiology, 2005. **15**(2): p. 153-64.
162. Bano-Polo, M., et al., *N-glycosylation efficiency is determined by the distance to the C-terminus and the amino acid preceding an Asn-Ser-Thr sequon.* Protein Sci, 2011. **20**(1): p. 179-86.
163. Rao, R.S., O.T. Buus, and B. Wollenweber, *Distribution of N-glycosylation sequons in proteins: how apart are they?* Comput Biol Chem, 2011. **35**(2): p. 57-61.

164. Wang, H., et al., *One-step generation of mice carrying mutations in multiple genes by CRISPR/Cas-mediated genome engineering.* Cell, 2013. **153**(4): p. 910-8.
165. D'Antonio, M., M.L. Feltri, and L. Wrabetz, *Myelin under stress.* J Neurosci Res, 2009. **87**(15): p. 3241-9.
166. Pennuto, M., et al., *Ablation of the UPR-mediator CHOP restores motor function and reduces demyelination in Charcot-Marie-Tooth 1B mice.* Neuron, 2008. **57**(3): p. 393-405.
167. Saporta, M.A., et al., *MpzR98C arrests Schwann cell development in a mouse model of early-onset Charcot-Marie-Tooth disease type 1B.* Brain, 2012. **135**(Pt 7): p. 2032-47.
168. Vogt, G., et al., *Complementation of a pathogenic IFNGR2 misfolding mutation with modifiers of N-glycosylation.* J Exp Med, 2008. **205**(8): p. 1729-37.
169. Jerath, N.U. and M.E. Shy, *Hereditary motor and sensory neuropathies: Understanding molecular pathogenesis could lead to future treatment strategies.* Biochim Biophys Acta, 2015. **1852**(4): p. 667-78.
170. Bai, Y., et al., *Myelin protein zero mutations and the unfolded protein response in Charcot Marie Tooth disease type 1B.* Ann Clin Transl Neurol, 2018. **5**(4): p. 445-455.
171. Meyer Zu Horste, G. and K.A. Nave, *Animal models of inherited neuropathies.* Curr Opin Neurol, 2006. **19**(5): p. 464-73.
172. Prada, V., et al., *Sural nerve biopsy and functional studies support the pathogenic role of a novel MPZ mutation.* Neuropathology, 2015. **35**(3): p. 254-9.
173. Vallat, J.M., et al., *Diagnostic value of ultrastructural nerve examination in Charcot-Marie-Tooth disease: two CMT 1B cases with pseudo-recessive inheritance.* Acta Neuropathol, 2007. **113**(4): p. 443-9.
174. Goebbels, S., et al., *Genetic disruption of Pten in a novel mouse model of tomaculous neuropathy.* EMBO Mol Med, 2012. **4**(6): p. 486-99.

175. Sander, S., et al., *Clinical syndromes associated with tomacula or myelin swellings in sural nerve biopsies.* J Neurol Neurosurg Psychiatry, 2000. **68**(4): p. 483-8.
176. Campagnoni, A.T., *Molecular biology of myelin proteins from the central nervous system.* J Neurochem, 1988. **51**(1): p. 1-14.
177. D'Urso, D., P. Ehrhardt, and H.W. Muller, *Peripheral myelin protein 22 and protein zero: a novel association in peripheral nervous system myelin.* J Neurosci, 1999. **19**(9): p. 3396-403.
178. Baets, J., et al., *Genetic spectrum of hereditary neuropathies with onset in the first year of life.* Brain, 2011. **134**(Pt 9): p. 2664-76.
179. Wrabetz, L., et al., *P(0) glycoprotein overexpression causes congenital hypomyelination of peripheral nerves.* J Cell Biol, 2000. **148**(5): p. 1021-34.
180. Filbin, M.T. and G.I. Tennekoon, *The role of complex carbohydrates in adhesion of the myelin protein, P0.* Neuron, 1991. **7**(5): p. 845-55.
181. Griffith, L.S., B. Schmitz, and M. Schachner, *L2/HNK-1 carbohydrate and protein-protein interactions mediate the homophilic binding of the neural adhesion molecule P0.* J Neurosci Res, 1992. **33**(4): p. 639-48.
182. Ishii, A., M. Furusho, and R. Bansal, *Sustained activation of ERK1/2 MAPK in oligodendrocytes and schwann cells enhances myelin growth and stimulates oligodendrocyte progenitor expansion.* J Neurosci, 2013. **33**(1): p. 175-86.
183. Sheean, M.E., et al., *Activation of MAPK overrides the termination of myelin growth and replaces Nrg1/ErbB3 signals during Schwann cell development and myelination.* Genes Dev, 2014. **28**(3): p. 290-303.
184. Das, I., et al., *Preventing proteostasis diseases by selective inhibition of a phosphatase regulatory subunit.* Science, 2015. **348**(6231): p. 239-42.
185. Khajavi, M., et al., *Oral curcumin mitigates the clinical and neuropathologic phenotype of the Trembler-J mouse: a potential therapy for inherited neuropathy.* Am J Hum Genet, 2007. **81**(3): p. 438-53.

186. Patzko, A., et al., *Curcumin derivatives promote Schwann cell differentiation and improve neuropathy in R98C CMT1B mice.* Brain, 2012. **135**(Pt 12): p. 3551-66.
187. Dwek, R.A., et al., *Targeting glycosylation as a therapeutic approach.* Nat Rev Drug Discov, 2002. **1**(1): p. 65-75.
188. Elbein, A.D., *Glycosidase inhibitors: inhibitors of N-linked oligosaccharide processing.* Faseb j, 1991. **5**(15): p. 3055-63.
189. Leonard, A., et al., *Miglustat effects on the basal nasal potential differences in cystic fibrosis.* J Cyst Fibros, 2013. **12**(1): p. 89.
190. Ficicioglu, C., *Review of miglustat for clinical management in Gaucher disease type 1.* Ther Clin Risk Manag, 2008. **4**(2): p. 425-31.
191. Lyseng-Williamson, K.A., *Miglustat: a review of its use in Niemann-Pick disease type C.* Drugs, 2014. **74**(1): p. 61-74.

Journal of Neurology (2019) 266:2629–2645
https://doi.org/10.1007/s00415-019-09453-3

ORIGINAL COMMUNICATION

Mutation update for myelin protein zero-related neuropathies and the increasing role of variants causing a late-onset phenotype

Ilaria Callegari[1,2,7] · C. Gemelli[2] · A. Geroldi[2] · F. Veneri[2] · P. Mandich[2,3] · M. D'Antonio[4] · D. Pareyson[5] · M. E. Shy[6] · A. Schenone[2,3] · V. Prada[2] · M. Grandis[2,3]

Received: 13 March 2019 / Revised: 21 June 2019 / Accepted: 26 June 2019 / Published online: 5 July 2019

Abstract

Mutations of myelin protein zero gene (*MPZ*) are found in 5% of Charcot–Marie–Tooth patients. In 2004, Shy et al. identified two main phenotypes associated with them: an early-onset subtype with mainly demyelinating features and a late-onset subgroup with prominent axonal impairment. We evaluated whether novel *MPZ* mutations described in literature during the last 14 years could still fit with this classification. We collected and revised reports of 69 novel *MPZ* mutations. Almost 90% of them could be alternatively classified as responsible for: (a) an early-onset phenotype, with first limitations starting before 3 years (2.5 ± 0.50 years), motor milestones delays, frequently severe course and upper limb MNCVs below 15 m/s; (b) late-onset neuropathy, with mean age of onset of 42.8 ± 1.5 years and mean upper limbs motor nerve conduction velocities (MNCVs) of 47.2 ± 1.4 m/s; (c) a phenotype more similar to typical CMT1A neuropathy, with onset during the 2nd decade, MNCV in the range of 15–30 m/s and slowly progressive course. The present work confirms that P0-related neuropathies may be separated into two main distinct phenotypes, while a third, relatively small, group comprehend patients carrying *MPZ* mutations and a childhood-onset disease, substantiating the subdivision into three groups proposed by Sanmaneechai et al. (Brain 138:3180–3192, 2015). Interestingly, during the last years, an increasing number of novel *MPZ* mutations causing a late-onset phenotype has been described, highlighting the clinical relevance of late-onset P0 neuropathies. Since the family history for neuropathy is often uncertain, due to the late disease onset, the number of patients carrying this genotype is probably underestimated.

Keywords Charcot–Marie–Tooth · Myelin protein zero · Phenotype classification · Genotype–phenotype correlation

Introduction

Charcot–Marie–Tooth disease (CMT), with a prevalence of 9.37–20.1/100.000 [1], is one of the most common hereditary disorders of the nervous system. The clinical hallmarks of the disease are distal weakness, muscle wasting

Electronic supplementary material The online version of this article (https://doi.org/10.1007/s00415-019-09453-3) contains supplementary material, which is available to authorized users.

V. Prada and M. Grandis contributed equally to this work.

✉ Ilaria Callegari
ilaria.callegari01@universitadipavia.it

✉ M. Grandis
mgrandis@neurologia.unige.it

[1] Neuroscience Consortium Monza Policlinico and Pavia Mondino, University of Pavia, Pavia, Italy

[2] Department of Neuroscience Rehabilitation Ophthalmology Genetics, Maternal and Child Health (DiNOGMI), University of Genova, Genoa, Italy

[3] Ospedale Policlinico San Martino, IRCCS, Largo P. Daneo 3, 16132 Genoa, Italy

[4] Division of Genetics and Cell Biology, San Raffaele Scientific Institute, Milan, Italy

[5] Unit of Rare Neurodegenerative and Neurometabolic Diseases, Department of Clinical Neurosciences, Fondazione IRCCS Istituto Neurologico Carlo Besta, Milan, Italy

[6] Department of Neurology, University of Iowa Hospitals & Clinics, Iowa City, USA

[7] IRCCS Mondino Foundation, Pavia, Italy

and sensory loss; nevertheless, the clinical phenotype can be quite variable in terms of age of onset, disease progression and severity. Based on nerve conduction velocity, CMT can be distinguished into two main forms: demyelinating (CMT1), characterized by upper limb motor nerve conduction velocities (MNCVs) below 38 m/s, and axonal (CMT2), with preserved or mildly slowed nerve conduction velocities in the upper limbs (> 38 m/s). From a molecular point of view, CMT is a complex disorder, with more than 1000 putative mutations in 80 different disease-associated genes [2]. Mutations in myelin protein zero gene (*MPZ*), encoding for P0, are found in 4.1% of all CMT patients [3, 4], and were initially described as responsible for CMT1B; subsequently, mutations in this gene have been found also in cases of congenital hypomyelinating neuropathy/Dejerine Sottas disease and CMT2. To analyse the phenotypes associated with *MPZ* mutations, Shy et al. [5] evaluated patients seen in their clinic and re-evaluated clinical data from 64 cases of CMT1B reported in literature until 2004. They found that most patients could be classified as having either an early-onset or a late-onset neuropathy, the former presenting with onset of the disease during the 1st decade of life and with upper extremity MNCVs lower than 15 m/s, the latter with an age of onset over 20 years of age and with upper extremity MNCVs faster than 30 m/s. In a more recent work examining clinical severity of patients from Inherited Neuropathy Consortium [6], 47 *MPZ* mutations, of whom 15 were novel and 6 were described in literature after 2004, were classified as responsible for three phenotypes with onset in infancy, childhood and adulthood, respectively.

In the present study, we collected literature data related to novel *MPZ* mutations described between 2005 and 2018 to assess whether the distinction between early- and late-onset neuropathy can still be considered a landmark and to provide further insight into the disease mechanisms.

Methods

Literature evaluation

Reports about novel *MPZ* mutations described between 2005 and 2018 were collected from a search on PubMed and on the online database http://molgen-www.uia.ac.be/CMTMutations/. We used the following search terms: "myelin protein zero", "Charcot–Marie–Tooth disease", and "novel *MPZ* mutation". Reports of novel *MPZ* mutations not providing adequate clinical and neurophysiological data, i.e., a complete description of the clinical presentation and an upper limb neurophysiological study were excluded (Fig. 1). Mutations described by more than one author and associated with more than one phenotype were included in each of the described groups. *MPZ* mutations found in patients with a negative or not available family history were included if segregation analysis had been performed or if the mutation was absent in unrelated healthy controls. For each mutation, clinical (age of onset, number of affected family members, severity and additional clinical features) and neurophysiological data (upper and lower limbs motor conduction velocities and compound motor action potentials)

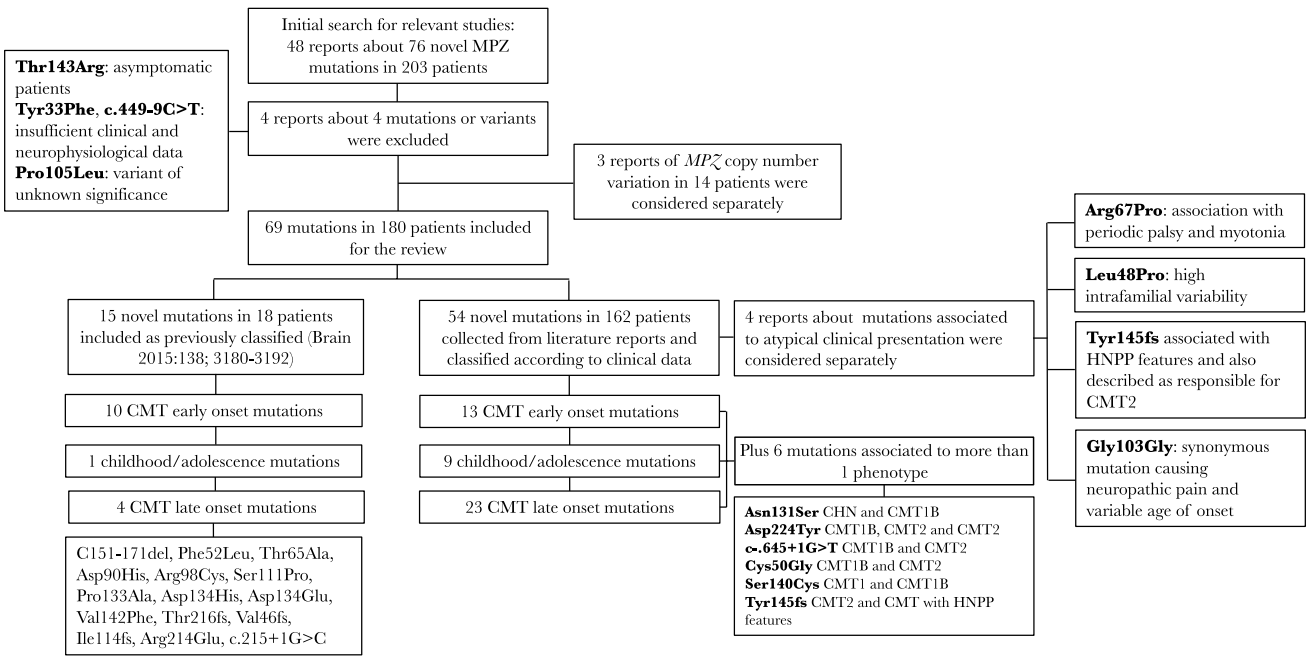

Fig. 1 Flowchart of the inclusion process for the review

were derived from the considered study for all the available patients. Mutations were classified as responsible for early-, childhood–adolescence- or late-onset neuropathy according to age of onset of the neuropathy (≤ 5 years, 6–20 years; ≥ 21 years), defined by the age at which the proband or another family member started to manifest clinical and/or neurophysiological signs; for each group, average values and standard error were calculated for the considered variables. The severity of the disease was classified based on CMTNS, when reported, or on clinical aspects described in the report.

Results

Between 2005 and 2018, 76 novel *MPZ* mutations in 203 patients have been reported in the literature [6–51] as responsible for Dejerine–Sottas disease, congenital hypomyelinating neuropathy, CMT1B or CMT2 neuropathies. We excluded three mutations described in five patients for insufficient clinical and neurophysiological data and one report about one variant of unknown significance (Figs. 1, 2; Supplementary Table 4); three reports [21, 29, 47] on *MPZ* copy number variation in 14 patients were considered separately (Supplementary Table 5). Reports about 69 novel *MPZ* mutations in 180 patients contained adequate clinical and neurophysiological data, thus allowing us to derive the phenotype, including a group of 15 novel *MPZ* mutations in 18 patients newly described in 2015 [6] and whose phenotype had already been classified has responsible for early-onset, CMT1B or late-onset neuropathy (Fig. 1).

Overall, 60 out of 69 mutations (87%) in 144 patients could be unambiguously classified, according to clinical and neurophysiological parameters, as responsible for an early-onset neuropathy (35 patients—24%; 23 mutations—38%), a late-onset neuropathy (74 patients—51%; 27 mutations—45%) or a childhood-onset phenotype (36 patients—25%; 10 mutations—17%). Six (9%) other mutations in 18 patients (10%) have been described in more than one report and associated by the authors to more than one phenotype and were therefore considered in each of the described groups; eventually, 3 further *MPZ* mutations (4%) in 14 patients (7%) were associated with an atypical phenotype [14, 20, 48] (Fig. 2).

From the descriptions of *MPZ* mutation in the literature, excluding those already classified in 2015 [6], we can derive as follows (Table 1, Fig. 3).

Twenty-six patients with 15 different novel mutations could be classified as having an early-onset neuropathy (Table 2). Among them, 17 patients with eight different mutations were described by the authors as having DSS, five patients with four different mutations were described as affected by CHN, and four patients with three different

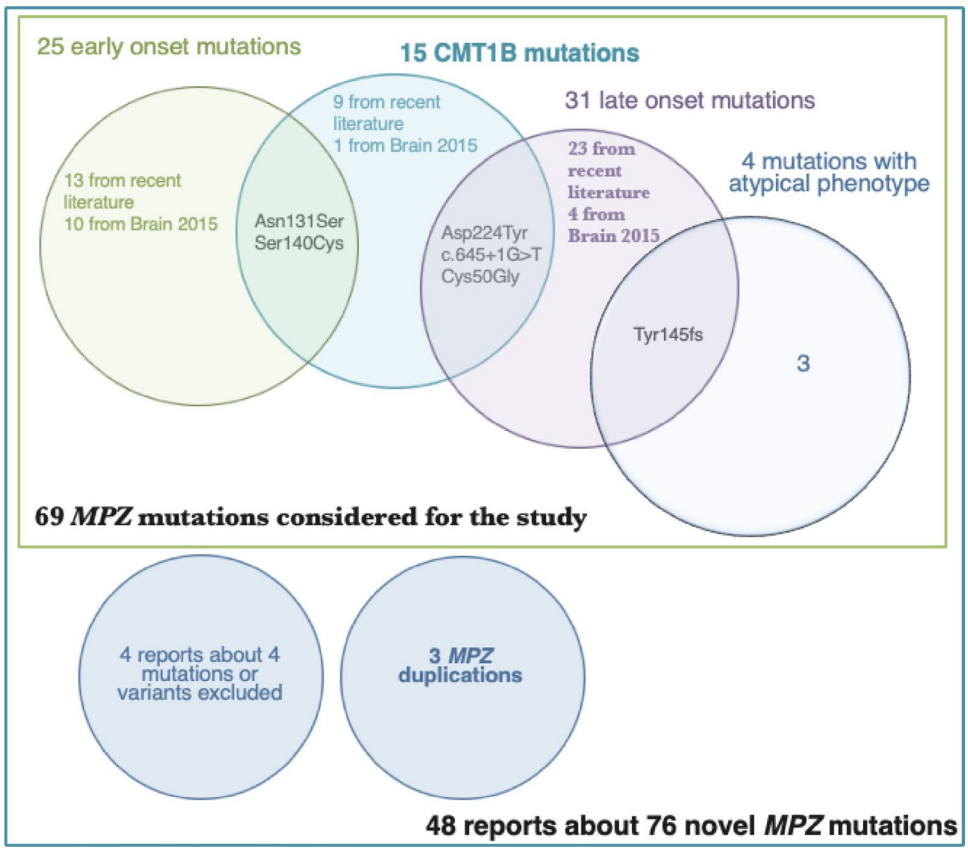

Fig. 2 Venn diagram showing mutations included and excluded from the review

Table 1 MPZ mutations phenotypes; literature review

	Early onset	Childhood/ adolescence	Late onset
Mutations (*N*)	15	14	27
Patients	26	44	76
Families	6 (40%)	9 (64%)	18 (66%)
Sporadic cases	9 (60%)	5 (36%)	9 (33%)
Age of onset (years)	2.5 ± 0.50	15.1 ± 1.1	42.8 ± 1.5
Pupillary abnormalities	Six patients with two mutations	0	One patient with one mutation
Hearing loss	Two patients with one mutation	0	Five patients with three mutations
Scoliosis	6 (24%)	0	0
CMTNS ≤ 10	3 (12%)	36 (82%)	59 (78%)
CMTNS 11–20	3 (12%)	8 (18%)	12 (16%)
CMTNS > 20	19 (76%)	0	5 (7%)
Mean UL mNCV (m/s)	7.4 ± 1.2	31.2 ± 2.6	47.2 ± 1.4
Mean UL CMAP (mV)	1.8 ± 0.4	6.6 ± 0.6	8.3 ± 0.7

mutations received a diagnosis of CMT1. The mean age at onset was 2.5 ± 0.50 years (median 2 years; range 0–9), with eight cases where the neuropathy started within the 2nd year of life and seven patients presenting at birth as floppy babies. Family history was negative in the nine cases (60%) and six families (40%) with at least two affected members were described. A severe clinical course, defined by a CMTNS > 20 was associated with 13 mutations in 19 cases (76%); 2 mutations in 6 cases were responsible for a mild to severe neuropathy. The phenotype was complicated by the occurrence of kyphoscoliosis in six patients (24% of patients, 33% of all mutations). Cranial nerves involvement was reported for several patients with early-onset neuropathy. In particular, five patients carrying the His81Gln [13] mutation and one patient carrying the Ile30Thr mutation [19] showed Adie's pupils, while two patients carrying the Gly137Gly mutation [50] had sensory-neural hearing loss and ptosis as adjunctive features. Neurophysiology was consistent with a severe hypo- or demyelinating neuropathy with secondary axonal degeneration. All but three cases presented with MNCV of the median and ulnar nerves below 15 m/s, with mean MNCV of the median nerve of 7.4 ± 1.2 m/s; three patients showed absence of sensory and motor nerve responses both in upper and lower limbs. When obtainable, conduction velocities from lower limbs were similar to those obtained from the upper limbs. Compound muscle action potentials (CMAPs) and sensory nerve action potentials (SNAPs) were reduced, with mean CMAP = 1.8 ± 0.4 mV.

Seventy-six patients carrying 27 novel mutations could be classified as affected by a late-onset neuropathy (Table 3). In most cases, symptoms ensued after the 4th decade of life, and in several cases they started during the 6th or 7th decade (median 43 years; range 15–75; mean age of onset of 42.8 ± 1.5 years). Family history was negative in 33% of the cases. Emerging features of late-onset P0 neuropathy were consistent with a sensory-motor neuropathy with prominent involvement of lower limbs and causing a relatively low disability, with 56 patients (78%) having a slowly progressive, mild neuropathy (CMTNS < 10). Nevertheless, cases of rapidly progressive symptoms, appearing late in life but quickly conducting to severe disability and ambulation aid requirement have been described for Arg36Gly, Pro70Ser and His81Leu mutations [15, 27, 29]. Moreover, neuropathic pain was a prominent feature in several cases of late-onset P0 neuropathies, as in the case of Arg36Trp [11] and Arg36Gly [15]: in both cases, patients started to complain of spontaneous burning pain and tingling of hands and feet, and showed neurophysiologic features of an axonal sensory-motor neuropathy in all limbs. Additional clinical findings included slow or absent pupillary light reflexes in one patient carrying the Phe95Leu mutation [38], and sensory-neural hearing impairment in five patients harbouring the Phe95Leu, Pro105Thr or Arg106Cys mutations [23, 33, 37].

Electrophysiological analysis was consistent with an axonal neuropathy, with mean MNCV from ulnar nerve of 47.2 ± 1.4 m/s, and normal CMAP amplitudes from the upper limbs. Lower limbs neuronography, when recorded, was consistent with an axonal neuropathy (mean CMAP of common peroneal nerve = 2 ± 0.5 mV).

Forty-four patients with 14 different mutations presented a childhood–adolescence-onset phenotype that fits neither with an early- nor with a late-onset neuropathy, resembling rather CMT1A (Table 4). Usually patients showed a normal motor development and started to complain of sensory-motor symptoms during the 1st or 2nd decade of life, with a mean age of neuropathy onset of 15.1 ± 1.1 years (median 15 years; range 6–40). Nine cases were familiar (64%) and five sporadic (36%). The clinical course of disease within this group was mild in 82% of the cases, with a mean age of 39.1 ± 3.3 years at first neurological visit, usually 2 decades

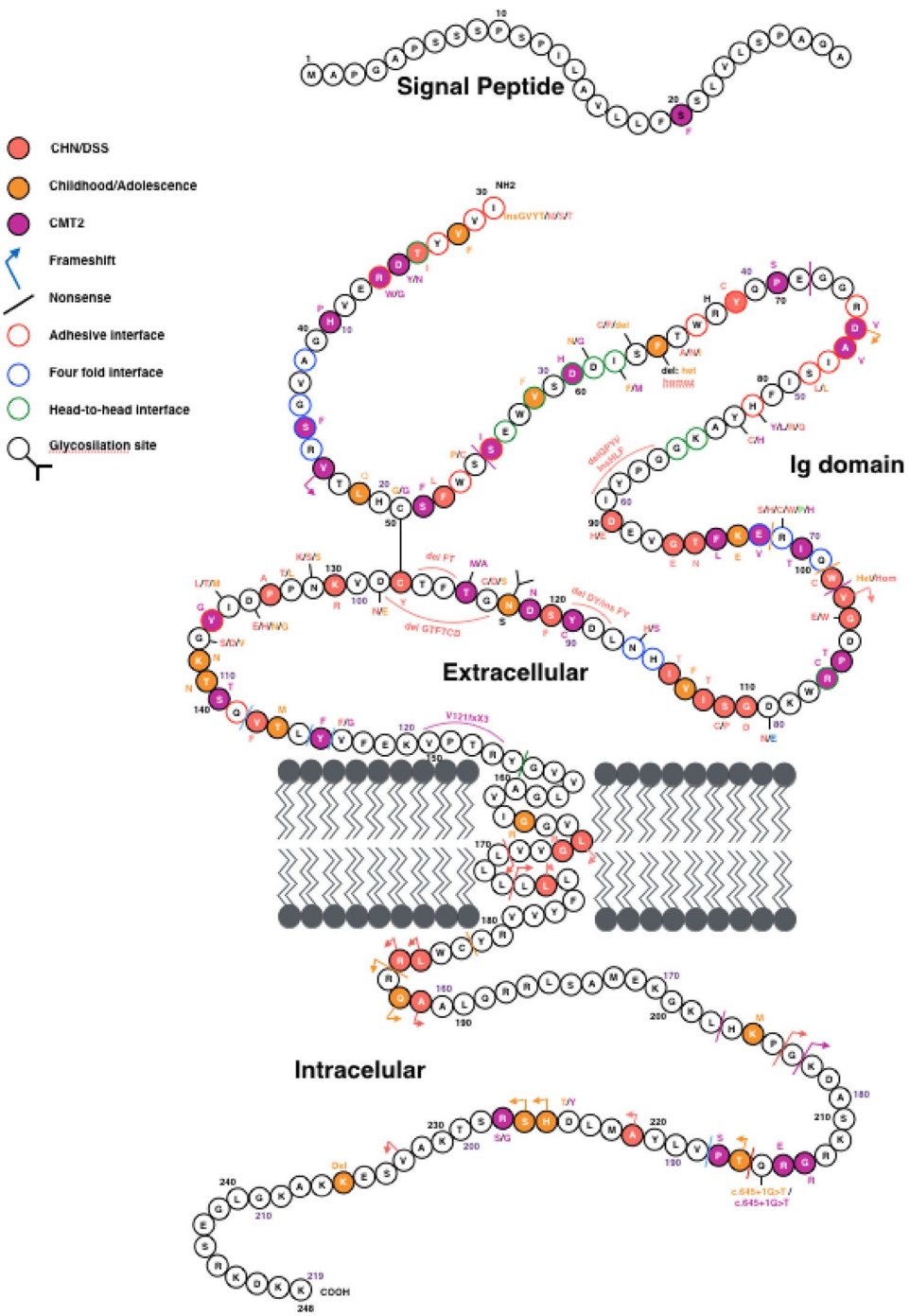

Fig. 3 Mutations in the MPZ gene associated with inherited neuropathies. Adhesive interface, fourfold interface and head-to-head interface, marked with colour to the border of circle, refer to amino acid residues deemed essential for *cis* and *trans* adhesion between adjacent myelin wraps. Both the numbering systems for MPZ mutations, including or not the 29 amino acid leader peptide cleaved before insertion in the myelin sheath, are reported. Mutations demonstrated by adding the letters that represent amino acid change, arrows that represent frameshift mutation and lines that represent nonsense mutation. Mutations causing early-onset phenotype are filled or noted with red colour, while those causing childhood-onset phenotype are in orange, and those causing late-onset phenotype are in purple (updated from Sanmaneechai et al. [6])

after first signs or symptoms' onset. Only eight patients with six mutations experienced a neuropathy of moderate severity (CMTNS 10–20). Cranial nerves involvement was never reported and patients had no additional features other than the polyneuropathy. Neurophysiological examination was consistent with a demyelinating polyneuropathy with MNCV approaching the so-called intermediate range, a mean ulnar nerve MNCV of 31.2 ± 2.6 m/s, and usually preserved upper limbs CMAP (6.6 ± 0.6 mV).

Eventually, four mutations were associated with a phenotype slightly different from the classical ones (Table 5): Gly103Gly synonymous mutation [14] has been described in two families with variable age of onset, neuropathic pain and predominant sensory involvement; Arg67Pro [20] has been described in a family with a compound genotype and phenotype of periodic palsy and myotonia, Leu48Pro [49] has been reported in two families with high intrafamilial variability in terms of age of onset, electrophysiological findings and

Table 2 Features of P0-related neuropathies—early-onset neuropathies

Mutation	Author diagnosis	Age of onset of first limitations	Age walked	Clinical course	NCV	CMAP	Pathology	Family history	Other clinical features	Author
Ile30Ser	CMT1	2 y	ND	Severe	*m* 4 m/s	*m* 0.8 mV	Not performed	1 pt	–	Miltenberger-Miltenyi et al. [35]
Ile30Thr	DSS	2–3 y	2.5–6 y	Severe (CMTNS 29–35)	*u* 0–9 m/s	*u* 0–1.5 mV	Not performed	AD 1F; 2 pt	Scoliosis, neuropathic pain, Adie's pupils	Floroskufi [19]
Thr65Asn	DSN/HMSN III	Infancy	> 18 months	Severe	*m* 4–12 m/s *u* 6–11 m/s *t* NE	*m* 1.8 mV *u* 1.7 mV *t* NE	Not performed	1pt de novo	Scoliosis	Brozkova et al. [10]
His81Gln	CMT1/DSS	1st dec (2–9 y)	–	Mild to severe (CMTNS 7–27)	*m* 6.2–14.9 m/s *u* 4.5–14.3 m/s *p* NE *t* NE	*m* 0.1–3.8 mV *u* 0.4–8.1 *p* NE *t* NE	Severe loss of MFs of all calibres; onion bulbs, regenerative clusters	AD 1F; 7 pt	Adie's pupils, tremor, ataxia	Choi et al. [13]
Gly103Trp	DSN/HMSN III	Infancy	> 18 months	Mild to Severe	*m* 17.6–22 m/s *u* 27–28.3 m/s *t* 0–6 m/s	*m* 2–5.8 mV *u* 7.5 mV *t* 0.1 mV	Not performed	1F, 2 pt	Scoliosis	Brozkova et al. [10]
Ser121Phe (Ser111Phe)	CHN	4 m	Never walked	Severe (unable to perform any voluntary movement)	*m* 2.9 m/s *u* 3.3 m/s *t* 3.6 m/s	*m* 0.56 mV *u* 0.99 mV *t* 0.143 mV	Severe loss of myelinated fibres; atypical onion bulbs	1 pt de novo	Respiratory insufficiency; CSF proteins: 87 mg/dl	Sevilla et al. [44]
Gly123Asp	DSS	2 y	–	Severe (CMTNS: 26)	*m* 6.7 m/s *u* 6.9 m/s *p* 9.2 m/s	*m* 4.0 mV *u* 2 mV *p* 0.7 mV	Not performed	1 pt de novo	Ataxia, kyphoscoliosis	Braathen et al. [9]
Asn131Ser[a]	CHN	2 y	2.5 y	Severe	*m* NE *u* NE *p* NE *t* NE	*m* NE *u* NE *p* NE *t* NE	Severe loss of myelinated fibres; onion bulb-like formations	1 pt de novo	–	McMillan et al. [34]
Pro132Thr	DSN/HMSN III	Early in infancy	>18 months	Severe	*m* NE *u* 3 m/s *t* NE	*m* NE *u* NE *t* NE	Not performed	1 pt de novo	Hypotonia	Brozkova et al. [10]
Ser140Cys (Ser111Cys)[a,b]	CMT1	1st dec	–	Severe	*m* 14.6 m/s *u* 12 m/s *p* 7.5 m/s	–	Not performed	AD 1F; 2 pt	–	Mandich et al. [32]

Table 2 (continued)

Mutation	Author diagnosis	Age of onset of first limitations	Age walked	Clinical course	NCV	CMAP	Pathology	Family history	Other clinical features	Author
Gly137Gly	DSS	0–5 y	Delayed	Severe	*m* 5 m/S *u* 9 m/s *p* 5.5 m/s	*m* 1 mV *u* 0.2 mV *p* 0.15 mV	Loss of large myelinated fibres; onion bulbs	AD 1F; 2 pt	Ptosis, bilateral hypoacusia, scoliosis	Taioli et al. [50]
Leu184AlafsX51	CHN	At birth	Delayed	Severe	*m* 0–4 m/s *p* NE	*m* 0.8–3.3 m/S *p* NE	Absence of myelin sheaths	AD 1 F; 2 pt	–	Smit et al. [47]
Arg185AlafsX6	CMT1	1 y	ND	Severe	*m* 11 m/s	ND	Not performed	1 pt de novo	Macrocephalia	Miltenberger-Miltenyi et al. [35]
c.368_382delGCACGTTCACTTGTG	CHN	At birth	ND	Severe	Absent sensory and motor nerve responses in his upper and lower extremities	Absent sensory and motor nerve responses in his upper and lower extremities	Complete absence of myelination of both large or small fibres, despite intact axons	1 pt de novo	CSF proteins: 95 mg/dl	McMillan et al. [34]
c.618_619 insT	DSS	1st month of life	Delayed	Severe	*m* NE *u* 3 m/s *p* NE	*m* NE *u* 1.4 mV *p* NE	Not performed	1 pt de novo	CSF proteins: 3 g/ml; RMN: nerve and spinal roots enlargement	Zschüntzsch et al. [51]

Dec decade, *y* years, *m* median, *u* ulnar, *p* peroneal, *t* tibial, *s* sural, *NE* not evocable, *NR* not recorded, *AD* autosomal dominant, *F* family, *pt* patients

[a]Mutations described by more than one author

[b]Mutation also included in Brain 2015:138; 3180–3192

Table 3 Features of P0-related neuropathies—late-onset neuropathies

Mutation	Author diagnosis	Age of onset of first limitations	Age walked	Clinical course	NCV	cMAP	Pathology	Family history	Other clinical features	Author
Ser20Phe	CMT1B	60 y	ND	Slowly progressive	Normal median and ulnar conduction *p* NE *t* NE *s* 44 m/s	Normal median and ulnar conduction *t* NE *p* NE *s* 12 uV	Reduced thick myelinated fibres density, increased endoneurial connective tissue, absent demyelination	1 pt	Thigh and calf cramps after exercise and increased CK levels	Finsterer et al. [18]
Asp35Asn	CMT2	3rd to 7th dec	ND	CMTNS: 12–15	*m* 42–49 m/s *u* 52–60 m/S *p* 0–31 m/s *t* NE	*m* 4.4–7.5 mV *u* 5–7.7 mV *p* 0–0.4 *t* 0–0.5	Not performed	AD 2F; 3pt	–	Braathen et al. [9]
Arg36Trp[b]	CMT2	47 y	ND	–	*m* 45.6 m/s *u* 46.4–63.5 m/s *p* 28.9–41.9 m/s *t* 29.1–32.6 m/s	*m* 8 mV *u* 9.9–6.6 mV *p* 1.1–0.8 mV *t* 0.2–0.5 mV	Not performed	1F, 2 pt	Painful, acute onset, remitting CSF protein 60 mg%	Burns et al. [11]
Arg36Gly	CMT2	5th to 8th dec	–	Progressive unsteady gait	*t* 33.9–36.2 m/s *p* 35.2–40.7 m/S *s* 37.8–40.7 m/S	*t* 1–5.9 mV *p* 1.9–7.4 mV *s* 1.9–1.7 mV	Severe loss of myelinated fibres with sporadic axonal degeneration and regenerating clusters	AD 1F; 3 pt	Rapidly progressive clinical course	Dacci et al. [15]
Cys50Gly[a]	CMT1B	66 y	Normal	Mild	*m* 27.1 m/s *u* 29.2 m/s *p* NE *t* 19.5 m/s	*m* 9.9 mV *u* 12.05 mV *p* NE *t* 5.8 mV	Not performed	1 pt	Diffuse swelling and slight gadolinium enhancement of the cauda equina	Nishiyama et al. [36]
Ser54 fs	CMT1B	4th to 6th dec	Normal	Mild in the father, rapidly progressive in the son	*m* 24–37 m/s *u* 29–37 m/s	*m* 3.5–8.2 mV *u* 1.5–7.7 mV	Not performed	AD 1F; 2 pt	CSF protein 551 mg/L; benefit from PE	Chavada et al. [12]
Ser55Ile	CMTI	6th dec	–	Mildly progressive	*m* 37.3 m/s *u* 36.8 m/s *t* 25.6 m/s	*u* 8 mV *t* 0.7 mV	Not performed	AD 1F; 2 pt	–	Kleffner et al. [25]

Table 3 (continued)

Mutation	Author diagnosis	Age of onset of first limitations	Age walked	Clinical course	NCV	cMAP	Pathology	Family history	Other clinical features	Author
Pro70Ser[b]	CMT2	5th to 6th dec	–	Moderate (CMTNS 10–18)	*m* 47–58 m/s *u* 50–53.7 m/s *p* 0–38.1 m/s *s* 33–44 m/s	*m* 6.5–17.8 mV *u* 13.3–16 mV *p* 0–0.3 *s* 0–0.57	Severe axonal neuropathy with wallerian-like degeneration and some clusters of regeneration	AD 2F; 5 pt and 1 sporadic case	–	Laurà et al. [27]
His81Leu	CMT2	5th to 6th dec	–	Severe (CMTNS: 24–25)	*m* 40–42 m/s	*m* 2–2.3 mV	Not performed	AD 1F; 3 pt	–	Liu et al. [29]
Tyr82His	CMT2	4th to 6th dec	ND	Mild	*m* 34–56 m/s *u* 48–59 m/s *p* NE–44 m/s	–	Loss of myelinated fibres, clusters of regenerating axons	AD 2F; 14 pt	–	Bienfait et al. [8]
Phe95Leu	CMT1B	4th to 7th dec	–	Slowly progressive or asymptomatic	*m* 41.1 m/s *u* 53 m/s *t* 25 m/s	*m* 9.6 mV *u* 11.6 mV *t* 0.3 mV	Not performed	AD 1F; 3 pt	Pupils abnormality; sensorineural hearing loss	O'Connor et al. [37]
Trp101Stop	CMTI	25 y proband (1st to 2nd to 4th dec)	–	Mild (CMTNS 6–8)	*m* 33–43 m/s *u* 36–50 m/s	*m* 5.6–10.2 mV *u* 2.2–7.7 mV	–	AD 1F; 6 pt	Neuropathic pain	Ramirez et al. [40]
Pro105Thr	CMT2	5th to 7th dec	–	Steppage gate	*m* 32.7–46.1 m/s *p* NE–30.2 m/s	*m* 6.9–8.0 mV *p* NE	Not performed	AD 1F; 4 pt	Sensory hearing loss; calf muscle hypertrophy; neuropathic pain	Kabzinska et al. [23]
Arg106Cys	CMT2	5th to 7th dec	Normal	Mild (CMTNS<10)	*m* 38–49 m/s *p* NE *s* NE	*m* 6.1–16 *p* NE *s* NE	Not performed	AD 2F; 4 pt	Sensory-neural hearing loss	Marttila et al. [33]
Asn116Ser	CMT1B	43 y	–	–	*m* 32 m/s *u* 34 m/s *p* 34 m/s *t* 32 m/s *s* NE	*m* 5 mV *u* 9.5 mV *t* 0.97 mV *s* NE	Not performed	1 pt de novo	–	Kleffner et al. [25]
Asp121Asn	CMT2	4th dec	–	Mild to moderate	*m* 46–55 m/s *u* 53 m/s *t* 33.3–37.9 m/s	*m* 3.7 mV *p* NE *t* 0.2–2.2 mV	Not performed	AD 1F; 6 pt	Sensory-neural hearing loss, pupils abnormalities	Duan et al. [16]

Table 3 (continued)

Mutation	Author diagnosis	Age of onset of first limitations	Age walked	Clinical course	NCV	cMAP	Pathology	Family history	Other clinical features	Author
Thr124Ala	CMT2	38 y	–	Mild	*t* 39 m/s *s* 42 m/s *u* 56 m/s	Reduced	Not performed	AD 1F: 3 pt		Mandich et al. [32]
Val136Gly	CMT1	45 y	–	Slowly progressive	*m* 34 m/s *p* 20 m/s	Decreased	Severe loss of myelinated fibres	1 pt Homozygous	Ataxia, tremor; MRI: multiple white matter lesions, with corpus callosum involvement	Reyes-Marin et al. [41]
V160fsX3 stop	CMT1B	3rd dec	Normal	Mild	*m* 36 m/s	Reduced	Not performed	AD 1F; 3 pt	–	Piazza et al. [38]
Leu144 fs	CMT1 presenting as acute remitting sensory neuropathy	44 y	Normal	Mild, remitting	*m* 30.6 m/s *u* 35.8 m/s	*m* 2.4 mV *u* 3.7 mV	Not performed	1 pt de novo	–	Simpson and Rajabally [46]
Tyr145 fs[a]	CMT2	40 y	–		*m* 38 m/s *t* 32.5 m/s *s* 30 m/s	Reduced	Not performed	1 pt de novo	Postural tremor of arms and legs	Mandich et al. [32]
Val146Gly	CMT1B	40 y	–	Mild	*m* 35.4 m/s *u* 43.9–45 m/s *t* 29.5–31.8 m/s	*m* 9.5 mV *u* 7.7 mV *t* 0.9–2.6 mV	Not performed	AD 1 F; 2 pt	–	Brozkova et al. [10]
Pro217Ser	CMT2I	27 y	–	–	*m* 53.8 m/s *p* 34.8 m/s *t* 28–31.3 m/s	*m* 11.4 mV *p* 5.8 mV *t* 6.5–5.3 mV	Not performed	1 pt de novo	–	Kleffner et al. [25]
Asp224Tyr[a]	CMT2/CMTI	43 y (proband)	–	Mild to moderate	*m* 34 m/s	*m* 12 mV	–	AD 1F; 3 pt	–	Miltenberger-Miltenyi et al. [35]
Asp224Tyr[a]	CMT2/CMTI	25–45 y	Normal	Mild to moderate	*m* 34–45 m/s *t* 35–43 m/s	*m* 3.8–12 mV *t* 2–11 mV	Mild axonal loss of myelinated fibres, groups of regenerating fibres	AD 1 F, 4 pt	Electrophysiological signs of inflammatory neuropathy	Schneider-Gold et al. [43]
Arg227Gly	CMT2	68 y	Normal	Mild	*m* 42.6 m/s *u* 43.1 m/s *t* 24.7 m/s	*m* 10.1 mV *u* 9.5 mV *t* 0.40 mV	Selective loss of large myelinated fibres; regenerating clusters; no onion bulbs	1 pt de novo	–	Shimizu et al. [45]

Table 3 (continued)

Mutation	Author diagnosis	Age of onset of first limitations	Age walked	Clinical course	NCV	cMAP	Pathology	Family history	Other clinical features	Author
c.645 + 1 G > T[a]	CMT1B	42 y	–	–	*p* 22.5 m/s *t* 28.8 m/s	*p* 1.5 mV *t* 2.4 mV	Not performed	1 pt de novo	–	Kleffner et al. [25]
c.614 + 2T > G[b]	CMT1B	3rd to 4th dec	Normal	Mild to moderate	*u* 38.8–42 m/s *p* 26.1–32.9 m/s	*u* 6.1–8 mV *p* 0.4–4.5 mV	Not performed	AD 1F; 4 pt	–	Sabet et al. [42]

Dec decade, *y* years, *m* median, *u* ulnar, *p* peroneal, *t* tibial, *s* sural, *NE* not evocable, *NR* not recorded, *AD* autosomal dominant, *F* family, *pt* patients

[a]Mutations described by more than one author

[b]Mutation also included in Brain 2015:138; 3180–3192

severity of the disease. Moreover, Tyr145 fs has been found by two different groups, in one case in a family with classical CMT2 phenotype [32], in the other [31] in three patients from one family with onset during the 4th decade of life and electrodiagnostic and pathologic findings of HNPP. In all the atypical cases, the identified mutation segregated with the disease in the families.

In addition to the classical small intragenic mutations, cases of *MPZ* copy number variation have recently been described (Supplementary Table 5). Hoyer [21] first described a family carrying an extra copy of the *MPZ* gene from exon 1 to exon 6, associated with a demyelinating neuropathy with onset within the 1st decade of life and slowly progressive course, while Maeda [30] described a family carrying *MPZ* triplication, affected by a demyelinating sensory-motor neuropathy with pupillary abnormalities and high intrafamilial heterogeneity in terms of age of onset and disease severity. Recently, Speevak [48] reported another case of *MPZ* duplication in a child affected by motor hypodemyelinating neuropathy with onset during the 1st year of life and a copy number variation of a region including *MPZ* and succinate dehydrogenase complex subunit C (*SDHC*) genes.

Six patients among all those included in our study, six carrying late-onset variants (Arg36Trp, Cys50Gly, Ser54 fs, Asp224Tyr, Arg36Gly, Val136Gly) [11, 12, 15, 36, 41, 43] initially received a diagnosis of inflammatory neuropathy, given an acute/subacute fluctuating clinical course eventually associated with pain as a prominent feature, markedly increased CSF protein concentration, and diffuse hypertrophy and slight gadolinium enhancement of the cauda equina roots at MRI. Moreover, co-occurrence with multiple sclerosis or asymptomatic CNS myelin abnormalities has been described for the Asp224Tyr [17] and Val136Gly [41] mutations, respectively.

Discussion

In this study, we aimed to define the spectrum of *MPZ*-associated phenotypes [5, 6] collecting and reviewing literature data regarding novel *MPZ* mutations described during the last 14 years (2005–2018), to better characterize the clinical features associated with them.

We identified 76 novel *MPZ* mutations associated with CMT in the recent literature. We excluded one VUS and other three mutations (5%) from the current work because of inadequate clinical data and considered separately three *MPZ* copy number variations (5%). Four mutations resulted in an atypical phenotype and six were described by more than one author as responsible for distinct phenotypes. The remaining 60 mutations, including 15 newly reported in a recent paper [6] analysing the clinical records of patients

Table 4 Features of P0-related neuropathies—CMT1B neuropathies

Mutation	Author diagnosis	Age of onset of first limitations	Age walked	Clinical course	NCV	CMAP	Pathology	Family history	Other clinical features	Author
Leu48Gln	CMT1B	2nd dec	Normal or delayed	Mild	*m* 29–35 m/s *u* 32–41 m/s *s* 27–40 m/s or NR	*m* 5.1–11.4 mV	Not performed	AD 2F; 3 + 7 pt	–	Brozkova et al. [10]
Cys50Gly[a]	CMT1	6 y	ND	–	*m* 16 m/s	*m* 6 mV	Not performed	1 pt	–	Miltenberger-Miltenyi et al. [35]
Glu97 fs	CMT1B	2nd dec	Instable walk	Mild	*m* 31–42 m/s *u* 37–42 m/s *s* 36–37 m/s	*m* 1.4–9.3 mV	Not performed	AD 1F; 5 pt	–	Brozkova et al. [10]
Gln100X	CMT1	Childhood	–	–	*m* 29 m/s	*m* 2 mV	Not performed	AD 1 F, 5 pt	–	Miltenberger-Miltenyi et al. [35]
Gly123Ser	CMT1B	2nd dec	Normal	Slowly progressive	*m* 15.7–19.6 m/s	ND	Severe loss of myelinated fibres, some onion bulb formation with clusters of regenerative fibres, and a large endoneurial area	AD 1 F, 9 pt	–	Lee et al. [28]
Asn131Ser[a]	CMT1B	Childhood	Normal	–	*m* 16.3 m/s	*m* 0.1 mV	Severe loss of myelinated fibres	1 pt de novo	Upper limbs predominant weakness with initial symptoms of entrapment neuropathy	Iida et al. [22]
Ile135Met	CMT1	Childhood	Normal	Mild	*m* 12.9 m/s *u* 13.6 m/s *t* NE *s* NE	*m* 1.4 mV *u* 4.8 mV *t* NE *s* NE	Not performed	AD 1 F; 2 pt	–	Lin et al. [26]
Gly137Val	CMT1B	10 y	–	Slowly progressive, CMTNS 15	NE	NE	Severe loss of myelinated fibres, onion bulbs	1 pt		Prada et al. [39]
Ser140Cys[a]	CMT1B	2nd dec (10–19 y)	–	CMTNS: 3–19	*m* 17–21.3 m/s	*m* 10.6–14.5 mV	–	AD 1 F; 2 pt	–	Liu et al. [29]

Table 4 (continued)

Mutation	Author diagnosis	Age of onset of first limitations	Age walked	Clinical course	NCV	CMAP	Pathology	Family history	Other clinical features	Author
Gln187ProfsX63	CMT1	Childhood	Normal	Moderate	*m* 13.6 m/s *u* 15.1 m/s *t* NE *s* NE	*m* 3.8 mV *u* 3.6 mV *t* NE *s* NE	Not performed	1 pt de novo	–	Lin et al. [26]
Lys214Met (Lys-204Met)	DI-CMT	2nd dec (14–17 y)	–	Very mild	*m* 35.3–41.6 m/s *p* 25.8–36.9 m/s	*m* 1.6–8.8 mV *p* 2–4.3 mV	Not performed	AD 1F; 9 pt	Calf hypertrophy in 3 pt	Banchs et al. [7]
Asp224Tyr[a]	CMT1B	2nd dec	Normal	Mild to moderate	*m* 17–44 m/s *u* 20–50 m/s *p* 16–42 m/s	*m* 4.9–12 mV *p* 0.9–6 mV	Chronic demyelinating process with complex onion bulbs and abnormally thickened myelin sheaths	1F, 4 pt; Proband homozygous	Multiple sclerosis in the proband	Fabrizi et al. [17]
c.645 + 1G > T[a]	CMT1B	12 y	Normal	Mild	*m* 32.6 m/s *t* 22.7 m/s *s* 31 m/s	*m* 8.4 mV *t* 1.3 mV *s* 2.58 uV	Not performed	1 pt de novo	–	Brozkova et al. [10]
c.674_675insA (His225Glnfs*10)	CMT1	2nd dec	Normal	Mild to moderate	*m* 15.3–23.9 m/s *u* 11.9–14.9 m/s *p* NE–21.2 m/s *s* NE	*m* 4–4.5 mV *u* 3–6.7 mV *p* NE–2.5 mV	Not performed	AD 1 F; 5 pt	–	He et al. [68]

Dec decade, *y* years, *m* median, *u* ulnar, *p* peroneal, *t* tibial, *s* sural, *NE* not evocable, *NR* not recorded, *AD* autosomal dominant, *F* family, *pt* patients

[a]Mutations described by more than one author

Table 5 Features of P0-related neuropathies—*MPZ* mutations with atypical phenotype

Mutation	Author diagnosis	Age of onset of first limitations	Age of walk	Disease course	NCV	CMAPs	Pathology	Family history	Other clinical findings	Author
Arg67Pro	CMT1	35 y (51)	ND	ND	*m* 28 m/s	ND	–	AD 1 F, 13 pt	Periodic palsy, myotonia	Hisama [20]
Leu48Pro	CMT1B	0–41 y	–	Highly variable	*m* 19.3–43 m/s *p* 20.5–32 m/s	*m* 3.68–7.5 mV *p* 1.9–8.4 mV	Decrease of large and small myelinated fibres, thin myelin sheath or concentric and eccentric thickenings. Cluster of regenerating fibres	AD 1 F, 7 pt	High intrafamilial variability in terms of age of onset and ENG findings	Szabo et al. [49]
Gly103Gly	CMT1B	2nd dec	Normal	Mild	*m* 33–42 m/s *t* 19–33 m/s	*m* 5–12 mV *t* 3.2–5.4 mV	Not performed	AD 2F; 3 + 3 pt	Neuropathic pain	Corrado et al. [14]
Tyr145 fs	HNPP	30–45 y	Normal	Mild	*m* 39–53 m/s *u* 33–48 m/s *p* 30–45 m/s	*m* 4.6–6.5 mV *u* 3.9–6.1 mV *p* 1.5–4.7 mV	Presence of tomacula	AD 1 F, 4 pt	Electrodiagnostic and pathologic features of HNPP	Magot et al. [31]

Dec decade, *y* years, *m* median, *u* ulnar, *p* peroneal, *t* tibial, *s* sural, *NE* not evocable, *NR* not recorded, *AD* autosomal dominant, *F* family, *pt* patients

carrying *MPZ* mutations recruited by the Inherited Neuropathy Consortium in a natural history study, corresponded to either early demyelinating, a childhood demyelinating or the late axonal phenotype.

In more detail, one quarter of the cases presented an early-onset phenotype, manifesting during motor development and characterized by very slow MNCV, while one half of the patients with novel *MPZ* mutations had an adult-onset axonal neuropathy with normal or minimally impaired MNCV. Interestingly, another quarter of the cases evaluated in this study had a distinct phenotype, presenting with motor and sensory symptoms usually during the 2nd decade of life and showing a slowly progressive course, with MNCV in the lower limit of the intermediate range. Such a phenotype, definable as childhood–adolescence onset, has been also highlighted, with a similar percentage, by Sanmaneechai et al. [6].

Myelin protein zero is the most abundant protein of the peripheral compact myelin, where it maintains the cohesion between adjacent myelin wraps through homophilic interactions [52]. As P0 is a prominent myelin protein, the mechanisms whereby MPZ mutations act in the generation of disorders alternatively affecting myelin or axons remain to be elucidated.

In the last years, different pathomechanisms for *MPZ* mutations have been dissected, particularly for mutations causing an early-onset neuropathy, ranging from endoplasmic reticulum retention and activation of the canonical unfolded protein response [53–56] to altered trafficking of the protein to non-myelin plasma membranes and altered radial axonal sorting during the early phases of myelination [57]. Other proposed mechanisms include the disruption of the intercellular adhesion properties with a structural packing defect [53] and mis-glycosylation of P0 with either loss of the native glycosylation site, the Asp122, frequently associated to a late-onset axonal neuropathy, or the gain of a new glycol site, resulting in an hyperglycosylated P0 variant, observed for mutations causing a severe demyelinating neuropathy [54, 58].

Advances have been achieved by the evidence that P0 not only localises in the compact myelin but also at the paranode and node of Ranvier, where it interacts with neurofascin 155 (NF155) and neurofascin 186 (NF186), participating in the maintenance of the nodal structure [59] and that Asp6Tyr, Asp32Gly, and His52Tyr mutations, responsible for late-onset CMT, display homophilic adhesion properties comparable to wild-type P0, but are unable to interact with components of the paranodal and nodal complexes.

CMT2 accounts for 30% of all CMT patients [60]. From our results, in the last decade, there was an increasing amount of novel *MPZ* mutations associated with late-onset axonal neuropathies rather than early-onset hypo- or demyelinating neuropathies. If we consider that while severe early-onset P0 variants often occur de novo and remain limited to a restricted number of cases, late-onset mutations are frequently familial and involve a larger number of subjects and recessive transmission, usually more common in severe early-onset diseases, has been described as associated with a late-onset phenotype in a patient carrying Val136Gly mutation, located in the same residue of Val136Glu but associated with heterozygous DSS and the prevalence of late-onset *MPZ* mutations, which has long been underestimated, is likely to be higher than expected, as growing awareness is increasing diagnostic rate and patients without overt family history may still be misdiagnosed.

Our data also include cases with presenting or superimposed features of an acquired inflammatory neuropathy. Given that the association between hereditary and inflammatory neuropathies is not yet clarified, and that neurophysiological and laboratory findings once considered typical for acquired inflammatory neuropathies have been described in various forms of CMT, genetic causes, including *MPZ* mutations, should be considered in the workup of patients with features of inflammatory neuropathy, especially if not all diagnostic criteria for inflammatory neuropathies are fulfilled and clinical response to immunosuppressive treatment is poor.

Molecular diagnosis of CMT can be achieved in 60–80% of cases [3, 56, 60, 61]. While up to 98% [56] of patients affected by CMT1 eventually receive a molecular diagnosis, this is still frequently challenging for patients suffering from late-onset CMT2, with the rate of diagnosis ranging between 25 and 63% using a gene-by-gene approach.

During the last years, the landscape of mutations responsible for CMT2 has expanded, ranging between the more common *GJB1* heterozygous mutations and autosomal dominant *GDAP1* mutations, and the incorporation of next-generation sequencing in the diagnostic practice has allowed the discovery of novel CMT genes, especially causing late-onset CMT2 [62], including *HARS* [63], *MARS* [64], *MME* [65] MORC2 [66] and NEFH [67].

The increasing amount of new genes associated with CMT2 and by the fact that other genetically determined neuropathies such as transthyretin-related amyloidosis, a systemic disease with involvement of peripheral nerves, can also manifest after the 6th decade, it is conceivable that an increasing number of late-onset neuropathies, previously misdiagnosed as acquired or age related, have a genetic cause.

In conclusion, our data, focusing on P0-related neuropathies heterogeneity, confirms the existence of three distinct phenotypes deriving from *MPZ* mutations, and highlights the clinical relevance of late-onset P0 neuropathies as well as the need to increase our knowledge about their underlying molecular mechanisms.

Compliance with ethical standards

Conflicts of interest None of the authors have any conflict of interest regarding this work.

Ethical approval This article does not contain any studies with human participants or animals performed by any of the authors.

Informed consent For this type of study formal consent is not required.

References

1. Barreto LC, Oliveira FS, Nunes PS et al (2016) Epidemiologic study of Charcot–Marie–Tooth disease: a systematic review. Neuroepidemiology 46:157–165
2. Timmerman V, Strickland AV, Zuchner S (2014) Genetics of Charcot–Marie–Tooth (CMT) disease within the frame of the human genome project success. Genes (Basel) 5(1):13–32
3. Fridman V, Bundy B, Reilly MM et al (2015) CMT subtypes and disease burden in patients enrolled in the Inherited Neuropathies Consortium natural history study: a cross-sectional analysis. J Neurol Neurosurg Psychiatry 86(8):873–878
4. Pareyson D, Saveri P, Pisciotta C (2017) New developments in Charcot–Marie–Tooth neuropathy and related diseases. Curr Opin Neurol 30(5):471–480
5. Shy ME, Jani A, Krajewski K et al (2004) Phenotypic clustering in MPZ mutations. Brain 127(Pt 2):371–384
6. Sanmaneechai O, Feely S, Scherer SS et al (2015) Genotype–phenotype characteristics and baseline natural history of heritable neuropathies caused by mutations in the MPZ gene. Brain 138:3180–3192
7. Banchs I, Casasnovas C, Alberti A et al (2009) Diagnosis of Charcot–Marie–Tooth disease. J Biomed Biotechnol 2009:985415
8. Bienfait HM, Faber CG, Baas F et al (2006) Late onset axonal Charcot–Marie–Tooth phenotype caused by a novel myelin protein zero mutation. J Neurol Neurosurg Psychiatry 77(4):534–537
9. Braathen GJ, Sand JC, Russell MB (2010) Two novel missense mutations in the myelin protein zero gene causes Charcot–Marie–Tooth type 2 and Dejerine–Sottas syndrome. BMC Res Notes 3:99
10. Brozkova D, Mazanec R, Haberlova J, Sakmaryova I, Seeman P (2010) Clinical and in silico evidence for and against pathogenicity of 11 new mutations in the MPZ gene. Clin Genet 78(1):81–87
11. Burns TM, Phillips LH, Dimberg EL, Vaught BK, Klein CJ (2006) Novel myelin protein zero mutation (Arg36Trp) in a patient with acute onset painful neuropathy. Neuromuscul Disord 16(5):308–310
12. Chavada G, Rao DG, Martindale J, Hadjivassiliou M (2012) A novel MPZ gene mutation in exon 2 causing late-onset demyelinating Charcot–Marie–Tooth disease. J Clin Neuromusc Dis 13(4):206–208
13. Choi BO, Kim SB, Kanwal S et al (2011) MPZ mutation in an early-onset Charcot–Marie–Tooth disease type 1B family by genome-wide linkage analysis. Int J Mol Med 28(3):389–396
14. Corrado L, Magri S, Bagarotti A et al (2016) A novel synonymous mutation in the MPZ gene causing an aberrant splicing pattern and Charcot–Marie–Tooth disease type 1B. Neuromusc Disord 26:516–520
15. Dacci P, Taroni F, Bella ED et al (2012) Myelin protein zero Arg-36Gly mutation with very late onset and rapidly progressive painful neuropathy. J Peripher Nerv Syst 17(4):422–425
16. Duan X, Gu W, Hao Y et al (2016) A novel Asp121Asn mutation of myelin protein zero is associated with late-onset axonal Charcot–Marie–Tooth disease, hearing loss and pupil abnormalities. Front Aging Neurosci 8:222 **(eCollection)**
17. Fabrizi GM, Pellegrini M, Angiari C et al (2006) Gene dosage sensitivity of a novel mutation in the intracellular domain of P0 associated with Charcot–Marie–Tooth disease type 1B. Neuromuscul Disord 16(3):183–187
18. Finsterer J, Miltenberger G, Rauschka H, Janecke A (2006) Novel C59T leader peptide mutation in the MPZ gene associated with late-onset, axonal, sensorimotor polyneuropathy. Eur J Neurol 13(10):1149–1152
19. Floroskufi P, Panas M, Karadima G, Vassilopoulos D (2007) New mutation of the MPZ gene in a family with the Dejerine–Sottas disease phenotype. Muscle Nerve 35(5):667–669
20. Hisama FM (2005) Familial periodic paralysis and Charcot–Marie–Tooth disease in a 7-generation family. Arch Neurol 62(1):135–138
21. Hoyer H, Braathen GJ, Eek AK, Skjelbred CF, Russell MB (2011) Charcot–Marie–Tooth caused by a copy number variation in myelin protein zero. Eur J Med Genet 54(6):e580–e583
22. Iida M, Koike H, Ando T et al (2012) A novel MPZ mutation in Charcot–Marie–Tooth disease type 1B with focally folded myelin and multiple entrapment neuropathies. Neuromuscul Disord 22(2):166–169
23. Kabzinska D, Korwin-Piotrowska T, Drechsler H, Drac H, Hausmanowa-Petrusewicz I, Kochanski A (2007) Late-onset Charcot–Marie–Tooth type 2 disease with hearing impairment associated with a novel Pro105Thr mutation in the MPZ gene. Am J Med Genet Part A 143A(18):2196–2199
24. Keckarevic-Markovic M, Milic-Rasic V, Mladenovic J et al (2009) Mutational analysis of GJB1, MPZ, PMP22, EGR2, and LITAF/SIMPLE in Serbian Charcot–Marie–Tooth patients. J Peripher Nerv Syst 14(2):125–136
25. Kleffner I, Schirmacher A, Gess B, Boentert M, Young P (2010) Four novel mutations of the myelin protein zero gene presenting as a mild and late-onset polyneuropathy. J Neurol 257(11):1864–1868
26. Lin KP, Soong BW, Chang MH et al (2012) Clinical and cellular characterization of two novel MPZ mutations, p.I135 M and p.Q187PfsX63. Clin Neurol Neurosurg 114(2):124–129
27. Laurà M, Milani M, Morbin M et al (2007) Rapid progression of late onset axonal Charcot–Marie–Tooth disease associated with a novel MPZ mutation in the extracellular domain. J Neurol Neurosurg Psychiatry 78(11):1263–1266
28. Lee YC, Yu CT, Lin KP et al (2008) MPZ mutation G123S characterization: evidence for a complex pathogenesis in CMT disease. Neurology 70(4):273–277
29. Liu L, Li X, Zi X et al (2013) Two novel MPZ mutations in Chinese CMT patients. J Peripher Nerv Syst 18(3):256–260
30. Maeda MH, Mitsui J, Soong BW et al (2012) Increased gene dosage of myelin protein zero causes Charcot–Marie–Tooth disease. Ann Neurol 71(1):84–92
31. Magot A, Latour P, Mussini JM et al (2008) A new MPZ mutation associated with a mild CMT1 phenotype presenting with recurrent nerve compression. Muscle Nerve 38(2):1055–1059
32. Mandich P, Fossa P, Capponi S et al (2009) Clinical features and molecular modelling of novel MPZ mutations in demyelinating and axonal neuropathies. Eur J Hum Genet 17(9):1129–1134
33. Marttila M, Rautenstrauss B, Huehne K, Laitinen V, Majamaa K, Karppa M (2012) A novel mutation of myelin protein zero associated with late-onset predominantly axonal Charcot–Marie–Tooth disease. J Neurol 259(8):1585–1589
34. McMillan HJ, Santagata S, Shapiro F et al (2010) Novel MPZ mutations and congenital hypomyelinating neuropathy. Neuromuscular Disorders 20(11):725

35. Miltenberger-Miltenyi G, Schwarzbraun T, Loscher WN et al (2009) Identification and in silico analysis of 14 novel GJB1, MPZ and PMP22 gene mutations. Eur J Hum Genet 17(9):1154–1159
36. Nishiyama S, Sugeno N, Tateyama M, Aoki M (2013) Late-onset Charcot–Marie–Tooth disease type 1B due to a novel mutation in the extracellular disulfide bridge of MPZ gene. Clin Neurol Neurosurg 115(2):208–209
37. O'Connor G, McNamara P, Bradley D, Connolly S, Langan Y, Redmond J (2012) Late-onset CMT phenotype caused by a novel mutation in the MPZ gene. Eur J Neurol 19(7):e65–e66
38. Piazza S, Baldinotti F, Fogli A et al (2010) A new truncating MPZ mutation associated with a very mild CMT1 B phenotype. Neuromuscul Disord 20(12):817–819
39. Prada V, Capponi S, Ursino G et al (2015) Sural nerve biopsy and functional studies support the pathogenic role of a novel MPZ mutation. Neuropathology 35(3):254–259
40. Ramirez JD, Barnes PR, Mills KR, Bennett DL (2012) Intermediate Charcot–Marie–Tooth disease due to a novel Trp101Stop myelin protein zero mutation associated with debilitating neuropathic pain. Pain 153(8):1763–1768
41. Reyes-Marin K, Jimenez-Pancho J, Pozo L et al (2011) A novel myelin protein zero (V136G) homozygous mutation causing late onset demyelinating polyneuropathy with brain white matter lesions. Clin Neurol Neurosurg 113(3):243–244
42. Sabet A, Li J, Ghandour K et al (2006) Skin biopsies demonstrate MPZ splicing abnormalities in Charcot–Marie–Tooth neuropathy 1B. Neurology 67(7):1141–1146
43. Schneider-Gold C, Kotting J, Epplen JT et al (2010) Unusual Charcot–Marie–Tooth phenotype due to a mutation within the intracellular domain of myelin protein zero. Muscle Nerve 41(4):550–554
44. Sevilla T, Lupo V, Sivera R et al (2011) Congenital hypomyelinating neuropathy due to a novel MPZ mutation. J Peripher Nerv Syst 16(4):347–352
45. Shimizu H, Oka N, Kawarai T et al (2010) Late-onset CMT2 associated with a novel missense mutation in the cytoplasmic domain of the MPZ gene. Clin Neurol Neurosurg 112(9):798–800
46. Simpson BS, Rajabally YA (2010) Charcot–Marie–Tooth disease due to novel myelin protein zero mutation presenting as late-onset remitting sensory neuropathy. J Clin Neuromusc Dis 11(4):187–190
47. Smit LS, Roofthooft D, Van Ruissen F, Baas F, van Doorn PA (2008) Congenital hypomyelinating neuropathy, a long term follow-up study in an affected family. Neuromuscul Disord 18(1):59–62
48. Speekav MD, Farrel SA (2013) Charcot–Marie–Tooth 1B caused by expansion of a familial myelin protein zero (*MPZ*) gene duplication. Eur J Med Genet 56:566–569
49. Szabo A, Zuchner S, Siska E, Mechler F, Molnar MJ (2005) Marked phenotypic variation in a family with a new myelin protein zero mutation. Neuromuscul Disord 15(11):760–763
50. Taioli F, Cabrini I, Cavallaro T, Simonati A, Testi S, Fabrizi GM (2011) Dejerine–Sottas syndrome with a silent nucleotide change of myelin protein zero gene. J Peripher Nerv Syst 16(1):59–64
51. Zschuntzsch J, Dibaj P, Pilgram S, Kotting J, Gerding WM, Neusch C (2009) Severe demyelinating hypertrophic polyneuropathy caused by a de novo frameshift mutation within the intracellular domain of myelin protein zero (MPZ/P0). J Neurol Sci 281(1–2):113–115
52. Shapiro L, Doyle JP, Hensley P et al (1996) Crystal structure of the extracellular domain from P0, the major structural protein of peripheral nerve myelin. Neuron 1(7):435–449
53. Wrabetz L, D'Antonio M, Pennuto M et al (2006) Different intracellular pathomechanisms produce diverse *Myelin Protein Zero* neuropathies in transgenic mice. J Neurosci 26(8):2358–2368
54. Grandis M, Vigo T, Passalacqua M et al (2008) Different cellular and molecular mechanisms for early and late-onset myelin protein zero mutations. Hum Mol Genet 17(13):1877–1889
55. Pennuto M, Tinelli E, Malaguti M et al (2008) Ablation of the UPR-mediator CHOP restores motor function and reduces demyelination in Charcot–Marie–Tooth 1B mice. Neuron 57(3):393–405
56. Saporta ASD, Sottile SL, Miller LJ, Feely SME, Siskind CE, Shy ME (2011) Charcot–Marie–Tooth disease subtypes and genetic testing strategies. Ann Neurol 69(1):22–33
57. Fratta P, Ornaghi F, Dati G et al (2019) A nonsense mutation in Myelin Protein Zero causes congenital hypomyelination neuropathy through altered P0 membrane targeting and gain of abnormal function. Hum Mol Genet 28(1):124–132
58. Prada V, Passalacqua M, Bono M et al (2012) Gain of glycosylation: a new pathomechanism of myelin protein zero mutations. Ann Neurol 71(3):427–431
59. Brügger V, Engler S, Pereira JA et al (2015) HDAC1/2-dependent P0 expression maintains paranodal and nodal integrity independently of myelin stability through interactions with neurofascins. PLOS Biol 13(9):e1002258
60. Murphy SM, Laura M, Fawcett K et al (2012) Charcot–Marie–Tooth disease: frequency of genetic subtypes and guidelines for genetic testing. J Neurol Neurosurg Psychiatry 83(7):706–710
61. Sivera R, Sevilla T, Vílchez J et al (2013) Charcot–Marie–Tooth disease: genetic and clinical spectrum in a Spanish clinical series. Neurology 81(18):1617–1625
62. Rossor AM, Polke JM, Houlden H et al (2013) Clinical implications of genetic advances in Charcot–Marie–Tooth disease. Nat Rev Neurol 9(10):562–571
63. Brodzkova S, Deconinck T, Griffin LB et al (2015) Loss of function mutations in HARS cause a spectrum of inherited peripheral neuropathies. Brain 138(Pt8):2161–2172
64. Gonzalez M, McLaughlin H, Houlden H et al (2013) Exome sequencing identifies a significant variant in methionyl-tRNA synthetase (MARS) in a family with late-onset CMT2. J Neurol Neurosurg Psychiatry 84(11):1247–1249
65. Lupo V, Frasquet M, Sánchez-Monteagudo A et al (2018) Characterising the phenotype and mode of inheritance of patients with inherited peripheral neuropathies carrying MME mutations. J Med Genet 55(12):814–823. https://doi.org/10.1136/jmedgenet-2018-105650 **(Epub 2018 Nov 10)**
66. Sevilla T, Lupo V, Martínez-Rubio D et al (2016) Mutations in the MORC2 gene cause axonal Charcot–Marie–Tooth disease. Brain 139(Pt 1):62–72
67. Rebelo AP, Abrams AJ, Cottenie E et al (2016) Cryptic amyloidogenic elements in the 3' UTRs of neurofilament genes trigger axonal neuropathy. Am J Hum Genet 98(4):597–614
68. He J, Guo L, Xu G et al (2018) Clinical and genetic investigation in Chinese patients with demyelinating Charcot-Marie-Tooth disease. J Peripher Nerv Syst 23(4):216–226